2005

Analysis and Implementation of Ripple Current Cancellation Technique for Electronic Ballasts

Marius G. Marita
Cleveland State University

ANALYSIS AND IMPLEMENTATION OF RIPPLE CURRENT CANCELLATION TECHNIQUE FOR ELECTRONIC BALLASTS

MARIUS G. MARITA

Bachelor of Science in Electrical Engineering

Cleveland State University

Cleveland, Ohio

May, 2003

submitted in partial fulfillment of requirements for the degree

MASTER OF SCIENCE IN ELECTRICAL ENGINEERING

at the

Cleveland State University

October , 2005

Dedicated to my dear wife

Adela.

AKNOWLEDGEMENTS

I would like to thank all the faculty and staff from the Electrical and Computer Engineering Department at Cleveland State University for their help. Special thanks to my advisor Dr. Ana Stankovic and Dr. F. Eugenio Villaseca the Chairman of the Electrical and Computer Engineering Department. Many thanks to Dr. Zhiqiang Gao, Mr. Jack Zeller, Dr. Dan Simon, Dr. Fuqin Xiong, Dr Jerzy Sawicki and Ms. Adriene Fox for their guidance and support in making this happen.

I would also like to thank all the colleagues from General Electric Consumer & Industrial at NELA Park Electronics Design Team. Their guidance and support helped me get through my work in completing this thesis. Many thanks to my coordinator Dr. Louis Nerone, my manager Mr. John Kralik, Mr. James Mieskoski, and Virgil Chichernea all of G.E..

Thanks to all for making this happen.

ANALYSIS AND IMPLEMENTATION OF RIPPLE CURRENT CANCELLATION TECHNIQUE FOR ELECTRONIC BALLASTS

MARIUS G. MARITA

ABSTRACT

This thesis evaluates the effect of the Ripple Current Cancellation Technique on a particular Boost Power Factor Correction Converter of electronic ballasts for lighting industry. The design and analysis of a universal input 150-Watt boost power factor correction converter with the ripple current cancellation circuit is presented. In addition a simulation model is developed using Cadence-PSPICE and its results compared with the bench model. An EMI filter designed for the 150-Watt boost with ripple current cancellation is described to satisfy the Federal Communication Commission (FCC) regulations.

TABLE OF CONTENTS

LIST OF FIGURES

Figure **Page**

LIST OF TABLES

Table **Page**

CHAPTER I

LITERATURE REVIEW

1.1 Introduction

The demand for more reliable and more compact electronic ballasts for lighting industry has increased in the past years. Companies and individuals spend a lot of their research on studying different topologies of switch-mode power supplies that can be implemented in electronic ballasts, making them more reliable and more compact.

Power supplies are used in providing the load with a constant voltage, current, or power, while the input voltage and load resistance change. The topologies used for switch-mode conversion vary up to about seven different methods. Their effects on the load as well as the problems they cause on the input line are diverse.

Most of the topologies used in switch-mode conversion provide the output with a constant voltage. This constant voltage has some ripple due to the converter storage components, and this causes problems for some applications. The output ripple is mostly controlled by the filter capacitor, which can be increased such that more ripple current

will be bypassing the load through the capacitor. But the capacitor size increases as its capacitance value goes up and so does the size of the converter.

Another problem occurs when the input current waveform drawn from the source is distorted due to the high frequency switching of the converter as well as the input capacitor. This causes the apparent power, which is unnecessary for the load to be high and causes the current drawn from the line to be distorted.

Besides the distorted current waveform of the source, there is a lot of high frequency noise that is reflected back to the line, called conducted Electro-Magnetic Interference (EMI). One of the causes of this type of noise is due to the switching losses associated with the switch and the diode of the converter. When the switch or diode changes states from on to off or vice versa, this change cannot occur instantly and there are some losses associated with it. Forcing the switch to change states, or the diode to be turned on or off, require some transition time that is associated with power losses. This causes the high frequency noise reflected back to the line.

EMI filters are designed to reduce the noise level at the input of a converter to a value that is permitted by the regulatory agencies in charge. These EMI filters while doing their job they take a lot of space and add to the weight of the converter, making the converter increase in size, weight, and they add to the overall cost.

There is an increased interest from the industry to find ways to reduce the size of these filters while making the converters more reliable and more compact. A great deal of study had been made in reducing the ripple current caused by the inductor of the converter. The way to reduce the ripple is by adding a circuit that would generate a current that is of the same magnitude but opposite to the AC ripple current of the

inductor. Feeding this AC current to the output filter of the converter, will cancel out the AC ripple, and would leave the output with a constant DC required by the load [2], [3], [5], [6], [7], [8], [11]. Practically the ripple cannot be fully cancelled but only drastically reduced. Therefore the output filter capacitor will still have to remain but its size could be greatly reduced. Smaller ripple through the output filter would imply less AC current through the filter capacitor, and less ripple through the output load. A smaller ripple at the output would provide the feedback loop of the controller with a cleaner signal and this will eliminate some of the control problems associated with the output ripple.

1.2 DC-to-DC Converter – Boost Topology

More reliable power supplies are implemented today by means of switching power converters. These power converters are designed with two major goals. First they have to run at high efficiency so that the cost of the wasted energy due to conversion is low. Secondly, the wasted energy will generate heat that would imply adding heat sinks, causing to increase the size of circuit components. Other design criteria that results from the two previously mentioned factors are the cost, size, and weight of the converters [1].

Linear electronics, which has been the only way to convert energy up until about 1970's was greatly reduced to less than 50% of the energy conversion methods used in today's electronics [1]. In linear electronics the conversion is being implemented by means of transformers that would either step up or down the voltage load while operating at constant 50 or 60 Hz frequency. Due to the low frequency, these transformers have big

size, which implies more energy dissipation and therefore higher costs, weight, and size of the overall system [1]. These factors make the linear electronics to be unpractical.

The switch-mode power supplies are a more efficient way of converting power and they prove to be a lot more reliable. Advancement in microelectronics fabrication technology led to the development of computers, communication equipment, and consumer electronics which require regulated power supplies and in some cases, uninterrupted power supplies.

Energy conservation has become a priority for keeping a clean environment and many industries, such as the lighting industry have adopted the use of higher efficiency converters as well as lighting devices that give light while using less and less amount of energy.

While many of the power converters are used to have as an input the AC lines of the power grid of the electric company and output a load, some can be used to work in reverse direction (like power generating farms, or solar panels, or photovoltaic cells) to put energy back into the lines [1].

The boost converter topology is used in this case to analyze the ripple current cancellation technique. A boost converter is shown in Figure 1.1 below.

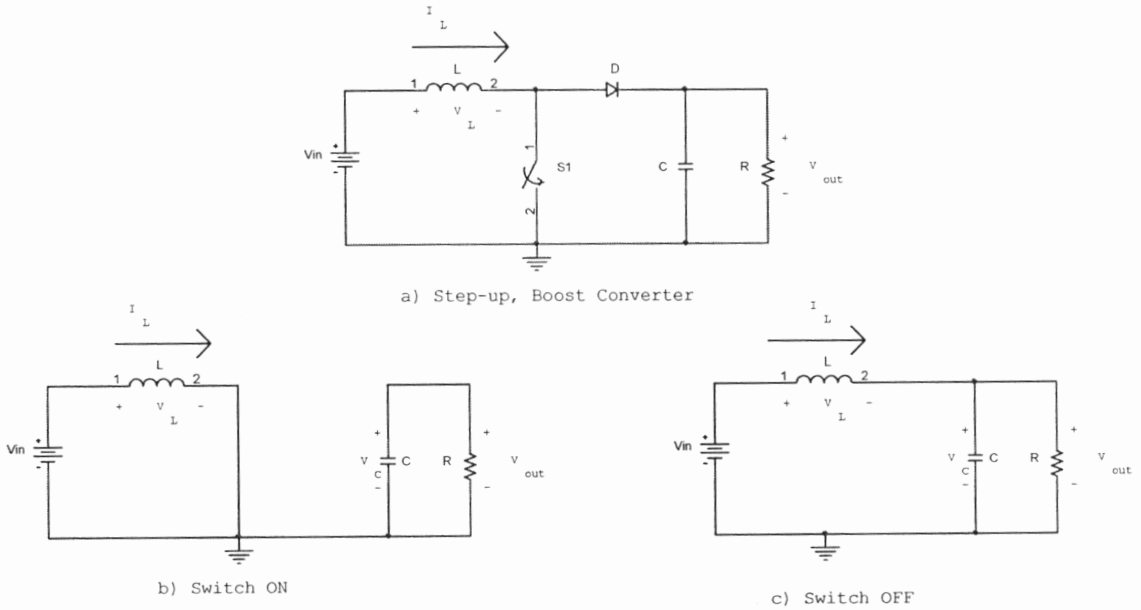

Figure 1.1: Boost Converter Schematic Representation a) Boost Schematic b) Switch On c) Switch Off

In a boost topology the output voltage is always greater than the input voltage [1], [25]. When the switch is on, the input supplies energy to the inductor and the output is isolated from the input (See Figure 1.1 b). When the switch is off the inductor is charged with energy and starts releasing it into the output along with the input supply voltage (See Figure 1.1 c).

When the switch is on, the following two equations hold.

$$\begin{aligned} i_L' &= \frac{1}{L} \cdot V_{in}(t) \\ v_c' &= -\frac{1}{R \cdot C} \cdot V_{out}(t) \end{aligned} \tag{1.1}$$

The output voltage is also the voltage across the capacitor, v_c.

The governing state space system of equations is of the form:

$$\begin{cases} X' = A \cdot X + B \cdot U \\ Y = C \cdot X + D \cdot U \end{cases} \tag{1.2}$$

In the above equation, the state variable X consists of the inductor current and capacitor voltage, U is represented by the input voltage, A is the state matrice, B is a vector, Y represents the output voltage, C is the transposed matrix, and D represents the initial conditions. Substituting in the above equation, the state space equation becomes:

$$\begin{cases} \begin{bmatrix} i_L' \\ v_c' \end{bmatrix} = \begin{bmatrix} 0 & 0 \\ 0 & -\dfrac{1}{R \cdot C} \end{bmatrix} \cdot \begin{bmatrix} i_L \\ v_c \end{bmatrix} + \begin{bmatrix} \dfrac{1}{L} \\ 0 \end{bmatrix} \cdot V_{in}(t) \\ V_{out}(t) = \begin{pmatrix} 0 & 1 \end{pmatrix} \cdot \begin{bmatrix} i_L \\ v_c \end{bmatrix} \end{cases} \tag{1.3}$$

The state space system of equations above describes the boost converter when the switch is on.

When the switch is off the equations describing the system in Figure 1.1c are:

$$\begin{aligned} i_L' &= -\frac{1}{L} \cdot v_c + \frac{1}{L} \cdot V_{in}(t) \\ v_c' &= \frac{1}{C} \cdot i_L - \frac{1}{R \cdot C} \cdot v_c \end{aligned} \tag{1.4}$$

The output voltage when switch is on is again equal to the voltage across the output capacitor. The state space equation describing the system in Figure 1.1c becomes:

$$\begin{cases} \begin{bmatrix} i_L' \\ v_c' \end{bmatrix} = \begin{bmatrix} 0 & -\dfrac{1}{L} \\ \dfrac{1}{C} & -\dfrac{1}{R \cdot C} \end{bmatrix} \cdot \begin{bmatrix} i_L \\ v_c \end{bmatrix} + \begin{bmatrix} \dfrac{1}{L} \\ 0 \end{bmatrix} \cdot V_{in}(t) \\ V_{out}(t) = \begin{pmatrix} 0 & 1 \end{pmatrix} \cdot \begin{bmatrix} i_L \\ v_c \end{bmatrix} \end{cases} \tag{1.5}$$

Let D be the duty ratio that describes the converter on time, and the following matrices representing the system with the switch on (1) and off (2) as:

$$A_1 = \begin{bmatrix} 0 & 0 \\ 0 & -\dfrac{1}{R \cdot C} \end{bmatrix} \tag{1.6}$$

$$A_2 = \begin{bmatrix} 0 & -\frac{1}{L} \\ \frac{1}{C} & -\frac{1}{R \cdot C} \end{bmatrix} \tag{1.7}$$

$$B_1 = \begin{bmatrix} \frac{1}{L} \\ 0 \end{bmatrix} \tag{1.8}$$

$$B_2 = \begin{bmatrix} \frac{1}{L} \\ 0 \end{bmatrix} \tag{1.9}$$

$$C_1 = (0 \quad 1) \tag{1.10}$$

$$C_2 = (0 \quad 1) \tag{1.11}$$

Then the overall system coefficient factors over one period can be calculated after the following formulas [1], [21], [24]:

$$A = A_1 \cdot D + A_2 \cdot (1 - D) \tag{1.12}$$

$$B = B_1 \cdot D + B_2 \cdot (1 - D) \tag{1.13}$$

$$C = C_1 \cdot D + C_2 \cdot (1 - D) \tag{1.14}$$

The resulting coefficients that describe the system in steady state become:

$$A = \begin{bmatrix} 0 & -\frac{1-D}{L} \\ \frac{1-D}{C} & -\frac{1}{R \cdot C} \end{bmatrix} \tag{1.15}$$

$$B = \begin{bmatrix} \frac{1}{L} \\ 0 \end{bmatrix} \tag{1.16}$$

$$C = (0 \quad 1) \tag{1.17}$$

Once the coefficients are calculated, solving for the steady state transfer function can be found from the following equation [1]:

$$\frac{V_{out}}{V_{in}} = -C \cdot A^{-1} \cdot B \tag{1.18}$$

The system in steady state, with no feedback behaves after the following formula:

$$\frac{V_{out}}{V_{in}} = -(0 \quad 1) \cdot \begin{bmatrix} 0 & -\frac{1-D}{L} \\ \frac{1-D}{C} & -\frac{1}{R \cdot C} \end{bmatrix}^{-1} \cdot \begin{bmatrix} \frac{1}{L} \\ 0 \end{bmatrix} \tag{1.19}$$

Simplifying the above equation results in the following equation that characterizes the system in continuous conduction mode:

$$\frac{V_{out}}{V_{in}} = \frac{1}{1-D} \tag{1.20}$$

Since D takes values between 0 and 1, the output voltage will always be greater than the input voltage, thus boost topology [1].

A quick modeling of the converter using small signal modeling method can be derived to obtain a control analysis.

It has been shown in references [1], [21], and [24] that by adding a small perturbation to D, V_{out}, i_L, and v_c, and assuming that V_{in} stays constant, the following equation holds in describing a system such as the boost converter:

$$H_p(s) = \frac{\tilde{V}_{out}(s)}{\tilde{d}(s)} = C \cdot [s \cdot I - A]^{-1} \cdot [(A_1 - A_2) \cdot \overline{X} + (B_1 - B_2) \cdot V_{in}] + (C_1 - C_2) \cdot \overline{X} \tag{1.21}$$

In the above equation the terms $\tilde{V}_{out}$ and $\tilde{d}$ represent the small perturbation added to the output and to the duty ratio, and $\overline{X}$ is a two rows and one column matrix that gives the average value of the i_L and v_c which represent the state variables.

For the boost topology, the average values of the state variables are:

$$v_c = V_{out} = V_{in} \cdot \frac{1}{1-D}$$
$$i_L = \frac{I_{out}}{1-D} = \frac{V_{out}}{R \cdot (1-D)} \tag{1.22}$$

The I in equation (1.21) represents the identity matrix.

Now that all the terms from equation (1.21) are defined, the calculation of the small signal model is possible. Substituting in the above H_p equation with all the terms and simplifying the equation, results in a second order system of the form:

$$H_p(s) = \frac{\frac{1-D}{L \cdot C} \cdot V_{out} - \frac{1}{C} \cdot I_L \cdot s}{s^2 + \frac{1}{R \cdot L} \cdot s + \frac{1}{L \cdot C} \cdot (1-D)^2} \tag{1.23}$$

A full calculation of the transfer function given by (1.23) is presented in appendix A of this thesis.

The system above describes the boost transfer function controlled by a simple voltage feedback loop. The system has two underdamped poles (-R±jI) located in the left hand plane, and one zero which is in the right half plane of the real vs. imaginary plane.

The system above is very difficult to control due to the zero situated on the right half plane and the poles that are very close to the imaginary axis. The gains of the controller cannot take high values because, as the gain increases, the poles tend to move towards the right half plane and this could also create stability problems. Therefore, the control feedback loop must be designed with small gains, which makes the system response to disturbances slow.

The system above is very sensitive to input changes, as well as load disturbances, as these factors make the pole location to change. The control problem becomes more

difficult for this system at light loads [24]. Due to these factors, a more simplified system is desired.

The best practice in eliminating these problems is by adding an inner current loop [24]. Due to this inner current loop, the poles of the system are overdamped, and therefore much easier to be controlled. This inner current loop is placing the pole due to the dynamics of the inductor far to the left of the origin so this pole can be practically eliminated. The pole due to the output capacitor that pretty much describes the system when the inner current loop is used is well under control by the voltage feedback loop. The poles in the current mode control are overdamped and this is also an important factor in making the system much easier to be controlled. Although this inner current loop ads slight complication to the design of the controller, it is necessary to ensure stability of the boost converter over a wide range of operation, from heavy loads to very light loads [24].

1.3 Power Factor Correction

A way to measure the utilization of the source is by looking at the ratio between the real power P and the apparent power S [1], [24]. The term used in the industry today is called the Power Factor.

This power factor (P.F.) is defined as:

$$P.F. = \frac{P}{S} \tag{1.24}$$

where

$$S = V_{rms} \cdot I_{rms} \tag{1.25}$$

For a pure resistor, the real power P is equal to the apparent power S and the power factor becomes 1. This is the best case for the utilization of the source.

For a pure inductor, or a pure capacitor, the real power is 0, and the result of the power factor is 0 as well. This is the worst case for the utilization of the source [24].

The voltage seen by the source is a sinusoidal waveform of the form:

$$V_s(t) = V_M \cdot \sin(\omega \cdot t) \tag{1.26}$$

The current seen by the source as a Fourier series is:

$$i(t) = \sum_{n=0}^{\infty} I_M \cdot \sin(n \cdot \omega \cdot t + \phi_n) \tag{1.27}$$

The real power drawn from the source becomes:

$$P = \frac{1}{2\pi} \cdot \int_{2\pi} V_s(t) \cdot i(t) \cdot d(\omega \cdot t) \tag{1.28}$$

Substituting for the voltage and the current, the equation above becomes:

$$P = \frac{1}{2\pi} \cdot \int_{2\pi} V_M \cdot \sin(\omega \cdot t) \cdot \sum_{n=0}^{\infty} I_M \cdot \sin(n \cdot \omega \cdot t + \phi_n) \cdot d(\omega \cdot t) \tag{1.29}$$

Simplifying the above equation it becomes:

$$P = \sum_{n=0}^{\infty} \frac{1}{2\pi} \cdot \int_{2\pi} V_M \cdot I_M \cdot \sin(\omega \cdot t) \cdot \sin(n \cdot \omega \cdot t + \phi_n) \cdot d(\omega \cdot t) \tag{1.30}$$

Carrying out the calculations of the above equation by applying orthogonality (the integral of the product of two different frequency components are individually zero), all terms cancel out except the fundamental component. Therefore the equation for power becomes:

$$P = \frac{1}{2\pi} \cdot \int_{2\pi} V_M \cdot I_1 \cdot \sin(\omega \cdot t) \cdot \sin(\omega \cdot t + \phi_1) \cdot d(\omega \cdot t) \tag{1.31}$$

Carrying out the calculations of the above equation results in:

$$P = \frac{V_M \cdot I_1}{2} \cdot \cos(\phi_1) = V_{rms} \cdot I_{1,rms} \cdot \cos(\phi_1) \tag{1.32}$$

The above equation shows that only the fundamental current component contributes to the real power [24]. Hence the power factor becomes:

$$P.F. = \frac{V_{rms} \cdot I_{1,rms}}{V_{rms} \cdot I_{rms}} \cdot \cos(\phi_1) \tag{1.33}$$

$$P.F. = \frac{I_{1,rms}}{I_{rms}} \cdot \cos(\phi_1) \tag{1.34}$$

Farther more the power factor can be broken down into two factors:

$\frac{I_{1,rms}}{I_{rms}}$, is the distortion factor that shows how much the utilization of the source is reduced due to the higher harmonics that do not contribute to the power, and;

$\cos(\phi_1)$, is the displacement factor and shows how much the utilization of the source is reduced due to phase shift between the voltage and fundamental current [24].

Another way of measuring the utilization of the source is called the Total Harmonic Distortion. The total harmonic distortion THD is defined as the ratio between the sums of the rms of all the higher harmonics over the fundamental:

$$THD = \sqrt{\frac{\sum_{n \neq 1} I_n^2}{I_1^2}} \tag{1.35}$$

It is always desired that the total harmonic distortion be as small as possible, and the power factor be as close to one as possible.

One of the most popular methods of power factor correction used in lighting industry today is by means of controlling the operation of a boost converter in shaping

the input current waveform to obtain a high power factor. One of the controllers used in power factor correction using boost topology is an L-6562 control chip designed by STMicroelectronics Inc [13]. This controller is designed to operate the boost converter in critical conduction mode, therefore increasing its efficiency due to zero current on switching. Figure 1.2 below shows the simplified version of the L-6562 chip principle of operation.

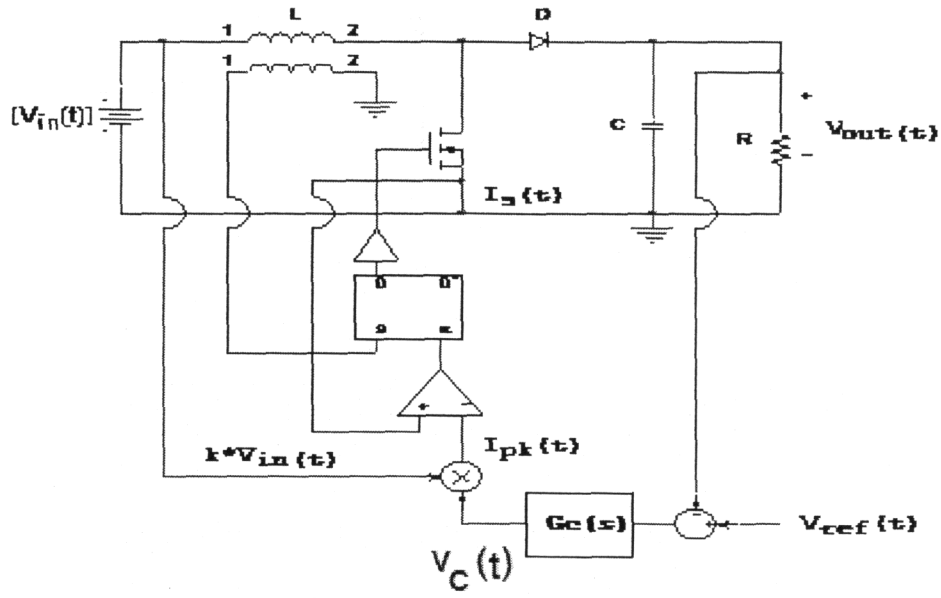

Figure 1.2: Boost Converter Controlled by an L-6562 Chip Schematic Diagram

The L-6562 controller is designed to sense the boost current and turn on the switch of the converter when the current reaches zero value. The converter current waveform is shaped to be in phase with the input voltage waveform. This is achieved by means of using a fraction of the input voltage waveform $k*|V_{in}(t)|$, and multiply it with a fraction of the output controlled voltage v_c. The resultant value of the multiplier, $I_{pk}(t)$, is then compared with the current sensed through the switch, $I_s(t)$. When the value of the

current sensed through the switch is equal to the value calculated by the L-6562 chip the chip turns off the switch. The switch stays off until the current through the inductor reaches zero value again [13]. A typical current waveform resulted from the control of a boost converter using an L-6562 Power Factor Correction (PFC) chip is shown in Figure 1.3 below.

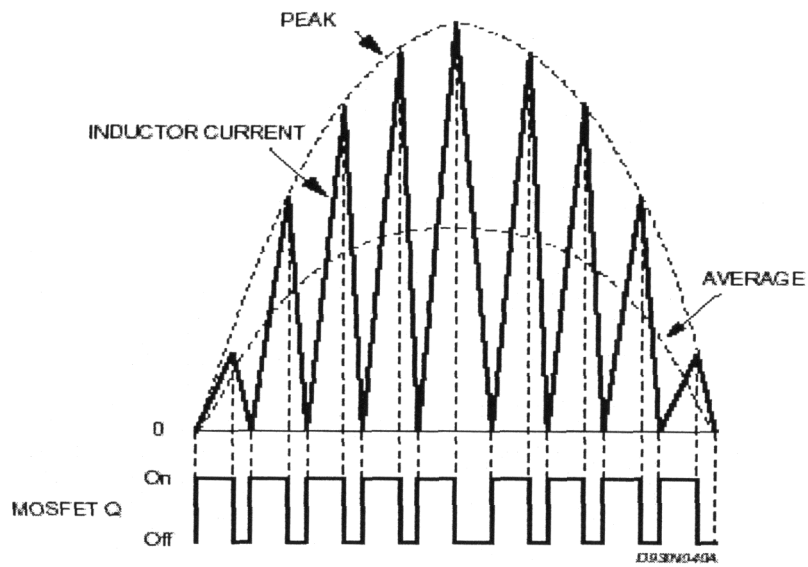

Figure 1.3: Current Waveform Generated by L-6562 Chip

The resultant input current value is the sinusoidal shaped high frequency ripple current of whose rms value is the average value of the peak seen in Figure 1.3 above. Although a high power factor (.99) can easily be achieved with this method, the input ripple needs to be eliminated such that Federal Communication Commission (FCC) restrictions for the maximum conducted noise back to the lines can be met. This is why an investigation of the methods for input as well as output ripple current cancellation is desired.

1.4 Ripple Current Cancellation Methods

The results obtained from using power converters are great, yet there is more work to be done in improving the efficiency and reliability of these devices. One of the biggest problems associated with the power converters is the noise generated due to high switching frequency. The ripple current at the output or input of a converter creates filtering difficulties, EMI noise, control issues, and output voltage ripple.

Ripple current cancellation techniques improve converter's performance by greatly reducing the ripple current at the output and input of a converter as well as reducing its size and ultimately its cost [2], [3], [11].

1.4.1 Output Ripple Current Cancellation

One way of canceling out the ripple is presented in reference [2]. In this technique the authors propose a new method that would cancel out the current ripple and leave the output DC current clean. A buck converter is used in this case to demonstrate the effect of Ripple Current Cancellation Circuit (RCCC). Figure 1.4 below represents the buck converter along with the ripple current cancellation circuit in it.

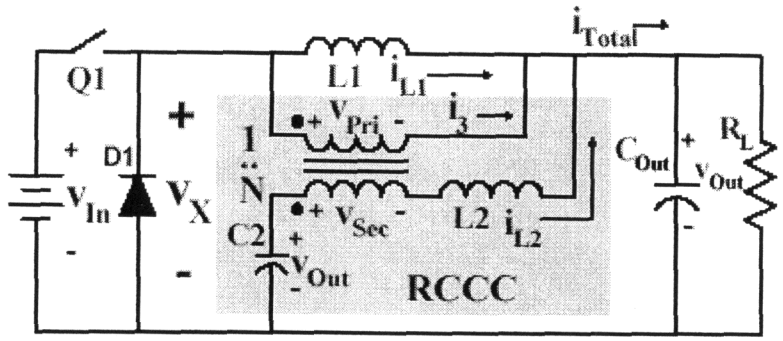

Figure 1.4: Ripple Current Cancellation Circuit on a Buck Converter

The technique presented in this paper injects current into the output that is of same magnitude but opposite in sign to the inductor AC current. Due to this injection, ideally the entire ripple current is cancelled and the remaining current is the DC required for the load. This technique allows the output filter to be designed with much smaller output capacitor and providing a cleaner control signal to the controller [2], [9]. The ripple current cancellation technique is applicable to other topologies as well such as the boost, cúk, flyback, and sepic [2]. The RCCC circuit is made up of an additional winding on the transformer along with an auxiliary inductor and a capacitor (See the grayed region of Figure 1.4). Inductor L_2 is selected such that it will give the correct ripple current and will cancel out the output ripple. Capacitor C_2 is selected so that it will bias itself to the value of the output voltage and will block any dc current from entering the circuit.

The circuit is being analyzed to obtain the values for the inductors and transformer secondary.

From Figure 1.4, the two inductors and the transformer are described by the following formulas:

$$V_{Pri} = V_x - V_{Out} = L_1 \cdot \frac{di_{L_1}}{dt} \tag{1.36}$$

$$V_{Sec} = N \cdot V_{Pri}$$

$$V_{Sec} = N \cdot L_1 \cdot \frac{di_{L_1}}{dt} \tag{1.37}$$

By KVL:

$$V_{L_2} = V_{C_2} - V_{Sec} - V_{Out} \tag{1.38}$$

Assume that V_{C2} charges up to V_{Out}:

$$V_{L_2} = V_{Out} - V_{Sec} - V_{Out} \tag{1.39}$$

$$V_{L_2} = -V_{Sec} \tag{1.40}$$

Voltage through the inductor L_2 is also derived as:

$$V_{L_2} = L_2 \cdot \frac{di_{L_2}}{dt} \tag{1.41}$$

Substituting (1.41) and (1.37) into (1.40) gives:

$$L_2 \cdot \frac{di_{L_2}}{dt} = -N \cdot L_1 \cdot \frac{di_{L_1}}{dt} \tag{1.42}$$

Current i_3 is $N/1 * i_2$ and of opposite direction due to transformers properties.

$$\frac{di_3}{dt} = -N \cdot \frac{di_{L_2}}{dt} \tag{1.43}$$

From (1.42):

$$\frac{di_{L_2}}{dt} = -N \cdot \frac{L_1}{L_2} \cdot \frac{di_{L_1}}{dt} \tag{1.44}$$

From (1.36):

$$\frac{\mathrm{d}i_{L_1}}{\mathrm{d}t} = \frac{(V_x - V_{Out})}{L_1} \tag{1.45}$$

The ripple free condition is that (1.43)+(1.44)+(1.45)=0, and that translates in:

$$\frac{di_3}{dt}+\frac{di_{L_2}}{dt}+\frac{di_{L_1}}{dt}=0 \tag{1.46}$$

Substituting (1.45) into (1.44) gives:

$$\frac{di_{L_2}}{dt}=-N\cdot\frac{(V_x-V_{Out})}{L_2} \tag{1.47}$$

Substituting (1.47) into (1.43) gives:

$$\frac{di_3}{dt}=-N^2\cdot\frac{(V_x-V_{Out})}{L_2} \tag{1.48}$$

Substituting (1.45), (1.47), and (1.48) into (1.46) gives:

$$\frac{(V_x-V_{Out})}{L_1}-N\cdot\frac{(V_x-V_{Out})}{L_2}+N^2\cdot\frac{(V_x-V_{Out})}{L_2}=0 \tag{1.49}$$

Simplifying the above equation and rearranging it gives:

$$N^2-N+\frac{L_2}{L_1}=0 \tag{1.50}$$

Equation (1.50) above is a second order equation that would give the following two solutions for N:

$$N=\frac{1}{2}\pm\sqrt{\frac{1}{4}-\frac{L_2}{L_1}} \tag{1.51}$$

From equation (1.51) above solving for L_2 gives:

$$L_2=L_1\cdot N\cdot(1-N) \tag{1.52}$$

Equation (1.52) above shows that N can take values between 0 and 1. N can take two values based on equation (1.51). It is preferable to select the smallest value of N since

this will reduce the copper losses in the RCCC circuit and will also reduce the value of the inductor L_2, as well as the ripple across capacitor C_2 [2].

Given the circuit in Figure 1.4, without the ripple current cancellation circuit, its transfer function will be solved for next.

By KCL, and using Laplace Transform:

$$\frac{V_x - V_{Out}}{s \cdot L_1} = \frac{V_{Out}}{\frac{1}{s \cdot C_{Out}}} + \frac{V_{Out}}{R_L} \tag{1.53}$$

$$\frac{V_x}{s \cdot L_1} = V_{Out} \cdot (\frac{1}{s \cdot L_1} + s \cdot C_{Out} + \frac{1}{R_L}) \tag{1.54}$$

$$V_x = V_{Out} \cdot (1 + s^2 \cdot C_{Out} \cdot L_1 + s \cdot \frac{L_1}{R_L}) \tag{1.55}$$

Solving for V_{Out} / V_x gives:

$$\frac{V_{Out}}{V_x} = \frac{1}{s^2 \cdot L_1 \cdot C_{Out} + s \cdot \frac{L_1}{R_L} + 1} \tag{1.56}$$

This equation can be rewritten as:

$$\frac{V_{Out}}{V_x} = \frac{\frac{1}{L_1 \cdot C_{Out}}}{s^2 + \frac{1}{R_L \cdot C_{Out}} \cdot s + \frac{1}{L_1 \cdot C_{Out}}} \tag{1.57}$$

This can easily be identified as a second order system of the form:

$$G(s) = \frac{\omega_n^{\,2}}{s^2 + 2 \cdot \zeta \cdot \omega_n \cdot s + \omega_n^{\,2}} \tag{1.58}$$

In the above equation the system bandwidth and damping ratios are:

$$\omega_n = \frac{1}{\sqrt{L_1 \cdot C_{Out}}}$$
$$\zeta = \frac{1}{2 \cdot R_L} \cdot \sqrt{\frac{L_1}{C_{Out}}} \tag{1.59}$$

The gain and phase of the transfer function from equation (1.58) is plotted in Figure 1.5 below.

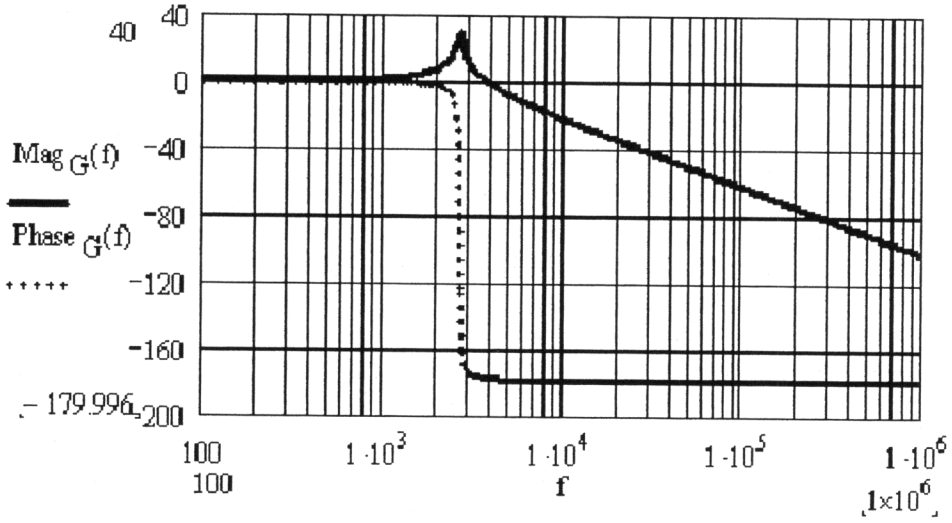

Figure 1.5: Buck Output Filter Transfer Function Plot

If the circuit in Figure 1.4 is analyzed with the ripple current cancellation circuit, then there are four storage components involved, and the transfer function can be calculated by applying the KCL on the circuit above.

$$i_{L_1} + i_3 + i_{L_2} = i_{Total} \tag{1.60}$$

The current through the inductors i_{L1}, i_{L2}, and current i_3 are derived from the basic laws of circuits as:

$$i_{L_1} = \frac{V_x - V_{Out}}{s \cdot L_1}$$

$$i_{L_2} = \frac{-N \cdot (V_x - V_{Out})}{s^2 \cdot L_2 \cdot C_2 + s \cdot C_2 \cdot R_D + 1} \cdot s \cdot C_2 \tag{1.61}$$

$$i_3 = -N \cdot i_{L_2}$$

Substituting for i_{L2}, i_3 can be expressed as:

$$i_3 = \frac{N^2 \cdot (V_x - V_{Out})}{s^2 \cdot L_2 \cdot C_2 + s \cdot C_2 \cdot R_D + 1} \cdot s \cdot C_2 \tag{1.62}$$

The total current i_{Total} is derived as:

$$i_{Total} = V_{Out} \cdot (s \cdot C_{Out} + \frac{1}{R_L}) \tag{1.63}$$

From equation (1.60), substituting with the expression for the currents obtained, the equation becomes:

$$\frac{V_x - V_{Out}}{s \cdot L_1} + \frac{-N \cdot (V_x - V_{Out})}{s^2 \cdot L_2 \cdot C_2 + s \cdot C_2 \cdot R_D + 1} \cdot s \cdot C_2 + \frac{N^2 \cdot (V_x - V_{Out})}{s^2 \cdot L_2 \cdot C_2 + s \cdot C_2 \cdot R_D + 1} \cdot s \cdot C_2 = V_{Out} \cdot (s \cdot C_{Out} + \frac{1}{R_L}) \tag{1.64}$$

Factoring out V_x-V_{Out} above gives:

$$\frac{V_x - V_{Out}}{V_{Out}} = \frac{(s \cdot C_{Out} + \frac{1}{R_L}) \cdot (s^2 \cdot L_2 \cdot C_2 + s \cdot C_2 \cdot R_D + 1) \cdot s \cdot L_1}{s^2 \cdot L_2 \cdot C_2 + s \cdot C_2 \cdot R_D + 1 + s^2 \cdot N^2 \cdot L_1 \cdot C_2 - s^2 \cdot N \cdot L_1 \cdot C_2} \tag{1.65}$$

Farther simplifying the above equation gives:

$$\frac{V_x - V_{Out}}{V_{Out}} = \frac{(s^2 \cdot L_1 \cdot C_{Out} + s \cdot \frac{L_1}{R_L}) \cdot (s^2 \cdot L_2 \cdot C_2 + s \cdot C_2 \cdot R_D + 1)}{s^2 \cdot L_2 \cdot C_2 + s \cdot C_2 \cdot R_D + 1 + s^2 \cdot N \cdot L_1 \cdot C_2 (N - 1)} \tag{1.66}$$

$$\frac{V_x - V_{Out}}{V_{Out}} = \frac{(s^2 \cdot L_1 \cdot C_{Out} + s \cdot \frac{L_1}{R_L}) \cdot (s^2 \cdot L_2 \cdot C_2 + s \cdot C_2 \cdot R_D + 1)}{s^2 \cdot L_2 \cdot C_2 + s \cdot C_2 \cdot R_D + 1 + s^2 \cdot L_1 \cdot C_2 (N^2 - N)} \tag{1.67}$$

Solving for V_x/V_{Out} gives:

$$\frac{V_x}{V_{Out}} = \frac{(s^2 \cdot L_1 \cdot C_{Out} + s \cdot \frac{L_1}{R_L}) \cdot (s^2 \cdot L_2 \cdot C_2 + s \cdot C_2 \cdot R_D + 1)}{s^2 \cdot L_2 \cdot C_2 + s \cdot C_2 \cdot R_D + 1 + s^2 \cdot L_1 \cdot C_2 (N^2 - N)} + 1 \tag{1.68}$$

$$\frac{V_x}{V_{Out}} = \frac{(s^2 \cdot L_1 \cdot C_{Out} + s \cdot \frac{L_1}{R_L}) \cdot (s^2 \cdot L_2 \cdot C_2 + s \cdot C_2 \cdot R_D + 1) + s^2 \cdot L_2 \cdot C_2 + s \cdot C_2 \cdot R_D + 1 + s^2 \cdot L_1 \cdot C_2 (N^2 - N)}{s^2 \cdot L_2 \cdot C_2 + s \cdot C_2 \cdot R_D + 1 + s^2 \cdot L_1 \cdot C_2 (N^2 - N)} \tag{1.69}$$

$$\frac{V_x}{V_{Out}} = \frac{(s^2 \cdot L_1 \cdot C_{Out} + s \cdot \frac{L_1}{R_L}) \cdot (s^2 \cdot L_2 \cdot C_2 + s \cdot C_2 \cdot R_D + 1) + s^2 \cdot L_2 \cdot C_2 + s \cdot C_2 \cdot R_D + 1 + s^2 \cdot L_1 \cdot C_2 (N^2 - N)}{s^2 \cdot L_2 \cdot C_2 + s \cdot C_2 \cdot R_D + 1 + s^2 \cdot L_1 \cdot C_2 (N^2 - N)} \tag{1.70}$$

$$\frac{V_x}{V_{Out}} = \frac{(s^2 \cdot L_1 \cdot C_{Out} + s \cdot \frac{L_1}{R_L} + 1) \cdot (s^2 \cdot L_2 \cdot C_2 + s \cdot C_2 \cdot R_D + 1) + s^2 \cdot L_1 \cdot C_2 \cdot N \cdot (N - 1)}{s^2 \cdot L_2 \cdot C_2 + s \cdot C_2 \cdot R_D + 1 + s^2 \cdot L_1 \cdot C_2 (N^2 - N)} \tag{1.71}$$

$$\frac{V_x}{V_{Out}} = \frac{(s^2 \cdot L_2 \cdot C_2 + s \cdot C_2 \cdot R_D + 1) \cdot (s^2 \cdot L_1 \cdot C_{Out} + s \cdot \frac{L_1}{R_L} + 1) + s^2 \cdot L_1 \cdot C_2 \cdot N \cdot (N - 1)}{s^2 \cdot L_2 \cdot C_2 + s \cdot C_2 \cdot R_D + 1 - s^2 \cdot L_1 \cdot C_2 \cdot N \cdot (1 - N)} \tag{1.72}$$

The condition for ripple current cancellation is:

$$L_2 = L_1 \cdot N \cdot (1 - N) \tag{1.73}$$

Based on this condition, and farther simplifying the equation (1.72), the transfer function for the system becomes:

$$\frac{V_{Out}}{V_x} = H(s) = \frac{(1 + s \cdot C_2 \cdot R_D)}{(s^2 \cdot L_1 \cdot C_{Out} + s \cdot \frac{L_1}{R_L} + 1) \cdot (s^2 \cdot L_2 \cdot C_2 + s \cdot C_2 \cdot R_D + 1) + s^2 \cdot L_1 \cdot C_2 \cdot N \cdot (1 - N)} \tag{1.74}$$

Ignoring the right hand component of the denominator in equation (1.74) due to its small contribution to the system behaviors, the remaining two second order equations in the denominator describe the system. The first equation on the left of the denominator is due to the converter output filter, and the second equation is due to the ripple current cancellation circuit (L_2-C_2). This indicates that the ripple current cancellation circuit can

be designed without affecting the operation of the conventional output filter [2]. The response of the system from (1.74) is plotted in Figure 1.6.

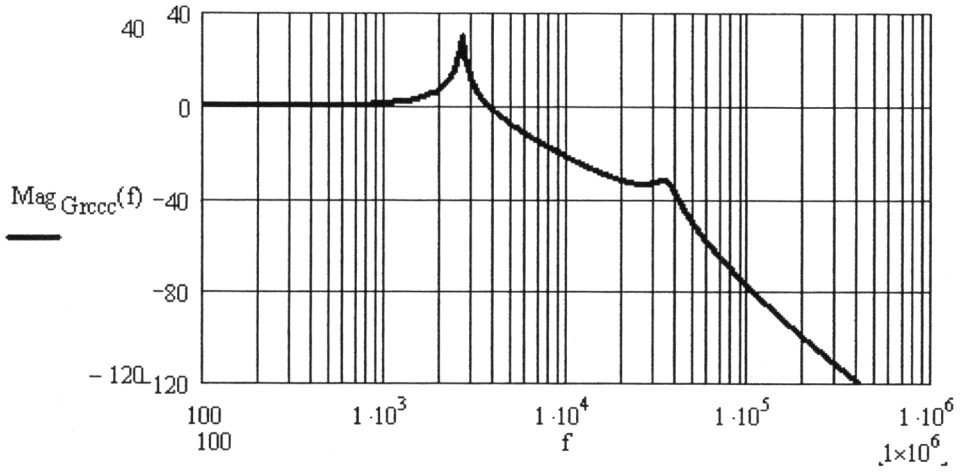

Figure 1.6: Magnitude Plot of the System Described in (1.74).

From Figure 1.6 it is noticed that the system described in (1.74) behaves as a fourth order system (rolls off at 80dB/dec). Due to R_D, the damping resistance, this prevents the peak to occur below the break frequency preventing the system stability problems. As a result the ripple current cancellation circuit reduces the ripple on the output of a buck converter without causing any stability problems, and without interfering with the output filter of the system [2].

1.4.2 Input Ripple Cancellation Method

While output ripple reduction can be achieved using the technique described above, input ripple reduction is also important. One of the input ripple reduction

techniques is described in reference [3]. This reference presents a method of input current ripple reduction based on coupled inductors technique. The method is implemented on a boost converter operating in discontinuous conduction mode. The direct result of input ripple cancellation is to reduce the converter size and weight.

Boost topology is very popular in correcting the power factor of a circuit, as well as eliminating the diode reverse recovery [13]. While achieving these benefits, the boost topology is well known of producing high input current content and electromagnetic interference effect. In order to prevent this from happening, the boost topology requires EMI filters at the input that are large in size and increase the cost of the converter.

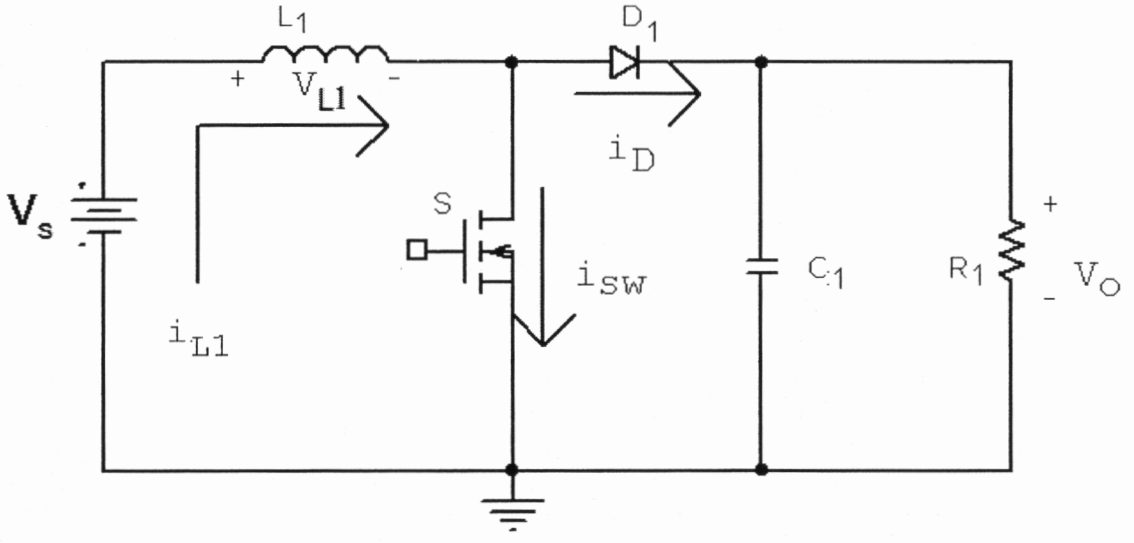

Figure 1.7: Boost Converter Topology

In boost topology pictured in Figure 1.7 above, when switch S is closed the current through L_1 is of the form:

$$i_{L_1 Stage1} = \frac{V_s}{L_1} \cdot t \tag{1.75}$$

When switch S is open, the current through L_1 is defined as:

$$i_{L_1 Stage2} = \frac{(V_s - V_o)}{L_1} \cdot (t - T_1) + I_{pk} \tag{1.76}$$

In order for the system to run in discontinuous conduction mode, the current through L_1 has to reach zero value and remain at that value for a given time. This implies that the inductor is fully de-energized.

The proposed method to reduce the input ripple is very similar to the one shown in Figure 1.4 and presented in reference [2]. This method as well has a capacitor in series with an inductor both connected in parallel with the switch S. In this topology the voltage across the capacitor is assumed to be constant.

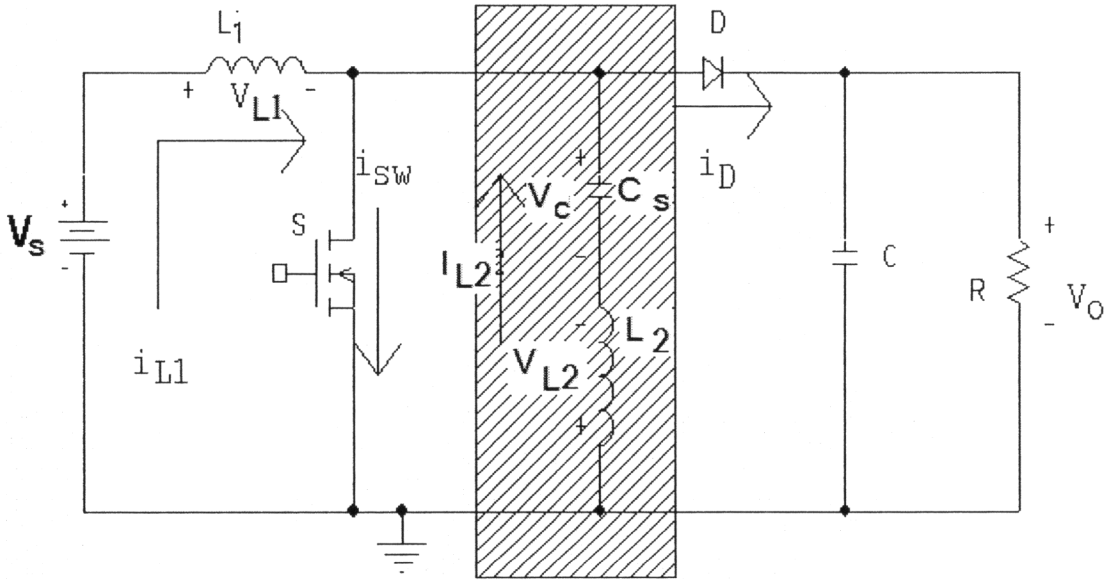

Figure 1.8: Boost Converter with Ripple Free Circuit

Figure 1.8 above shows the boost converter with its additional circuit to reduce the ripple. The additional circuit for ripple free condition is crossed selected. When the

system runs in discontinuous conduction mode, the inductor current goes through three stages over one period [3].

Stage 1, when the switch S is on, allows the current i_{L1} to increase. Voltage across L_1 is V_s, and the voltage across L_2 is V_c, which is charged up to V_s.

Stage 2 is when the switch S is off and now the inductor L_1 starts releasing energy. At this stage the voltage across L_1 is $(V_s - V_o)$ and the voltage across L_2 is $(V_c - V_o)$ which is also equal to $(V_s - V_o)$.

In stage 3, both the diode and the switch are off, and the current path is through capacitor C_s and inductor L_2. This path maintains the capacitor C_s charged to V_s therefore making the voltage across the two inductors to be zero.

The voltage across the two inductors, L_1 and L_2 is the same for all three stages discussed above. This allows the inductors to be built on the same core, therefore reducing the amount of material needed for built-up [3].

If both inductors are built on the same core, their voltage is described by the following formulas:

$$V_{L_1} = L_1 \cdot \frac{di_{L_1}}{dt} + L_M \cdot \frac{di_{L_2}}{dt} \tag{1.78}$$

$$V_{L_2} = L_2 \cdot \frac{di_{L_2}}{dt} + L_M \cdot \frac{di_{L_1}}{dt} \tag{1.79}$$

Where L_M is the mutual inductance and is defined as:

$$L_M = k \cdot \sqrt{L_1 \cdot L_2} \tag{1.80}$$

When the switch is on the input-current ripple-free condition is that $L_M = L_2$.

When the switch is off (stage 2), the ripple-free condition is derived to be again $L_M = L_2$.

When in stage 3, the current is zero for L_1 and L_2. Therefore the ripple-free condition becomes:

$$L_M = L_2$$

$$k \cdot \sqrt{L_1 \cdot L_2} = L_2$$

$$k = \sqrt{\frac{L_2}{L_1}} \tag{1.81}$$

Equation (1.81) is the ripple free condition for the topology described in reference [3]. This technique allows the circuit to have good EMI performance.

While second technique is designed to provide ripple free condition at the input of the converter, the first technique shows how to reduce the ripple output on a buck converter. Both techniques are made out of the same circuit components such us capacitor and inductor. While the second technique provides ripple free based on equation (1.81) which implies mutual inductance, first technique provides "zero ripple" by means of inductor selection based on equation (1.52).

1.5 EMI Filtering

Switch Mode Power Supplies (SMPS) are frequently used in today's technology. One of the reasons why these converters have become so popular is because they run at very high efficiency therefore eliminating losses. Another important factor in making the SMPS popular nowadays is their size, which is considerably reduced due to high frequency operation.

While the benefits of using the SMPS are obvious from the above statements, this method of power supply comes with its disadvantages. One of the disadvantages of SMPS is that they are a source of noise that is reflected back to the supply lines and radiated to other electronic products in the vicinity. The cause of this noise is due to the switching components that makeup the power supply. These switching components are used to transfer the desired energy to the load. Due to high frequency operation of these components and the high potential across these switching devices noise is generated. Regulatory agencies like FCC provide standards of how much noise can be allowed to reflect back into the lines. Due to these limitations the noise is being suppressed to meet the regulatory agencies requirements by means of shielding for radiated, and filtering for conducted noise [1].

Conducted type noise will be dealt with in this thesis. The conducted noise is measured using Line Impedance Stabilization Network (LISN), a system that looks like the schematic shown in Figure 1.9 below [30].

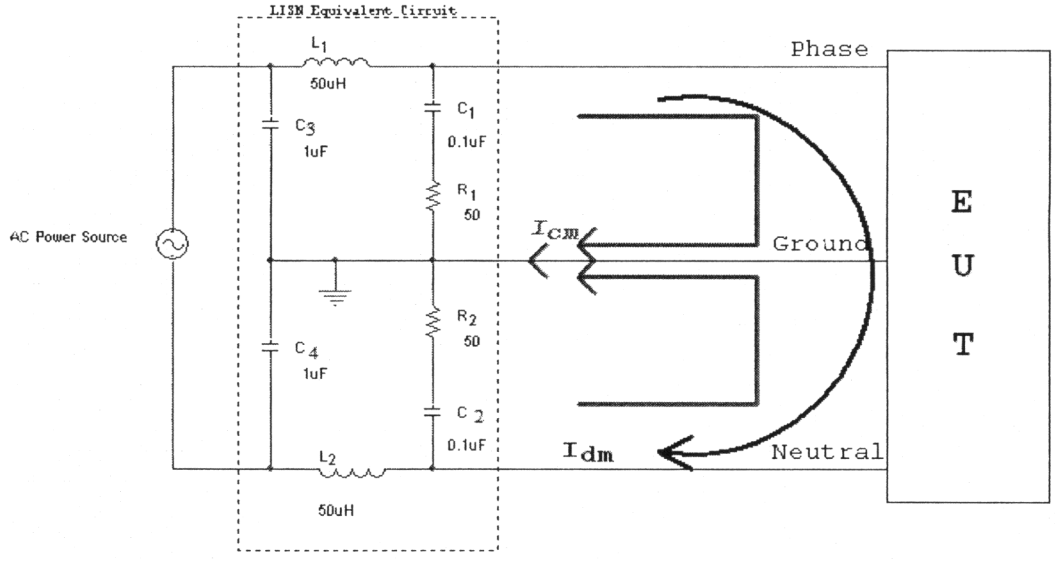

Figure 1.9: LISN Representation

System in Figure 1.9 above represents a functional equivalent circuit of the LISN. The noise level coming from the equipment under test (EUT) is measured across the two resistors R_1 and R_2. At low frequencies, the circuit in Figure 1.9 behaves as it would have the capacitors open and the inductors shorted, therefore the low frequency noise would be reflected back to the line through the L_1 and L_2 inductors [26], [27], [28], [30]. At high frequencies the inductors become open and the capacitors shorted therefore the noise level is passing through the 50 Ohms resistors. The high frequency schematic of the LISN is shown in Figure 1.10 below.

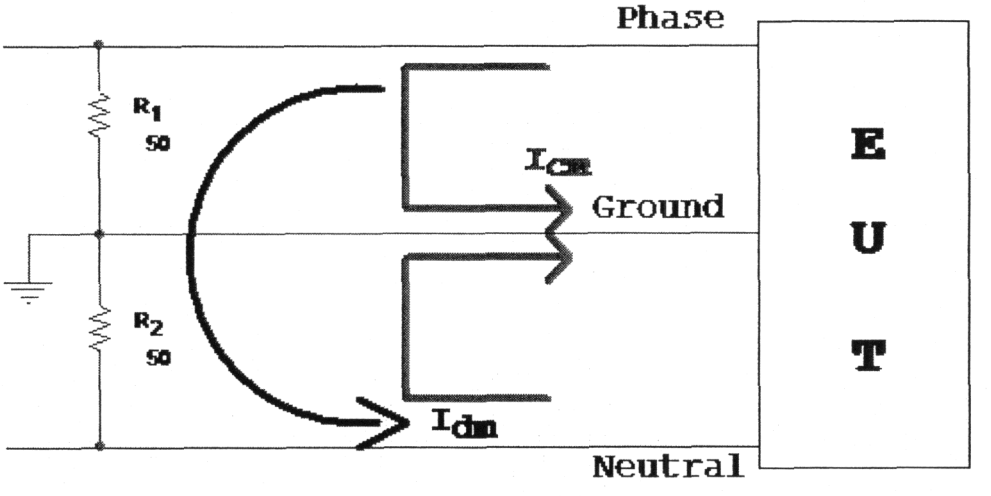

Figure 1.10: High Frequency Schematic Representation of the LISN Circuit

One of the 50 Ohms resistors is located in the spectrum analyzer that collects the noise level and plots the noise across a range of frequencies. The other resistor is added to the LISN as a BNC 50 Ohm impedance connector. The spectrum analyzer will run in most cases over a range of frequencies from 9kHz to 30MHz for European regulatory

agencies, and 450kHz to 30MHz for the U.S. regulatory agencies. The magnitude of the noise level will be plotted in frequency domain over the frequency range established by the regulatory agencies. Due to significant differences in noise level recorded, the voltage level is plotted in dBμV (decibels micro volts) and is calculated after the following formula:

$$dB\mu V = 20 \cdot \log(\frac{V_R}{1 \cdot \mu V}), \tag{1.82}$$

Where V_R is the voltage across one of the resistors in the LISN circuit [30]. By plotting the values recorded by the Spectrum Analyzer using formula (1.82), this allows a wide range of values to be seen on the same plot. For example, by using the above formula a voltage value of 10 microvolts gives 20dBμV while 10,000 microvolts gives 80dBμV, and 1Volt gives 120dBμV.

The noise level seen across one of the resistors of the LISN is the high frequency current signal reflected back to the line. Due to the LISN circuit, the path of the high frequency current flows through the two LISN resistors and this allows the Spectrum Analyzer to read the noise level over the high frequency range [26], [30]. It is mandatory that the electronic systems produced by any company around the world to be able to pass the requirements of the regulatory agencies where the product is being sold. As the specifications for the maximum allowed level of high frequency current becomes smaller and smaller, the electronics manufacturers fight harder and harder to make an electronic system pass these requirements. In designing the printed circuit boards of the electronic products, the manufacturer is forced to follow special design rules that would prevent the generation of the high frequency noise. Even when the special design rules are closely

followed, the high frequency noise is being generated and reflected back to the line. Many times this noise level is higher than the regulatory agencies maximum allowable level. Therefore the electronics manufacturers are forced to come up with additional filters that would suppress the noise level to a level that would be acceptable by the regulatory agencies. Figure 1.11 below shows some of the regulatory agencies requirements for the maximum allowed noise reflected back to the line [26].

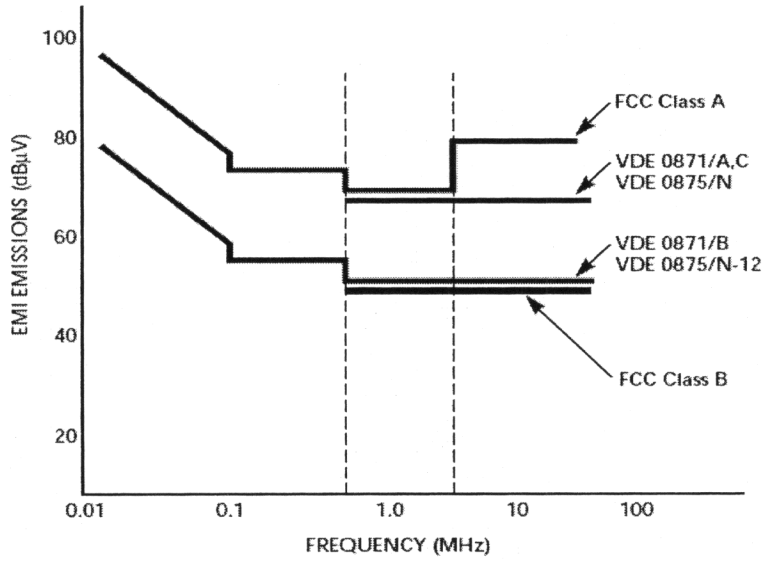

Figure 1.11: Regulatory Agencies Maximum Allowable Noise Level

The current reflected back to the lines generates the noise measured on one of the two LISN resistors. This noise comes in two flavors. Differential mode noise, marked as I_{dm}, is the equal flow of current that flows in opposite direction along a pair of conductors (Line and Neutral). Common mode noise, labeled as I_{cm}, flows in the same direction in a pair of conductors like the line and neutral seen in Figure 1.9 above and returns into the

ground path. Differential mode current is caused due to the circuit design methods and can be simulated using circuit ideal elements [30]. The common mode currents do not appear on the circuit schematic diagram and are caused by the parasitic inductors and capacitors that form due to circuit layout. The regulatory agencies requirements make a system with only picofarads stray capacitance, and nanohenries stray inductance to produce a common mode noise with a magnitude above the limit [30].

Common mode noise can be measured by clamping the phase and neutral wires together with a magnetic current probe like it is shown in Figure 1.12 below.

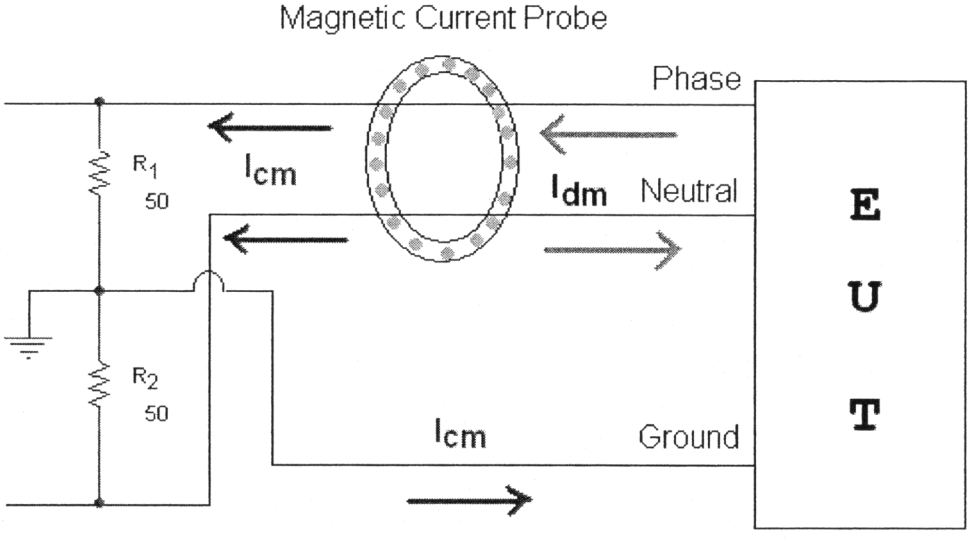

Figure 1.12: Common Mode Current Measurement

The differential mode current flows through phase and returns into the neutral path such that the magnetic field generated by this current is cancelled out. The common mode current flows in the same direction on both phase and neutral wires and returns to

ground. Therefore the magnetic field generated into the current probe will be of pure common mode type [30].

The differential mode current can also be measured by applying the same canceling technique used in Figure 1.12, but in this case one of the wires will loop around the outer wall of the magnetic current probe first and then return back through it, so that the magnetic field generated by the common mode current will be equal in magnitude but of opposite direction and the total magnetic flux left will be that of the differential mode current.

Filters are used to reduce the magnitude of the common as well as the differential mode currents reflected back to the line. The performance of a filter is measured based on the attenuation, which is the ratio of noise voltage at the load with and without the filter, expressed in decibels. The filter is designed in such a way that it will produce an impedance mismatch at the frequencies where the magnitude of the noise is above the required limits.

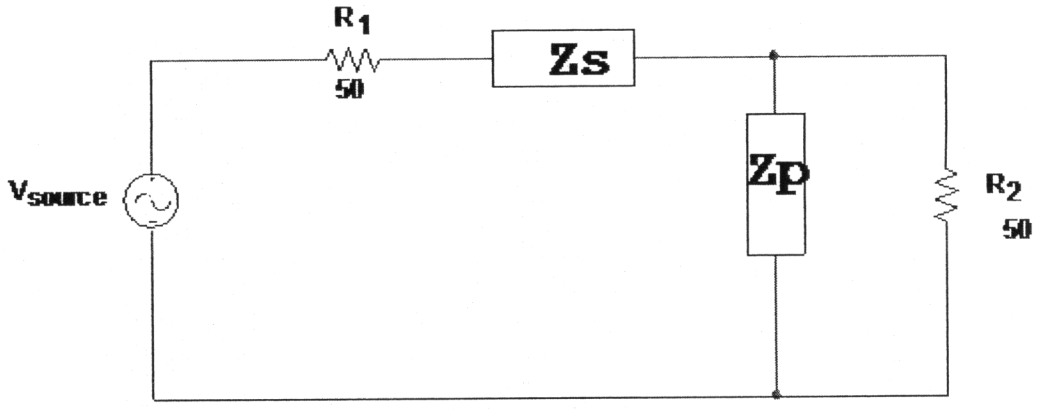

Figure 1.13: Filter Representation

Figure 1.13 represents a typical filter that is applied between the source of noise V_{source}, and LISN resistor R_2. The maximum power of the signal generated from the source is transmitted to the LISN resistor R_2 when the magnitude of the source and the load impedance are equal. The filter introduced between the source and load will have the impedance much larger or much smaller than the source of the LISN load R_2. In Figure 1.13, Z_S is typically an inductor with impedance much greater than the source (R_1) at the frequencies of concern. The parallel impedance Z_P is in general a capacitor that would provide low impedance at frequencies of concern and therefore provide a close path for the high frequency current, other than through LISN resistor R_2. A typical schematic representation of traditional filter used for Electro-Magnetic Interference (EMI) suppression is shown in Figure 1.14 [26], [27], [30].

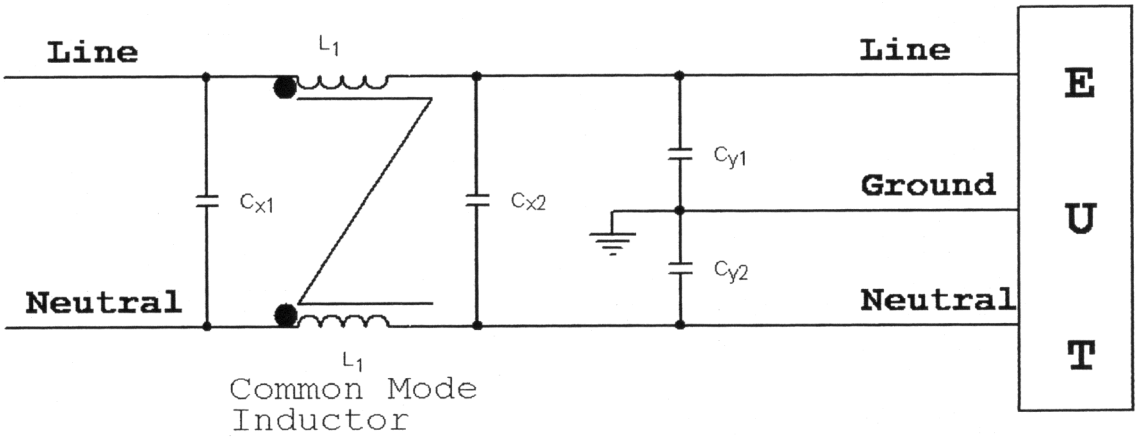

Figure 1.14: A Typical Traditional EMI Filter Configuration

The EMI filter shown in Figure 1.14 above is made out of four capacitors and one common mode inductor. The caps used for the input filter should meet certain specifications due to regulatory agencies regulations. The X type capacitors should be

the special class X suppression capacitors and their specific design should be able to stand very high pulse voltages that can be caused by lightning in overhead cables or switching surges in neighboring equipment. Based on the peak pulse voltage they can handle, the X type capacitors are divided into three categories according to EN-132400 European standards. The X_1 type can handle a peak voltage from 2.5 kV and up to 4kV. The X_2 type caps can handle a peak voltage up to 2.5kV and the X_3 caps can handle a peak pulse voltage of up to 1.2kV. The X type capacitors are used in places where their failure will not result in an electrical shock. The Y type capacitors are used in places where their failure could result in a dangerous electrical shock. Their mechanical and electrical characteristics prevent them from failing short-circuit. The value of these capacitors is limited based on the different safety regulations. The specifications for domestic and industrial applications of the maximum allowed ground leakage current at 120V line input is 5 milliamps and therefore the maximum allowed Y-cap value is limited by this factor. The Y type capacitors are used to bypass the high frequency noise from flowing into the earth. They also ensure that the amplitude of the common mode noise will be equal on both lines (Line and Neutral) [26], [27], [28], [30].

The phasing of the common mode inductor prevents the saturation of the core at low frequencies (50-60 Hz) and due to its arrangement the inductance at these frequencies cancels out [26], [27], [30]. The common mode inductor can be represented as it is shown in Figure 1.15 below.

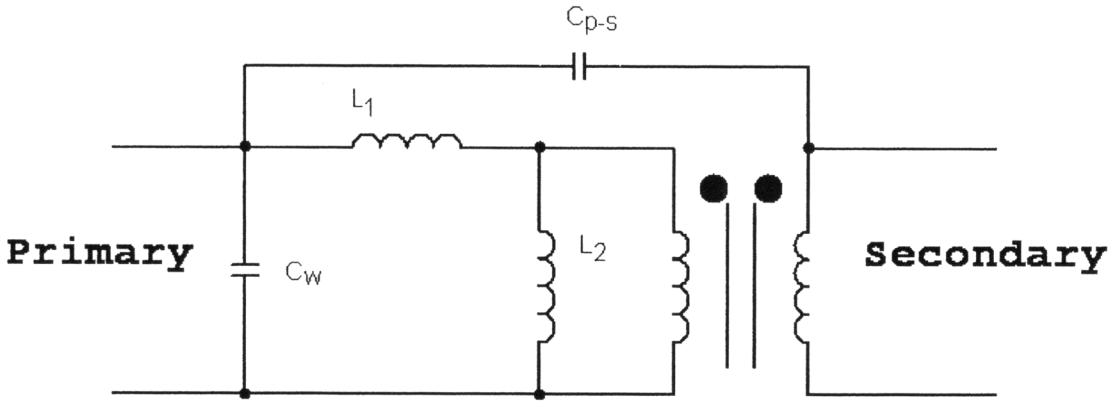

Figure 1.15: Common Mode Inductor Representation

The common mode inductor is made out of an ideal transformer and energy storing components such as C_w – Winding Capacitance, C_{p-s} – Capacitance between the primary and the secondary winding, L_1 – Leakage Inductance measured with the secondary winding shorted, and L_2 – Mutual Inductance (energy stored in the core). The ideal transformer turns ratio is typically 1 to 1 for the common mode inductors. This arrangement allows the high frequency noise to be attenuated before it reaches the LISN 50 Ohms resistance. By using the arrangement shown in Figure 1.14 the filter attenuates both the common and differential mode noise. Common mode noise filter derived from Figure 1.15 is shown in Figure 1.16 below [30].

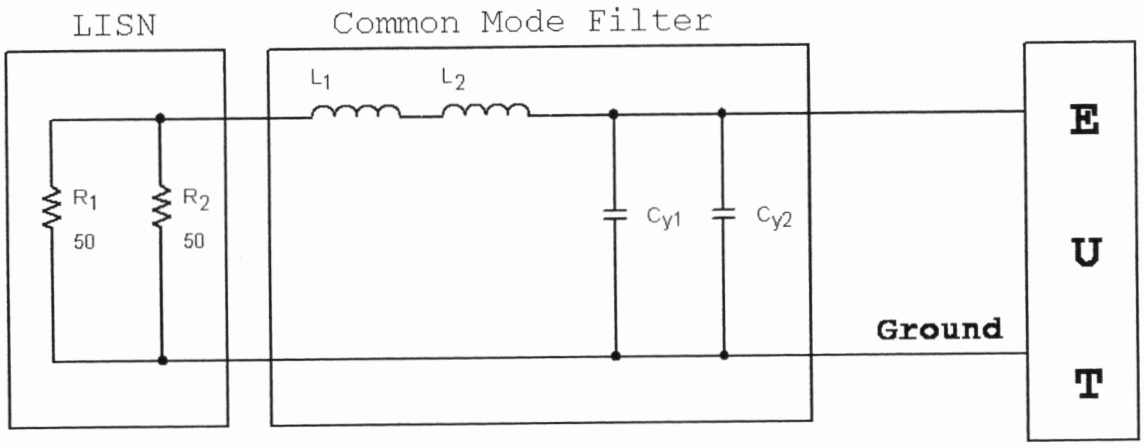

Figure 1.16: Common Mode Filter Representation

The Y type capacitors are adding together for the common mode filter, and the mutual as well as leakage inductance are both contributing to the noise attenuation. Differential mode filter derived from Figure 1.15 is shown in Figure 1.17 below [30].

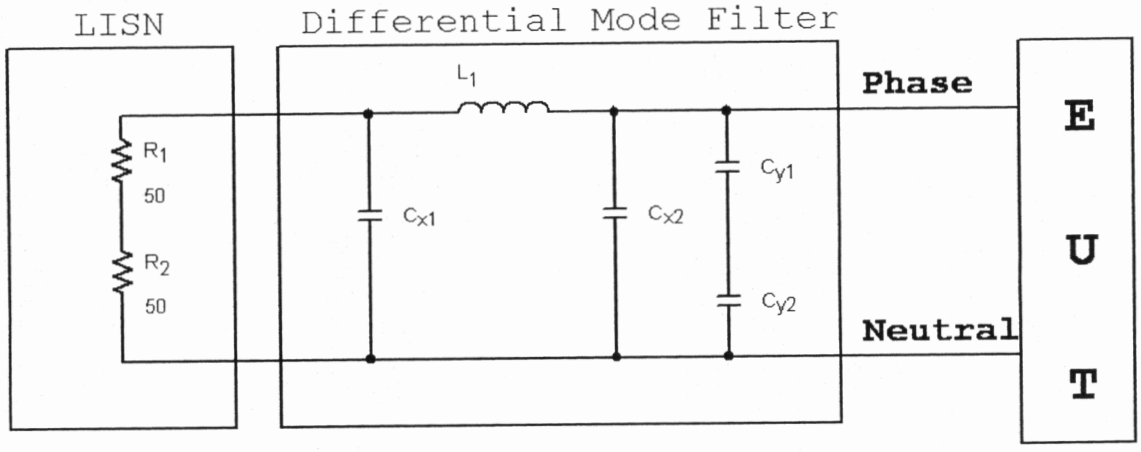

Figure 1.17: Differential Mode Filter Representation

For the differential mode filter both Y type capacitors add to the C_{x2}, while only the leakage inductance is part of the filter.

The problem with the traditional filter from Figure 1.15 is that it contributes significantly to the cost of the overall system, and adds considerable weight due to the common mode inductor. For systems where the predominant noise generated back to the line is of differential type, a new filter topology is proposed.

1.6 Motivation and Objectives

In this thesis the analysis, design, and implementation of the ripple current cancellation circuit on a boost power factor correction converter is presented. A 150-Watt boost PFC converter is designed based on the L-6562 control chip from STMicroelectronics Inc. Then the RCCC circuit is implemented on the boost such that the input ripple current is drastically reduced. A simulation of the 150-Watt boost PFC with RCCC is implemented. The results obtained from the simulation model are compared with the results obtained from the bench model implemented in the lab. A cost comparison between the RCCC method and the traditional filtering method is presented along with the EMI results obtained from the bench model.

Chapter 2 describes the design of the critical conduction mode boost PFC controlled by the L-6562 chip from STMicroelectronics. In addition, this chapter presents the analysis and implementation of the RCCC method on the 150-Watt boost PFC operated in critical conduction mode.

Chapter 3 presents the simulation and experimental results of the 150-Watt boost PFC with RCCC implemented on it.

Chapter 4 presents the comparison between a traditional filtering method and the RCCC method applied on the 150-Watt boost PFC, and cost analysis of both methods.

The thesis conclusion is described in chapter 5 with a short summary of the work presented in this thesis along with possible future work related to this topic.

CHAPTER II

RIPPLE CURRENT CANCELLATION CIRCUIT

2.1 Introduction

The use of the ripple current cancellation circuit has been investigated on a buck converter by the researchers at GE Global Research Center [2]. In this study it is desired to investigate the ripple current cancellation method at the input of a boost converter running in critical conduction mode. To provide a full understanding of this topology, the design of a 150-Watt boost power factor correction circuit is described next. Then the ripple current cancellation method is being discussed along with its application to the boost power factor correction circuit.

2.2 Design of a 150-Watt Universal Input Boost PFC Circuit

A universal 150-Watt boost PFC is to be design and controlled using the L-6562 IC chip. The boost is designed such that it can be run from a wide input range starting from 120 Vac up to 277 Vac. This wide range will make the input be practically universal, and would satisfy the input requirements of the European as well as North American standards. To be more accurate, the range of the input voltage is extended to be between 108 and 305 Volts, due to the power lines voltage variations. Since the topology used is Boost, this means that the voltage obtained at the output would be of greater or equal value with the input bus voltage [1]. Taking the maximum of the input range voltage $V_{inMax(rms)}$=305V this gives a maximum magnitude of:

$$V_{inMax} = \sqrt{2} \cdot V_{inMax(rms)} = 431.3V \tag{2.1}$$

Based on the V_{inMax} obtained above, a value of 450 Volts at the output of the boost PFC converter is desired. This would give an output resistance of:

$$R_{out} = \frac{V_{out}^{2}}{P_{out}} = 1350\Omega \tag{2.2}$$

Based on the design requirements obtained, the output current value will be:

$$I_{out} = \frac{V_{out}}{R_{out}} = 333mA \tag{2.3}$$

Based on the above calculations the following design requirements were set to build the 150-Watt boost PFC.

Table I: Summary of the Design Requirements

Design Requirements for a Universal input 150W Boost PFC								
Input			*Efficiency*	*Output*				*Minimum Frequency*
Voltage		*Power*		*Voltage*	*Power*	*Load*		
Min	Max					Current	Resistance	
108 V	305 V	166.7 W	90%	450 V	150 W	0.333 A	1350 Ohms	25kHz

Once these requirements are specified, the converter design can be started. The calculations were done based on the AN-966 application note from STMicroelectronics [13]. A Mathcad file was developed for designing the 150-Watt PFC and is available for viewing in Appendix B.

The peak current through the inductor is calculated as follows:

$$I_{Lpk} = 2 \cdot \sqrt{2} \cdot \frac{P_{in}}{V_{inMin(rms)}} = 4.37A \tag{2.4}$$

The converter is designed to run at variable frequency due to the L-6562 chip, but the minimum frequency of the switching has to be set above 14 kHz due to the L-6562 chip design. Another factor to be considered when deciding the minimum operating frequency of the boost converter is the audio signal that the human ear can hear. It is a design practice that in order to eliminate the audible noise caused by the switching devices as much as possible, the converter will be designed to run above 20 kHz. In this application the minimum switching frequency is set for 25 kHz.

Based on the assumptions made and the design requirements the inductor value can be calculated according to the following formula:

$$L = \frac{V_{inrmsMax}^{\ 2} \cdot (V_{out} - \sqrt{2} \cdot V_{inrmsMax})}{2 \cdot f_{sw} \cdot P_{in} \cdot V_{out}} \tag{2.5}$$

Substituting with the values obtained above, the inductor value turns out to be L=463μH.

Now that the value of the inductor is known, selecting the core material as well as the wire type and calculating the number of turns and the air gap becomes possible. The method used for selecting the core type is called the Core Geometry method shorted as K_g [22]. Based on this method the K_g is calculated from the following two formulas:

$$K_g = \frac{\rho \cdot (L \cdot I_{Lpk}{}^2)^2}{B_{\max} \cdot P_{cu}} \tag{2.6}$$

$$K_g = k \cdot \frac{W_a \cdot s^2}{t} \tag{2.7}$$

Where:

ρ - resistivity of the conductor used in windings (ρ_{copper}=1.724*10^(-6) Ω*cm)

B_{max} – maximum flux density of the material

P_{cu} – copper losses that are estimated at ~1% of input power

W_a – winding area of the bobbin

s – cross sectional area of the core

t – bobbin average length of turns.

Based on the K_g method the closest value obtained was with a core type E25/13/11 from Ferroxcube Inc. Using the K_g method will allow the selection of core that would best utilize the available winding area while ensuring the minimum core size that would satisfy the given requirements [22].

Once the core type and bobbin is selected, the winding of turns becomes possible. The total number of turns needed to get the desired inductance is obtained from the following formula:

$$N = \frac{L \cdot I_{pk}}{B_{\max} \cdot s} \tag{2.8}$$

The total number of turns required for the 150-Watt Boost converter was calculated at 87 turns.

The next step is to determine the wire type and it's cross sectional area. Because of high switching frequency multiple Litz wire-type is being selected to reduce the copper losses as well as the skin and proximity effect.

The cross sectional area of the wire is determined based on the following formula:

$$A_w = k \cdot \frac{W_a}{N} \tag{2.9}$$

Where k is the winding factor (typically between .3 and .6).

Once the cross sectional area of the wire is found, the diameter of the wire is calculated as:

$$D = \frac{1}{2} \cdot \sqrt{\frac{A_w}{\pi}} \tag{2.10}$$

The diameter of the wire allows the designer to select the type of wire that would fit in the window area available. For the 150-Watt Boost converter an AWG-38 Litz wire with 15 strands was selected.

The winding of the transformer was performed on a special winding machine. It is important while winding, that the tension in the wire is controlled so it will not exceed a certain limit that would damage the wire, while making sure that each layer is properly wound and aligned on the bobbin. Between each layer of windings a layer of insulated tape was wrapped around farther more protecting the windings from shorting each other in case of bare wire overlapping.

Once completed, the two ends of the wire are terminated into two pins that would allow the connection of the inductor to the boost circuit.

Next step in the design is the grinding of the core to provide an air gap and finally set the actual value of the inductor. The air gap length, l_g can be estimated based on the following formula:

$$l_g = \frac{\mu_0 \cdot N^2 \cdot s}{L} \tag{2.11}$$

Where μ_0 is the permeability of free space ($\mu_0 = 4x10^{-7}H / m$). The value obtained can give a rough estimate of what the actual air gap length would be.

The grinding is being performed typically on the middle leg of the "E" shaped core, since the cross sectional area is the greatest at that point. It is recommended to grind both sides of the E core, to uniformly distribute the fringing effect due to the magnetic flux lines in the air gap.

For the 150-Watt boost inductor, two extra windings were added, one for the zero current detector needed for L-6562 chip to sense the zero current and supply the L-6562 chip, and another for the ripple current cancellation circuit (RCCC).

The switching device of the boost converter is typically selected so that it would withstand the current and voltage characteristics of the system, while making sure that it can switch at much higher rate than what the maximum switching frequency is. Today's technology provides a wide range of MOSFETs that can switch at very high frequencies with minimum amount of losses during on time and minimum transition time. For the 150-Watt converter of this application a MOSFET type STP12NM50 N-Channel 500 Volts, 0.3 Ohms, and 12 Amps current from STMicroelectronics satisfied the design requirements.

The boost diode is typically selected based on the current it can stand while forward biasing, and the maximum voltage potential from the anode to the cathode of the

diode while it is reverse biasing. For the boost design an SF-5406 ultra fast Avalanche sinterglass recovery diode from Vishay Semiconductors was selected. This diode withstands up to 600 Volts and an average current of 3 Amps based on its datasheet. The input capacitor was selected to stand the maximum voltage seen at the input and its value was as small as 0.22uF based on the AN-966 application. The output capacitor has to stand a 450 Volts for this application, and its value is selected such that the output voltage ripple will be limited to the maximum allowed [13]. For this application two series capacitors of 68uF value and a maximum voltage of 350 Volts each were added at the output of the boost.

The controller was designed based on the application U-1089 from STMicroelectronics. A Mathcad file with the calculations of this controller is presented in Appendix C.

2.3 Design of RCCC on the Boost Input

The Boost converter described above was designed such that the ripple current cancellation technique can be implemented and its performance analyzed. The simplified diagram of the boost converter with the RCCC implemented on it is shown in Figure 2.1 below.

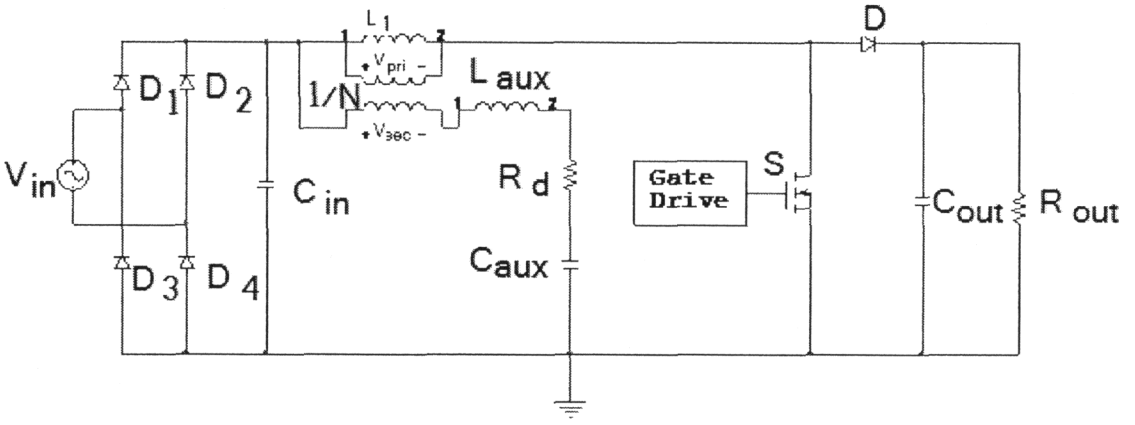

Figure 2.1: Boost Converter with the RCCC Circuit Implemented on it.

According to this method as applied for the boost the input current seen by the line is the sum of the current going through the boost inductor L_{boost}, and the current going through the RCCC and therefore through inductor L_{aux}. Due to the additional winding on the same core with the inductor L_{boost}, the current seen on the secondary of the transformer is the ripple current going through the L_{boost}. Adding the currents together results in the ripple cancellation and the remaining current will be the average current generated by the gate drive.

The auxiliary inductor of the RCCC circuit L_{aux}, is selected such that the current would follow closely with the boost inductor current and its value would be determined by the following formula:

$$L_{aux} = N \cdot (1 - N) \cdot L_{Boost} \tag{2.12}$$

N is the ratio of the number of turns of the auxiliary over primary winding of the transformer.

The auxiliary capacitor C_{aux}, value is selected typically between 0.2 and 2 μF and can be estimated based on the formula:

$$C_{aux} = \frac{1}{4 \cdot \pi \cdot L_{aux} \cdot f_{ripple} \cdot f_{BW}} \tag{2.13}$$

Where f_{ripple} is the converter switching frequency, and f_{BW} is a value that is higher than the closed-loop bandwidth and can be estimated as the geometric mean between the bandwidth of the power converter and the converter ripple frequency [2].

The additional resistor R_D seen in the RCCC is required to minimize the peaking from the L_{aux} and C_{aux} pole-pair. Because of the equivalent resistance of both L_{aux} and C_{aux}, this resistor is practically not required but it will be as part of the two storage devices. This resistor prevents the system to interfere with the bandwidth of the controller and avoids instability problems caused by 0dB crossing of the peak [2]. The quality factor that is associated with the damping resistance is defined as:

$$q = \frac{\sqrt{\frac{L_{aux}}{C_{aux}}}}{R_D} \tag{2.14}$$

The value of R_D runs typically small and its estimated value can be calculated after the following formula:

$$R_D = K \cdot \sqrt{\frac{L_{aux}}{C_{aux}}} \tag{2.15}$$

K is the quality factor, which typically is desired to be from 0.1 to 0.3. [2]

With this in mind, the RCCC of the 150-Watt boost converter got the following values:

L_{aux}=47μH C_{aux}=1μF R_D=0.4Ω.

2.4 RCCC Principle of Operation

The principle of operation of the ripple current cancellation circuit for the boost converter is similar with the buck converter. A schematic of the ripple cancellation circuit being implemented on a boost converter is shown in Figure 2.2 below.

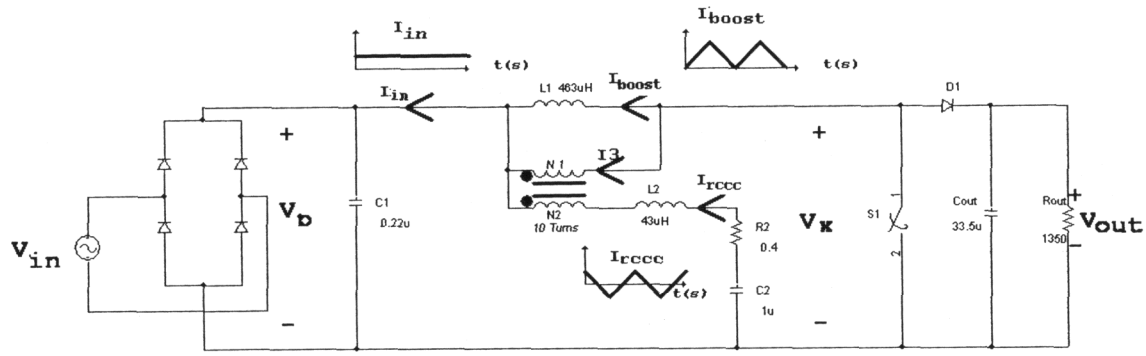

Figure 2.2: RCCC Schematics

Figure 2.2 above shows the schematic representation of the ripple cancellation circuit implemented on a boost converter. Since the value of the input capacitor C_1 is small, this allows the minimum amount of voltage to be stored in the capacitor and from this it can be assumed that the same voltage seen at the line input and rectified by the diode bridge is applied on the input capacitor C_1. The value of the input capacitor is desired to be as small as possible such that the voltage seen by the L-6562 control chip from the input has a perfect absolute value of the input sinusoid [13]. This allows the L-6562 chip to control the boost in critical conduction mode and provide an excellent power factor correction. The boost controller works great without the input capacitor, but this allows the high frequency noise to be bypassed through the diode bridge across the input lines and this causes high EMI noise. By keeping a small value capacitor at the input,

this prevents some of the high frequency noise to be sent to the line and deteriorating very little the power factor correction of the L-6562 control chip. The voltage V_x in Figure 2.2 above is the voltage across the switch MOSFET of the boost.

The current flowing through the boost over one switching period is represented in Figure 2.3 below.

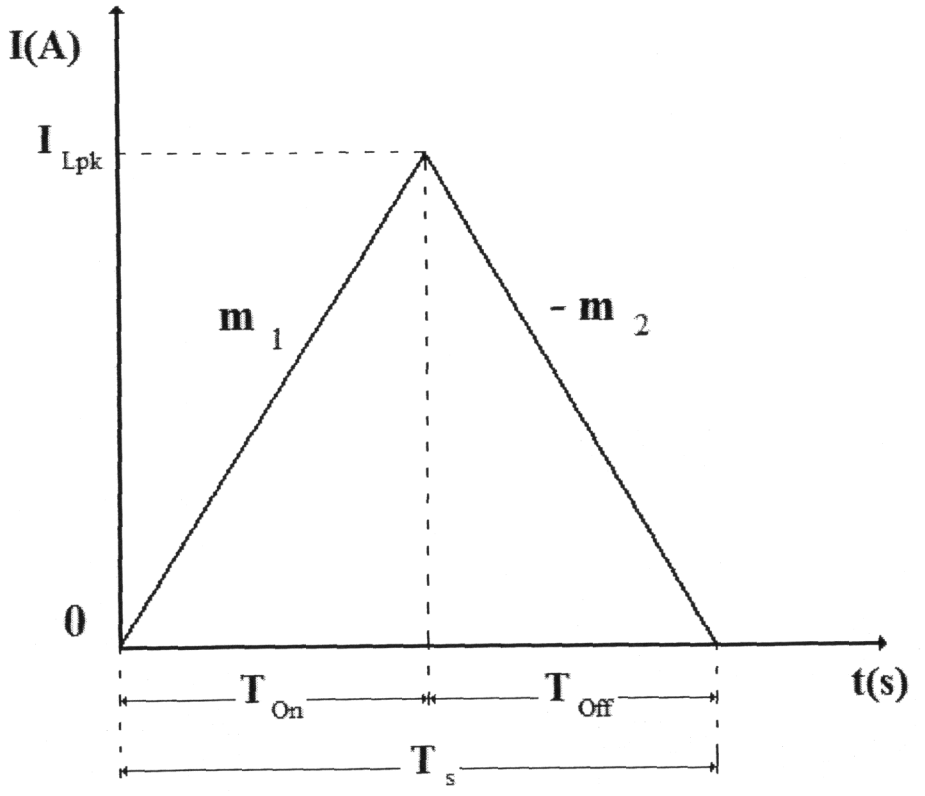

Figure 2.3: Boost Current Waveform over one Period

When the switch is closed, the value of the voltage V_x is zero (short circuit). Then the voltage applied across the inductor L_1 becomes:

$$V_{L\_boost\_Sw\_closed} = V_{in} = L_1 \cdot \frac{\Delta i_{s\_closed}}{\Delta t_{s\_closed}} \tag{2.16}$$

When switch is closed the change in current occurs over the period T_{On} and the current changes from zero to I_{Lpk}:

$$\begin{aligned} \Delta i_{s\_closed} &= I_{Lpk} \\ \Delta t_{s\_closed} &= T_{On} \end{aligned} \tag{2.17}$$

The peak current, I_{Lpk}, through the inductor, based on the L-6562 chip design is defined as:

$$I_{Lpk}(t) = k \cdot V_b(t) \cdot V_{comp}(t) \tag{2.18}$$

Where k represents scaled down factor of the input voltage, $V_b(t)$ is the absolute value of the input voltage due to bridge rectifier, and $V_{comp}(t)$ is the feedback of the controlled and stepped down output voltage. Based on the above formula the peak of the input current takes the shape of the input voltage, which makes the L-6562 chip give a power factor close to 1.

The on time can be defined as:

$$T_{On}(t) = L_1 \cdot \frac{I_{Lpk}(t)}{V_{in}(t)} \tag{2.19}$$

Then the inductor current while the switch is closed becomes:

$$i_{L_1\_Sw\_Closed}(t_{s1}) = \frac{V_b(t)}{L_1} \cdot t_{s1} \tag{2.20}$$

Where t_{s1} is defined over the range of: $t_{s1} \in (0 : T_{On}]$.

Equation (2.20) above is a first order equation that has the vertical axis intercept at the origin, and its slope is defined as:

$$m_1 = \frac{V_{b(t)}}{L_1} \tag{2.21}.$$

Once the controller of L-6562 chip senses that the peak current value through the inductor has been reached, the switch is turned off immediately and the boost diode is conducting.

When the switch is open, the voltage V_x is the output voltage V_{out} of the boost desired to be 450V (assuming there are no losses across the boost diode).

$$V_{x\_Sopen} = V_{Out} = 450V \tag{2.22}$$

The voltage across the inductor when the switch is open becomes:

$$V_{L\_boost\_Sw\_Open} = V_{in} - V_{Out} = L_1 \cdot \frac{\Delta i_{s\_open}}{\Delta t_{s\_open}} \tag{2.23}$$

The change in current when the boost switch is open based on Figure 2.3 above is:

$$\begin{aligned} \Delta i_{s\_open} &= -I_{Lpk} \\ \Delta t_{s\_open} &= T_{Off} \end{aligned} \tag{2.24}$$

The off time can be defined as:

$$T_{Off}(t) = L_1 \cdot \frac{I_{Lpk}(t)}{V_{Out} - V_{in}(t)} \tag{2.25}$$

Then the inductor current while the switch is open becomes:

$$i_{L_1\_Sw\_Open}(t_{s2}) = -m_2 \cdot t_{s2} + b_0 \tag{2.26}$$

The above equation describing the inductor current while the switch is open is a first order equation with the slope and y-axis intercept at:

$$\begin{aligned} m_2 &= \frac{V_{Out} - V_{in}(t)}{L_1} \\ b_0 &= I_{Lpk}(t) - \frac{V_{in}(t) - V_{Out}}{L_1} \cdot T_{On}(t) \end{aligned} \tag{2.27}$$

The above equation holds for the period when the switch is open and that is:

$t_{s2} \in (T_{On} : T_s]$, where

$$T_s = T_{On} + T_{Off} \tag{2.28}$$

Now that the equations for the boost inductor current are defined, the current through the ripple cancellation circuit can be calculated. The voltage of the secondary winding that picks up the ac, and proper selection of the auxiliary inductor based on the formula below determine the current through the ripple cancellation circuit.

$$L_2 = L_1 \cdot N \cdot (1 - N) \tag{2.29}$$

The proper selection of the capacitor C_2 of the ripple cancellation circuit makes the voltage across it to bias to the input voltage, and therefore this capacitor will block out any dc voltage from entering the circuit and show across the L_2 inductor. This makes the current across the inductor L_2 to be defined as:

$$\begin{aligned} i_{L_2\_Sw\_Closed}(t_{s1}) &= m_{1\_L_2} \cdot t_{s1} + b_{0\_closed} \\ i_{L_2\_Sw\_Open}(t_{s2}) &= m_{2\_L_2} \cdot t_{s2} + b_{0\_open} \end{aligned} \tag{2.30}$$

In the above first order equations, the slopes and y intercepts are determined after the following formulas:

$$\begin{aligned} m_{1\_L_2}(t) &= -N \cdot \frac{V_{in}(t)}{L_2} \\ m_{2\_L_2}(t) &= -N \cdot \frac{V_{in}(t) - V_{Out}}{L_2} \\ b_{0\_closed}(t) &= N \cdot \frac{V_{in}(t)}{L_2} \cdot \frac{T_{On}(t)}{2} \\ b_{0\_open}(t) &= N \cdot \frac{V_{in}(t) - V_{Out}}{L_2} \cdot (T_{On}(t) + \frac{T_{Off}(t)}{2}) \end{aligned} \tag{2.31}$$

The above formulas give the current waveform in the ripple current cancellation circuit, which is pure AC.

The current seen through inductor L_2 is reflected back to the primary winding of the transformer based on the following formulas:

$$\begin{aligned} i_{3\_Sw\_Closed}(t_{s1}) &= -N \cdot i_{L_2\_sw\_closed}(t_{s1}) \\ i_{3\_Sw\_Open}(t_{s2}) &= -N \cdot i_{L_2\_sw\_open}(t_{s2}) \end{aligned} \tag{2.32}$$

The resulting total current seen at the source of the boost converter becomes:

$$\begin{aligned} i_{Total\_Sw\_Closed}(t_{s1}) &= i_{L_1\_Sw\_Closed}(t_{s1}) + i_{L_2\_Sw\_Closed}(t_{s1}) + i_{3\_Sw\_Closed}(t_{s1}) \\ i_{Total\_Sw\_Open}(t_{s2}) &= i_{L_1\_Sw\_Open}(t_{s2}) + i_{L_2\_Sw\_Open}(t_{s2}) + i_{3\_Sw\_Open}(t_{s2}) \end{aligned} \tag{2.33}$$

The resulting waveforms of all currents defined in the equations above are plotted in Figure 2.4 below over one switching period.

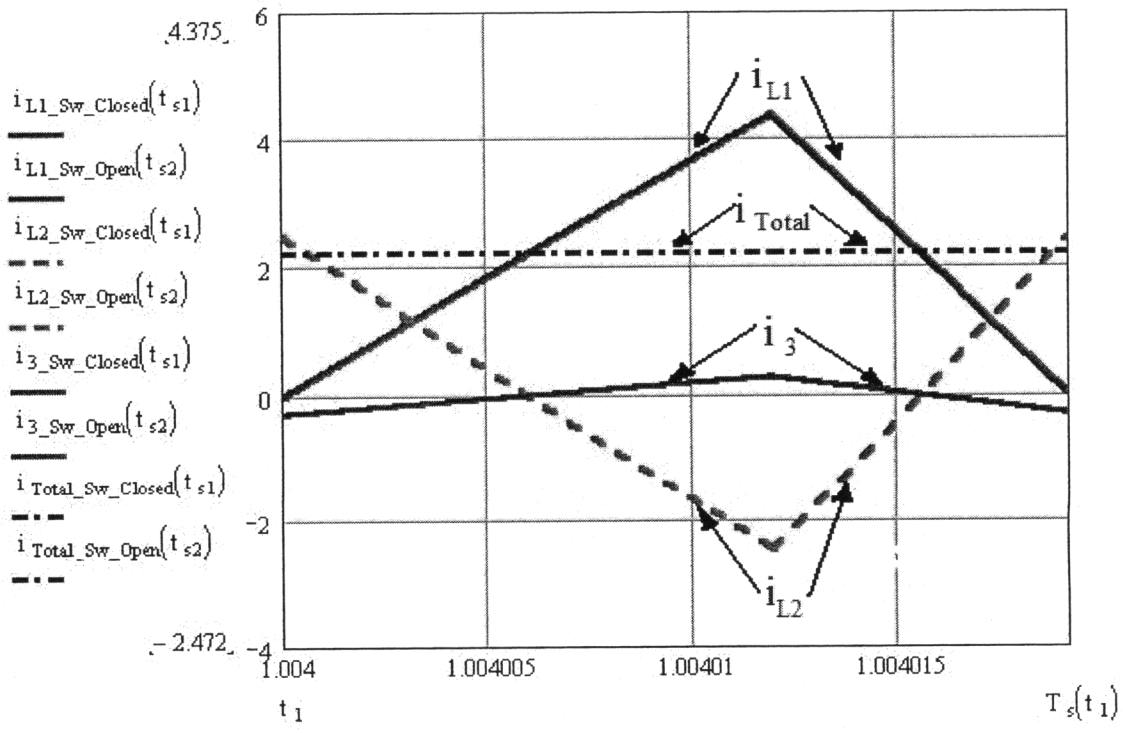

Figure 2.4: Plot of the Currents Over One Period

Figure 2.4 above shows the resulting waveforms of the currents plotted over one period. The total current seen at the input over one switching period is a pure DC current, which indicates that the ripple is fully cancelled out.

CHAPTER III

SIMULATION AND EXPERIMENTAL RESULTS

3.1 Simulation Model

A simulation model was developed based on the requirements obtained for the 150-Watt boost converter. The simulation model was evaluated using Cadence – Allegro SPB 15.2 software previously known as PSpice. The boost PFC L-6562 chip model was developed in reference [16] using Pspice software. The L-6562 model obtained was used to control the 150-Watt boost converter designed to evaluate the ripple cancellation circuit. In addition to the boost topology, the ripple cancellation circuit was implemented on the 150-Watt boost model and simulation results were obtained with it.

3.1.1 Schematic Diagram

Simulation model of the 150-Watt boost PFC converter controlled based on the L-6562 principle and the ripple current cancellation circuit is shown in Figure 3.1 bellow.

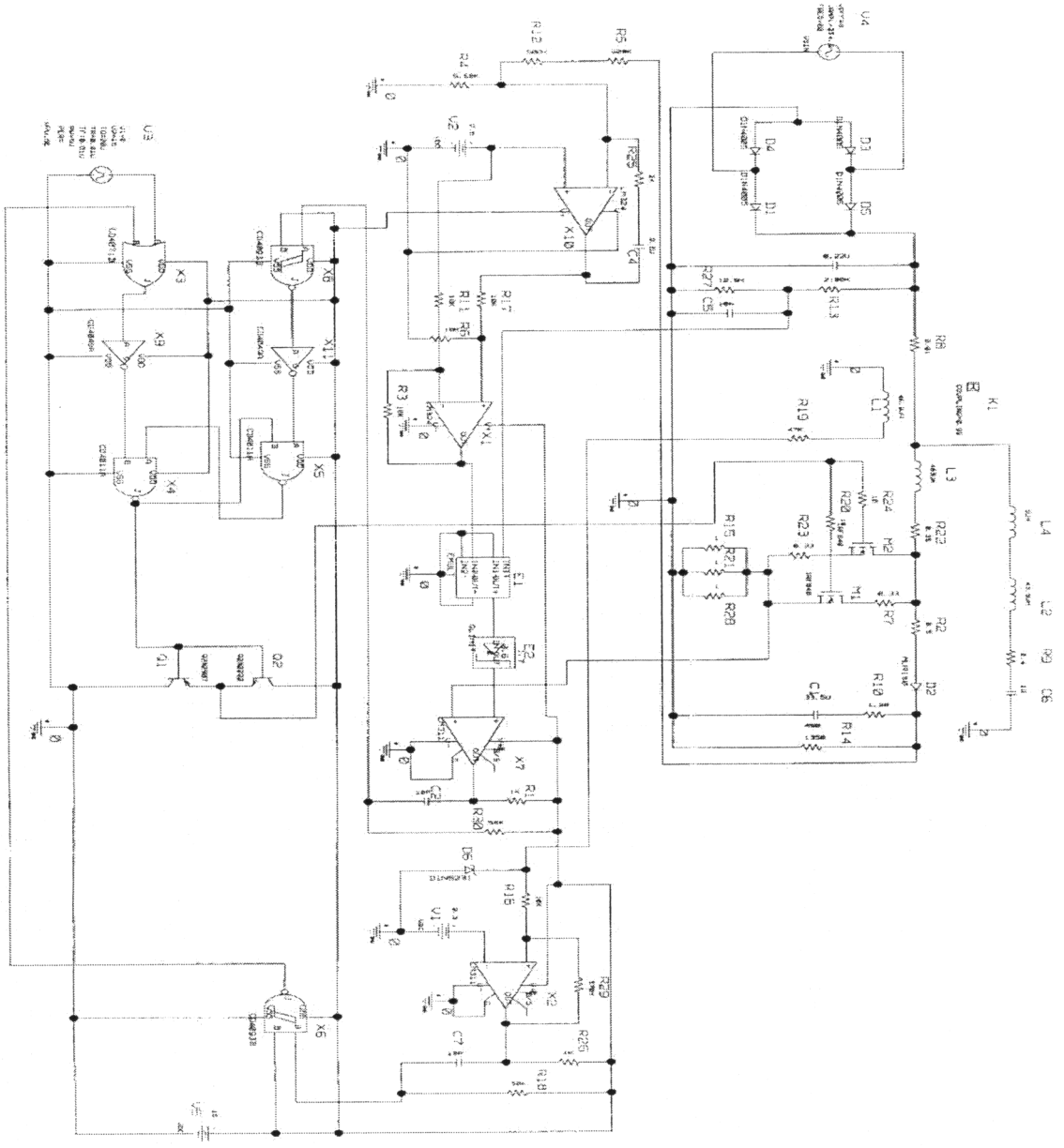

Figure 3.1: Simulation Schematic of the Cadence PSpice Model.

The schematic diagram of the simulation model is mainly divided into three parts: First there is the power side, which is basically all the electronic components that makeup the power converter, such as the bridge rectifier, input capacitor, boost inductor, MOSFETs, boost diode, output capacitor, and load resistance. Then there is the control part that makes the converter run according to L-6562 specifications. This part represents step down resistors for voltage input to the L-6562 chip and all the function blocks of the chip that allow transition mode operation of the boost converter while achieving a high power factor. These function blocks are made up of transistors, comparators, inverters, "AND" and "NAND" gates, a multiplier, and the gate drive circuit to turn on and off the MOSFETs. In addition a feedback controller made up of upper resistor of the output voltage divider and a capacitor in series with a resistor make up the feedback controller. Finally, there is the ripple current cancellation circuit that basically senses the current in the boost inductor and produces an ac current of the same magnitude as the boost current. The remaining current seen by the input source is the average current seen by the line with very small ripple. The ripple current cancellation circuit is made up of an additional winding on the boost inductor, along with an inductor and a capacitor. There is an additional resistor in the RCCC circuit that represents the equivalent series resistance of the inductor and the capacitor making up the RCCC.

3.1.2 Simulation Results

Once the circuit simulation was implemented, the results of the system behavior at different points in the circuit were tested. For comparison, the simulation result of the system with no input filtering and without the RCCC is shown in Figure 3.2 below.

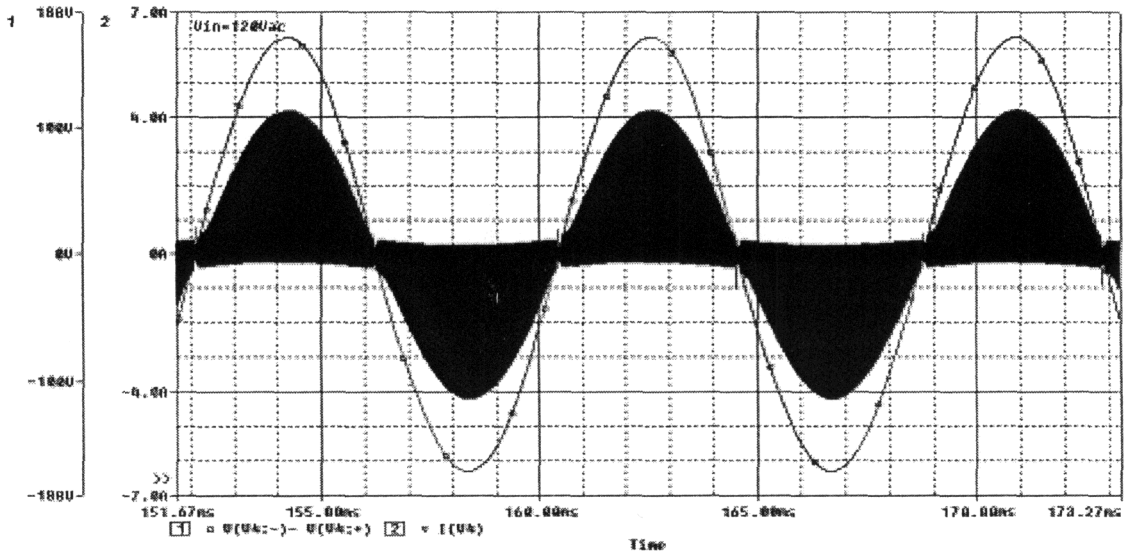

Figure 3.2: Simulation Results of the Input Voltage vs. Input Current at 120Vac without RCCC

Without any type of filtering the system input current waveform has a lot of ripple as it is shown in Figure 3.2.

Then the RCCC circuit was added and the system was tested over a wide input voltage range. The simulation was tested with the input voltage being at 120Vac, 180Vac, 230Vac, and 277Vac and the results obtained are shown in Figures 3.3-3.6 below.

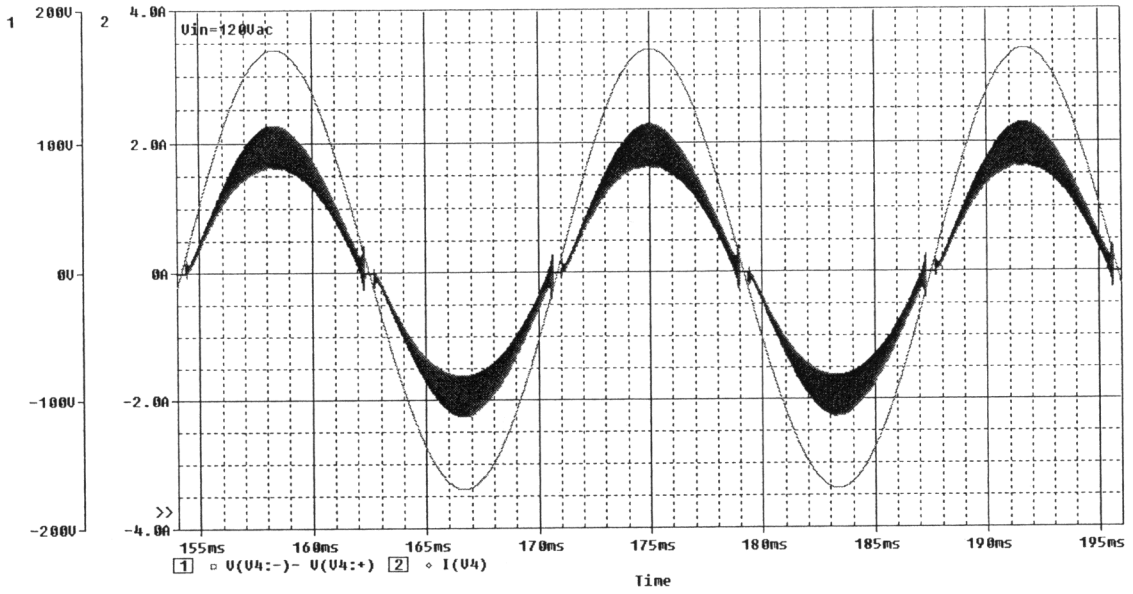

Figure 3.3: Simulation Results of Input Current and Input Voltage at 120Vac with RCCC

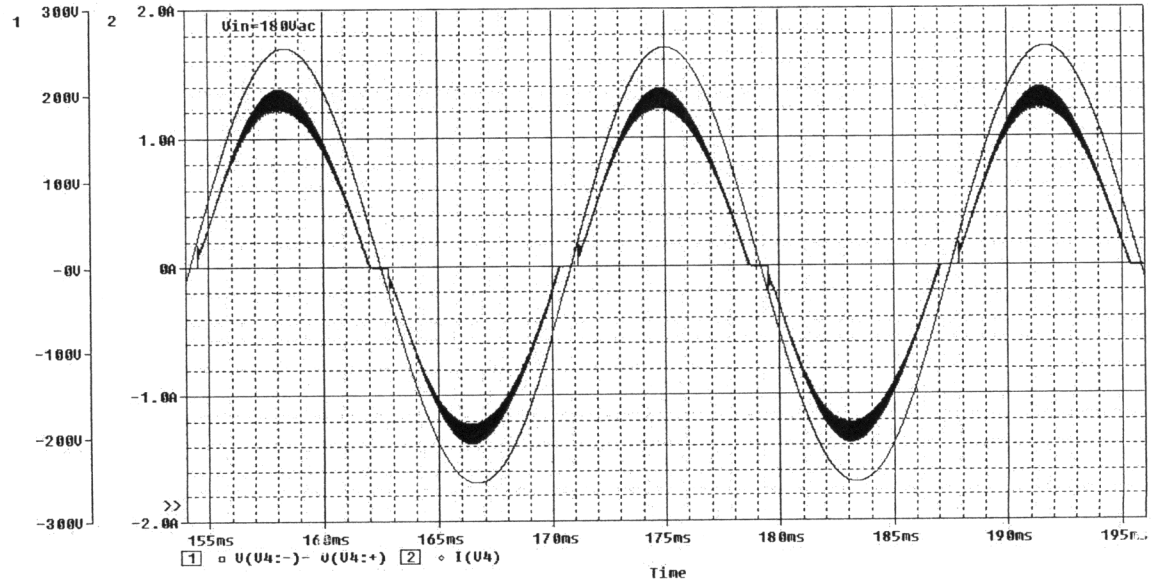

Figure 3.4: Simulation Results of Input Voltage and Input Current at 180Vac with RCCC

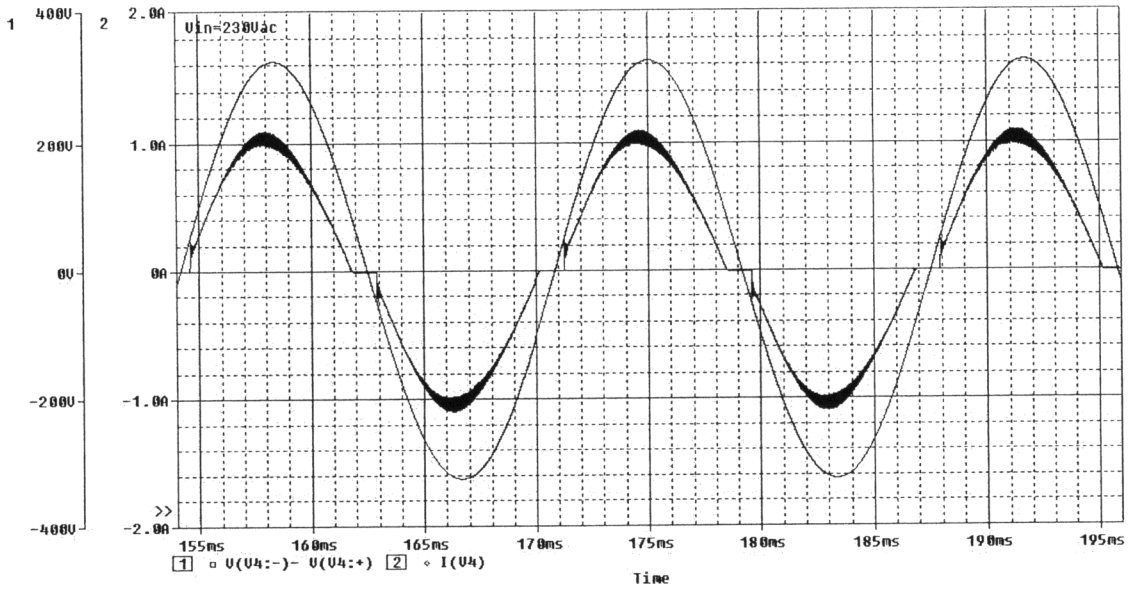

Figure 3.5: Simulation Results of Input Voltage and Input Current at 230Vac with RCCC

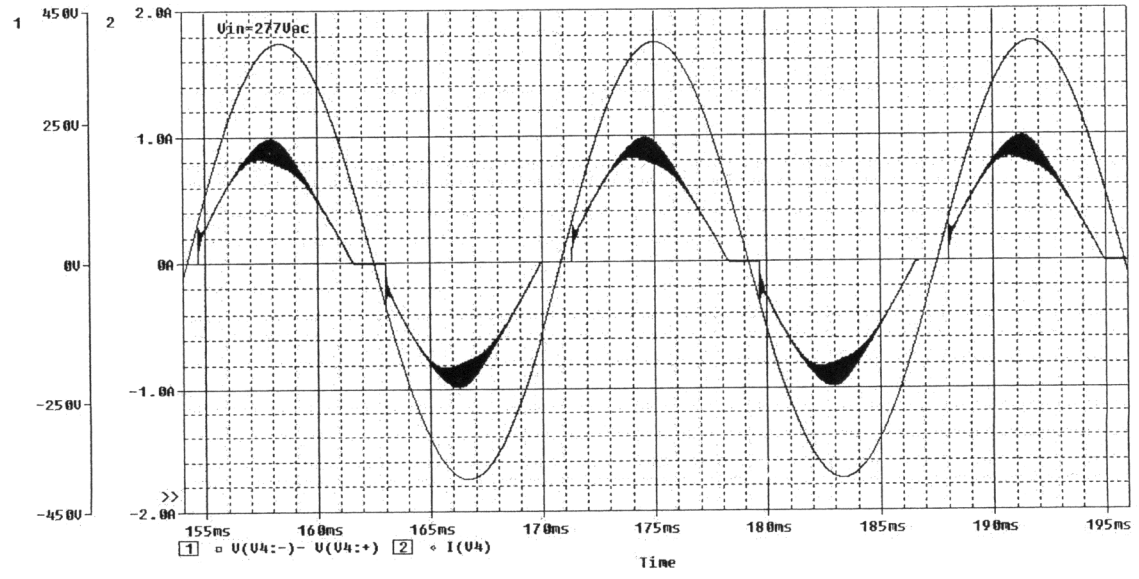

Figure 3.6: Simulation Results of Input Voltage and Input Current at 277Vac with RCCC

The four figures above represent the input current average that is seen at the input being cleaned out by the ripple current cancellation circuit, without affecting the power factor correction and total harmonic distortion.

By comparing the results obtained for the input current without the RCCC with the results of the input current with RCCC, there is more than 90% cancellation of the ripple at the input when the RCCC circuit is on.

The ripple current cancellation circuit does not affect the boost functionality and controllability. The current through the boost inductor remains the same rather there is a RCCC or not.

The output voltage of the 150-Watt boost PFC is plotted at different input voltages next.

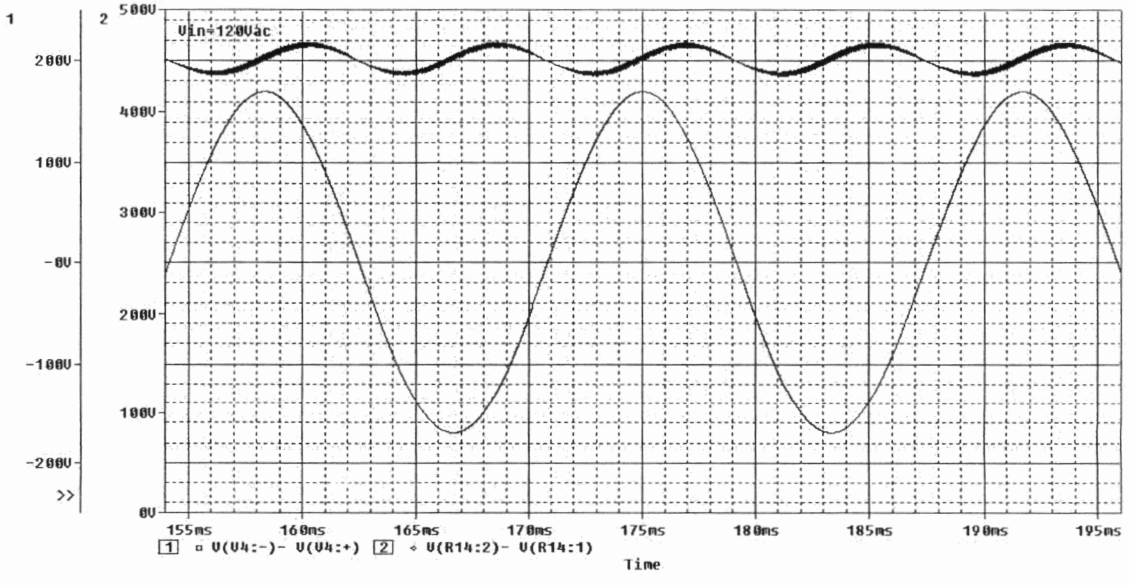

Figure 3.7: Simulation Results of Input Voltage and Output Voltage at 120Vac

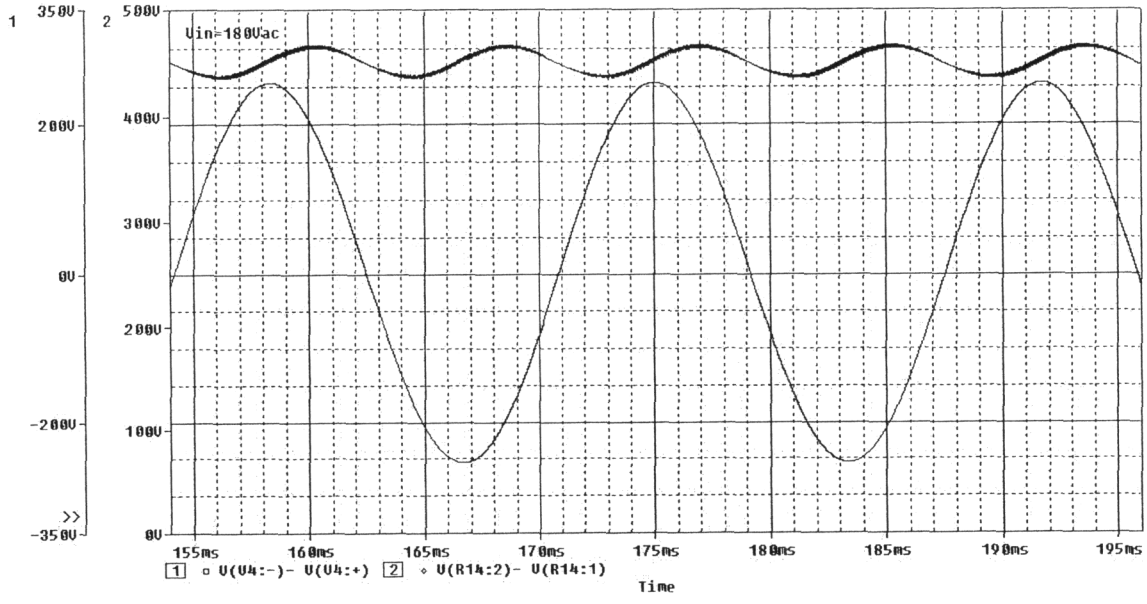

Figure 3.8: Simulation Results of Input Voltage and Output Voltage at 180Vac

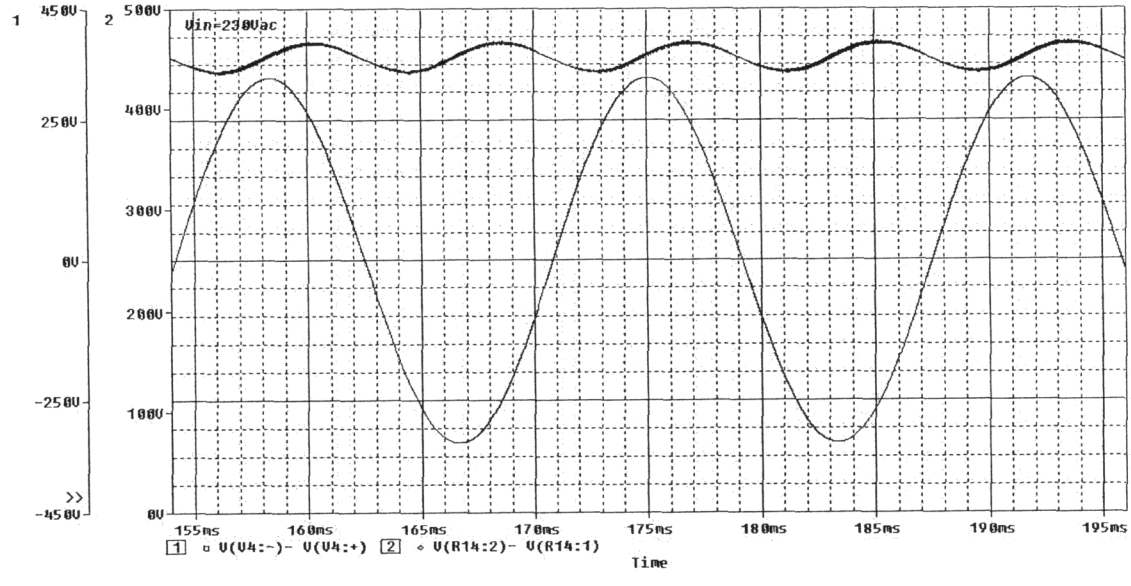

Figure 3.9: Simulation Results of Input Voltage and Output Voltage at 230Vac

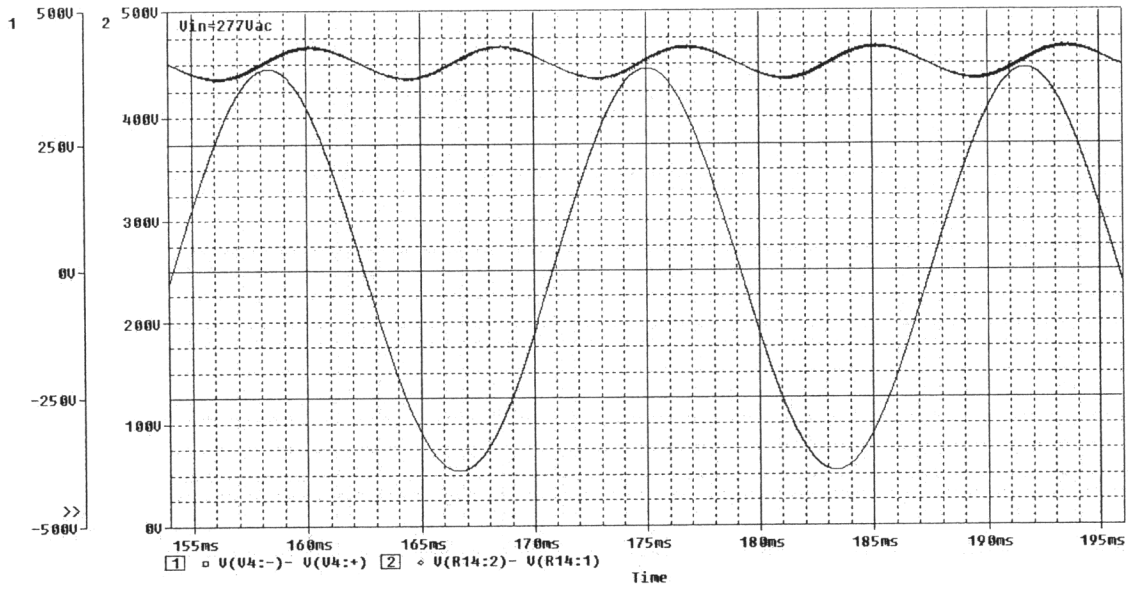

Figure 3.10: Simulation Results of Input Voltage and Output Voltage at 277Vac

The above plots represent the output voltage at four different input voltages. The results obtained are as expected. The output voltage has a dc value of 450Volts and a peak-to-peak ripple no greater than 40 Volts with frequency of twice the input frequency (120Hz).

The RCCC circuit will develop an ac current that would provide ripple cancellation at the input of the converter. Simulation results of the boost current vs. RCCC current are shown at different values to show how the RCCC works.

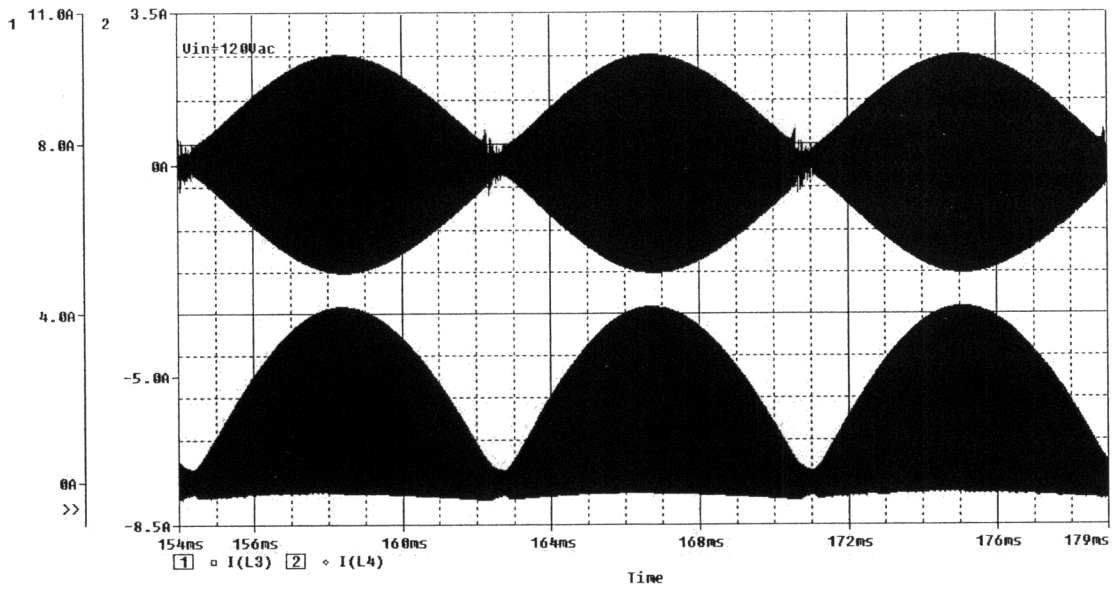

Figure 3.11: Simulation Results of Boost Current and RCCC Current at 120Vac

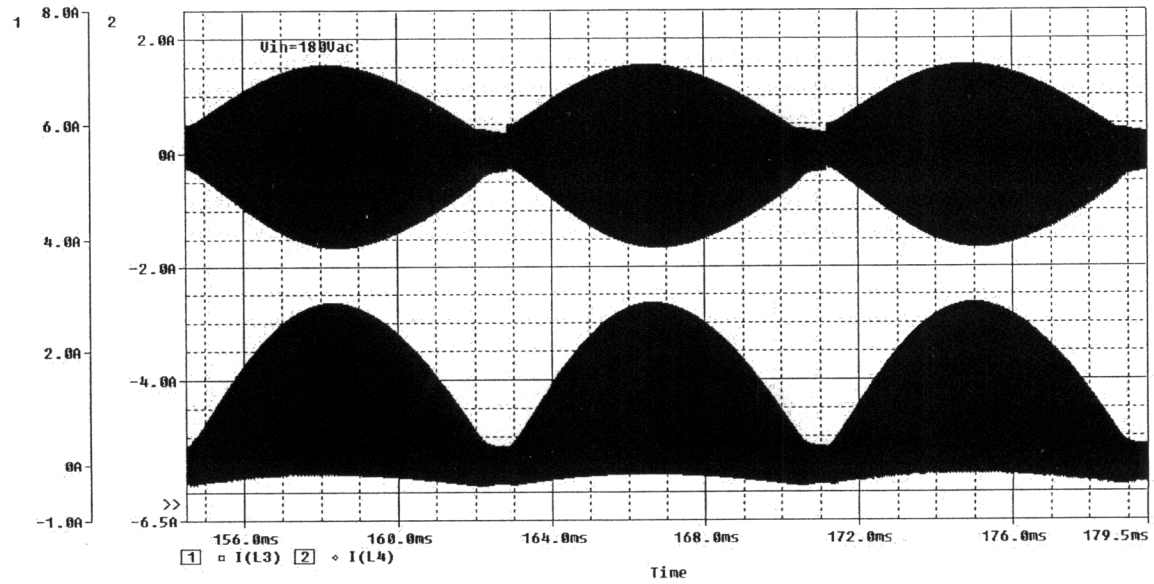

Figure 3.12: Simulation Results of Boost Current and RCCC Current at 180Vac

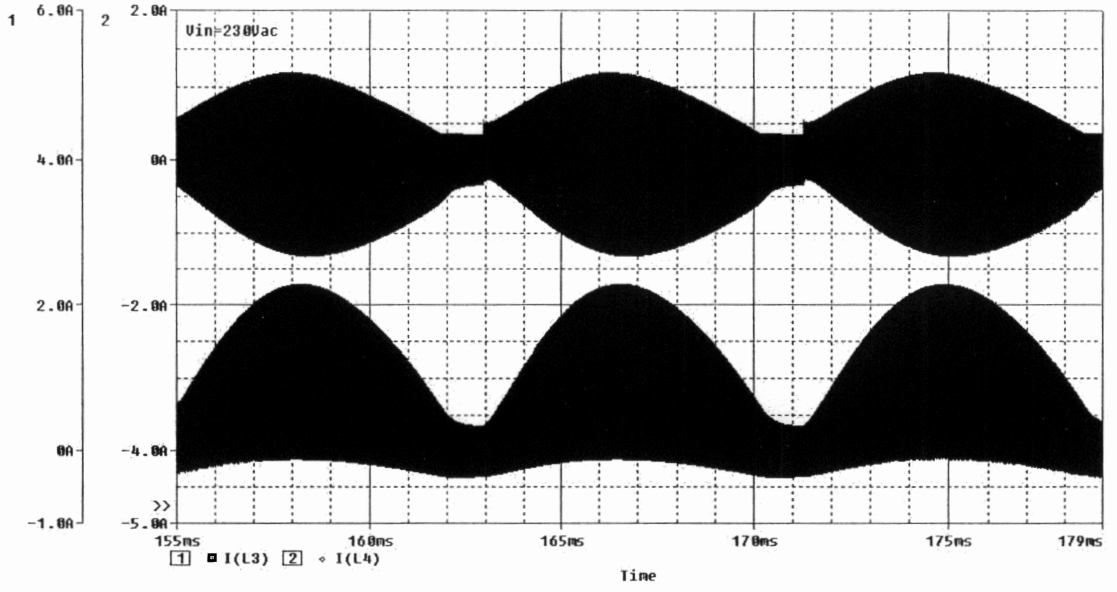

Figure 3.13: Simulation Results of Boost Current and RCCC Current at 230Vac

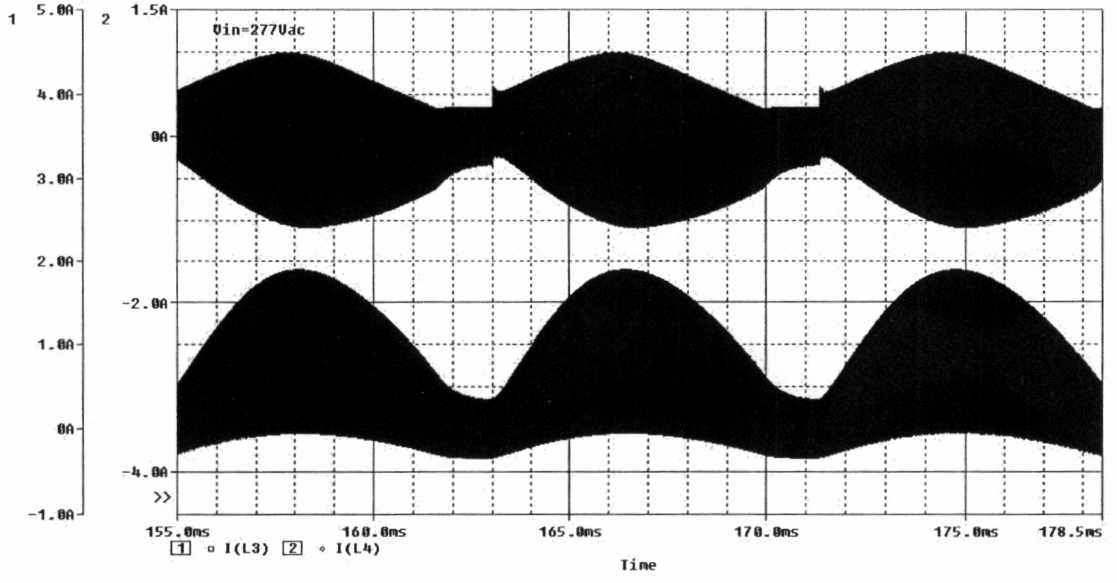

Figure 3.14: Simulation Results of Boost Current and RCCC Current at 277Vac

The above figures show how the RCCC develops the required ac current of same peak-to-peak magnitude as the boost current, therefore when added together these values would give a low ripple current at the input of the boost.

A close look at the boost current and ripple cancellation current can be observed by zooming in. Adding the input current to the boost current and ripple cancellation current gives a clear shot at how the RCCC works.

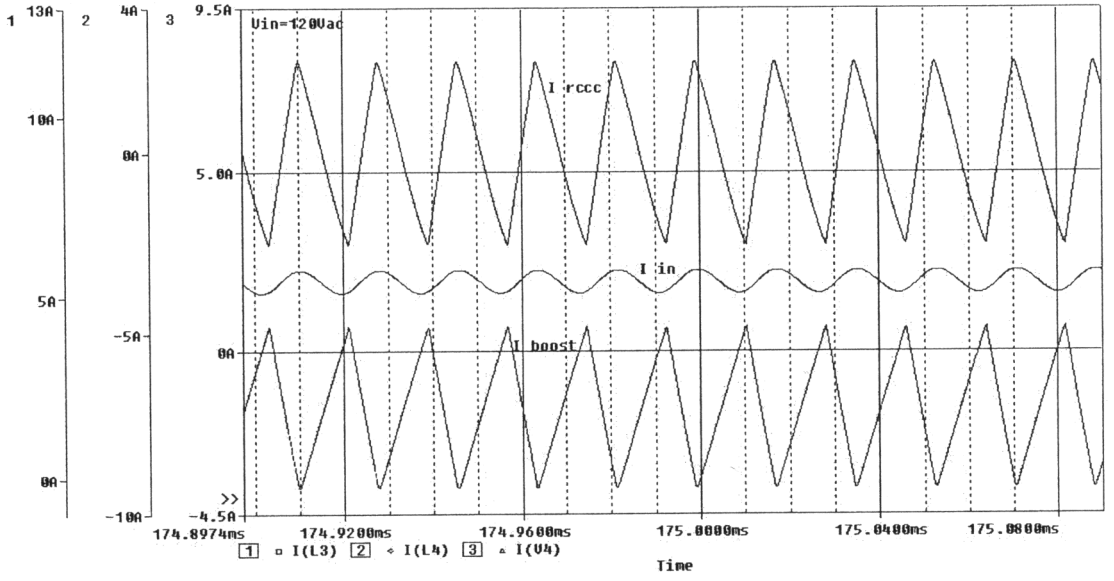

Figure 3.15: Simulation Results of Boost, RCCC, and Input Currents at 120Vac

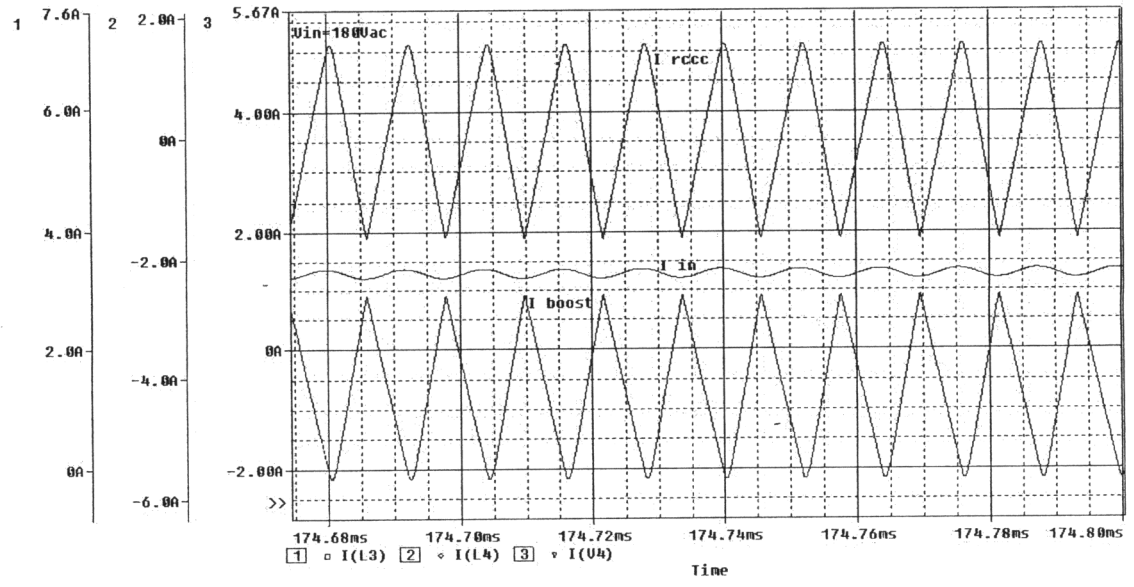

Figure 3.16: Simulation Results of Boost, RCCC, and Input Currents at 180Vac

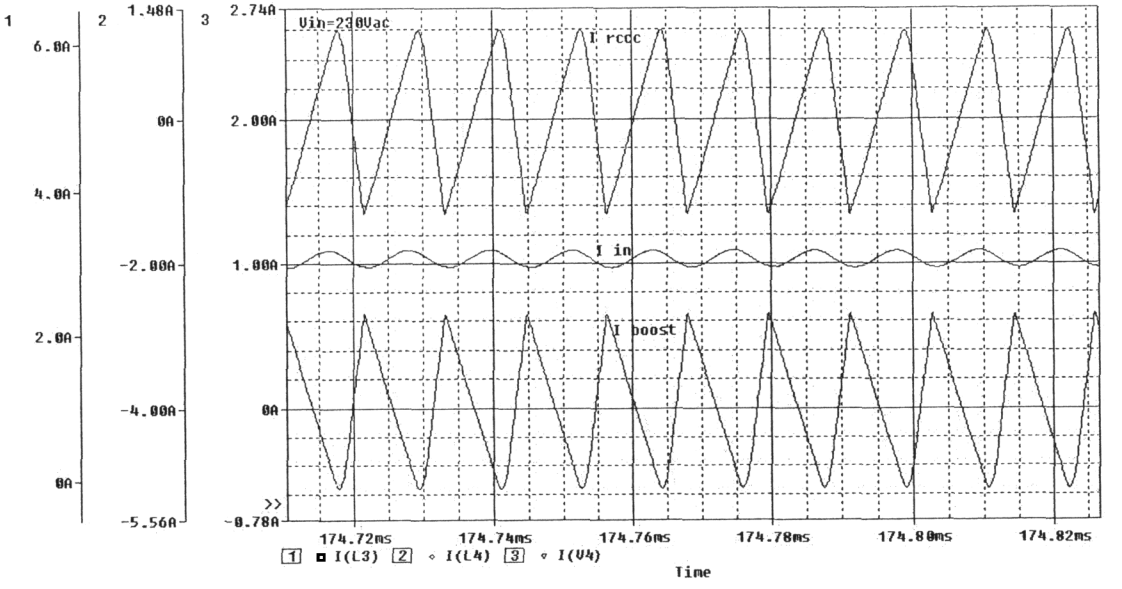

Figure 3.17: Simulation Results of Boost, RCCC, and Input Currents at 230Vac

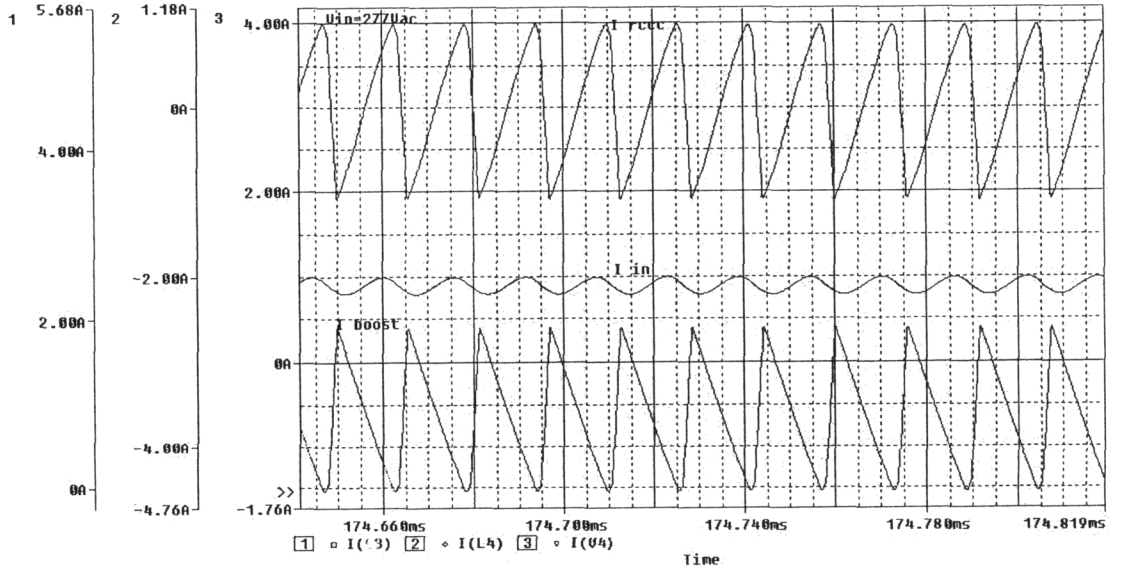

Figure 3.18: Simulation Results of Boost, RCCC, and Input Currents at 277Vac

The plots were taken by zooming in the boost, RCCC, and input currents at the peak of the waveform after the system reached steady state. A small ripple of the input current is still remaining due to the auxiliary inductor of the RCCC being off by a small

value in its inductance from the calculated one, and due to the auxiliary capacitor of the RCCC.

3.2 Experimental Model

The 150-Watt boost converter was built according to AN-966 application and the ripple cancellation circuit was implemented on it. The bench model obtained was tested and experimental results were obtained to verify the correct functionality of the converter with the ripple current cancellation circuit.

3.2.1 Experiment Setup

Circuit diagram shown in Figure 3.19 below represents the experimental setup of the 150-Watt boost PFC.

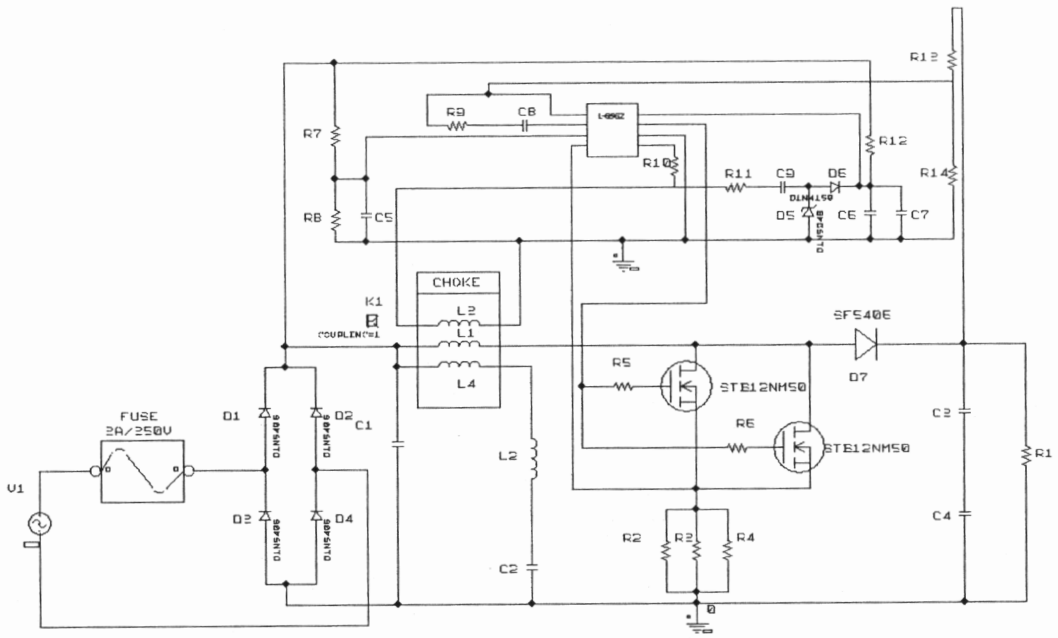

Figure 3.19: Experimental Set-up Diagram of the 150Watt Boost Converter

The values for the circuit components are listed in Table II below.

Table II: Parts List of the 150Watt Boost Circuit Components

Parts List			
Title:	150Watt Universal Boost PFC		
Project:	Ripple Current Cancellation Implementation		
Designer:	Marius G. Marita		
ITEM	DESCRIPTION	QUANTITY	SCHEMATIC DESIGN
1	CAPACITOR, 0.22uF, 630VDC, 10%, POLYESTER FILM	1	C1
2	CAPACITOR, 1uF, 305VDC, 10%, FILM CAPACITOR	1	C2
3	CAPACITOR, 67uF, 250VDC, 10%, ELECTROLYTIC	2	C3, C4
4	CAPACITOR, 0.01uF, 50VDC, 10%, CERAMIC	1	C5, C9
5	CAPACITOR, 0.1uF, 25V, CERAMIC	1	C6
6	CAPACITOR, 22uF, 25V, 20%, ELECTROLYTIC	1	C7
7	CAPACITOR, 2uF, 16V, 10%, CERAMIC	1	C8
8	DIODE, RECTIFIER, D1N5406	4	D1,D2,D3,D4
9	DIODE, ZENER, 15V, 6% D1N5248	1	D5
10	DIODE, SIGNAL, FAST, 1N4148	1	D6
11	DIODE, VERY FAST SOFT RECOVERY BYT43J	1	D7
12	FUSE, 3A/350V	1	FUSE
13	MOSFET, N-CHANNEL, 500V, 12AMPS, STB12NM50	2	M1,M2
14	RESISTOR, 1350V, 200W COSTUM MADE	1	R1
15	RESISTOR, 1.00 OHM, 1/2W, 1%	3	R2,R3,R4
16	RESISTOR, 10 OHM, 1/4W, 5%	2	R5,R6
17	RESISTOR, 2.1 M, 1/4W, 1%	1	R7
18	RESISTOR, 12.9K, 1/4W, 1%	1	R8
19	RESISTOR, 2K, 1/4W, 1%	1	R9
20	RESISTOR, 150K, 1/4W, 5%	1	R10
21	RESISTOR, 100 OHM, 1/4W, 5%	1	R11
22	RESISTOR, 360K, 1/4W, 5%	1	R12
23	RESISTOR, 1M, 1/4W, 1%	1	R13
24	RESISTOR, 5.65K, 1/4W, 1%	1	R14
25	INDUCTOR, 463uH, DELTA 25/19/13	1	L1
26	INDUCTOR, 43uH, EPCO XP13	1	L2

3.2.2 Experimental Results

The 150-Watt boost converter was built in the lab on a vector board. The response of the system was tested at different input voltages ranging from 105Vac to 300Vac and the response of the system was recorded in four situations. First, the boost PFC converter was tested without the input filtering and without the RCCC circuit. Then the RCCC was turned on and the results obtained were recorded. For a full comparison, the 150-Watt boost converter was tested with a traditional input filter and its response recorded in Table III below.

Table III: Experimental Results of 150-Watt Boost PFC

150Watt ;Universal Input Boost PFC Performance																				
	Vin (V)	Iin (A)	Pin (W)	Vout (V)	Vout-min (V)	Vout-max (V)	Vp-p (V)	Pout (W)	Efficiency (%)	PF	THD (%)	Iin p-p max (A)	Iin p-p min (A)	Iin p-p (A)	I L3 Peak (A)	Irrc p-p (A)
No Filtering	105	1.553	161.5	452.0	432	476	44	151.3	93.7%	0.996	7.00	4.60	0.00	4.60	4.58	-
	120	1.340	159.6	452.0	432	476	44	151.3	94.8%	0.996	6.80	4.04	0.00	4.04	3.98	-
	180	0.870	156.4	452.0	434	474	40	151.3	96.8%	0.999	3.65	2.80	0.00	2.80	2.70	-
	230	0.675	154.9	451.6	434	474	40	151.1	97.5%	0.999	4.40	2.32	0.00	2.32	2.22	-
	277	0.558	154.1	451.3	432	474	42	150.9	97.9%	0.997	6.78	1.92	0.00	1.92	1.86	-
	300	0.515	153.7	451.5	432	474	42	151.0	98.2%	0.996	7.80	1.74	0.00	1.74	1.70	-
With RCCC	Vin (V)	Iin (A)	Pin (W)	Vout (V)	Vout-min (V)	Vout-max	Vp-p	Pout (W)	Efficiency (%)	PF	THD	Iinp-p max (A)	Iin p-p min (A)	Iin p-p (A)	I L3 Peak (A)	Irrc p-p (A)
	105	1.554	161.5	451.0	430	474	44	150.7	93.3%	0.994	7.60	2.60	1.70	0.90	4.52	5.40
	120	1.341	159.8	451.2	432	476	44	150.8	94.4%	0.997	7.20	2.12	1.64	0.48	4.00	4.56
	180	0.868	155.6	451.4	430	474	44	150.9	97.0%	0.997	3.58	1.38	1.18	0.20	2.74	2.88
	230	0.679	154.6	451.6	430	476	46	151.1	97.7%	0.992	5.68	1.16	0.92	0.24	2.22	2.32
	277	0.567	154.2	451.3	428	474	46	150.9	97.8%	0.982	9.50	1.02	0.82	0.20	1.86	2.02
	300	0.528	154.0	451.2	428	474	46	150.8	97.8%	0.975	11.20	1.04	0.82	0.42	1.70	1.88
With Traditional Filter	Vin (V)	Iin (A)	Pin (W)	Vout (V)	Vout-min (V)	Vout-max	Vp-p	Pout (W)	Efficiency (%)	PF	THD	Iin p-p max (A)	Iin p-p min (A)	Iin p-p (A)	I L3 Peak (A)	Irrc p-p (A)
	105	1.560	162.2	450.7	432	474	42	150.5	92.8%	0.993	7.00	2.66	1.66	1.00	4.56	-
	120	1.340	160.0	451.3	432	474	42	150.9	94.3%	0.996	6.50	2.20	1.56	0.64	3.98	-
	180	0.872	156.4	451.4	432	474	42	150.9	96.5%	0.997	3.14	1.44	1.12	0.32	2.74	-
	230	0.681	155.1	451.8	430	472	42	151.2	97.5%	0.991	4.96	1.20	0.90	0.30	2.28	-
	277	0.569	154.4	451.5	430	472	42	151.0	97.8%	0.980	8.18	1.08	0.74	0.34	1.88	-
	300	0.529	154.0	451.1	432	474	42	150.7	97.9%	0.971	9.85	1.06	0.64	0.42	1.70	-

Table above summarizes the performance of the 150Watt boost PFC in three different situations. First the boost was tested without any input filtering, and without the ripple cancellation circuit. Then the RCCC was turned on and the performance of the converter was recorded. Finally, an EMI filter was added to the 150-Watts converter and its performance was recorded in table above.

The system input current and input voltage waveform performance was recorded at four different input voltages. The performance of the bench model with the RCCC circuit connected was tested at 120Vac, 180Vac, 230Vac, and 277Vac input.

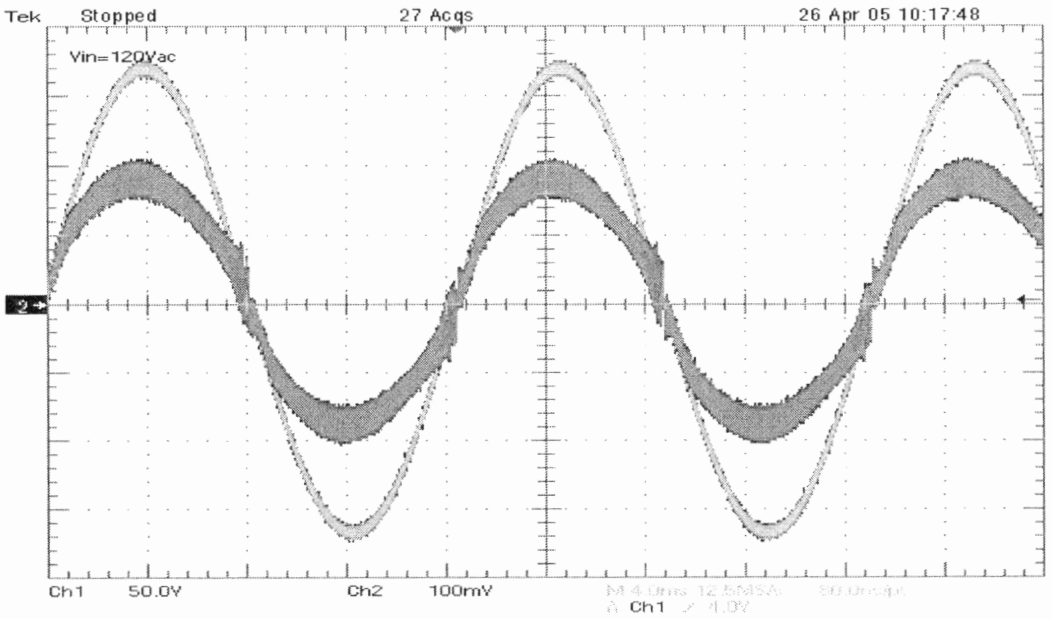

Figure 3.20: Experimental Results of Input Voltage and Input Currents at 120Vac (Ch2 – 100mV=1Amp)

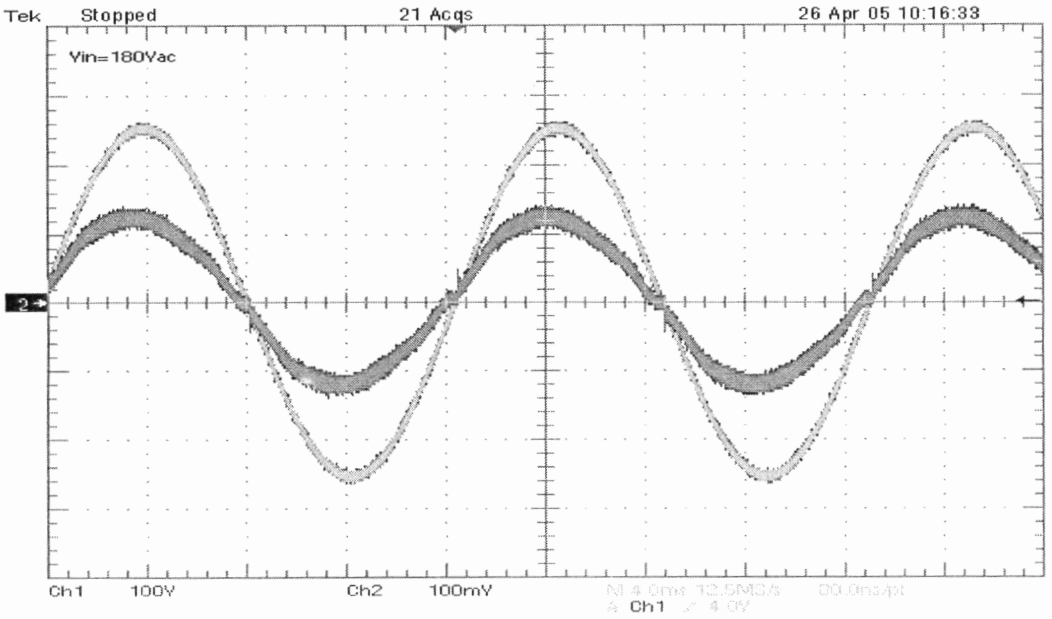

Figure 3.21: Experimental Results of Input Voltage and Input Currents at 180Vac (Ch2 – 100mV=1Amp)

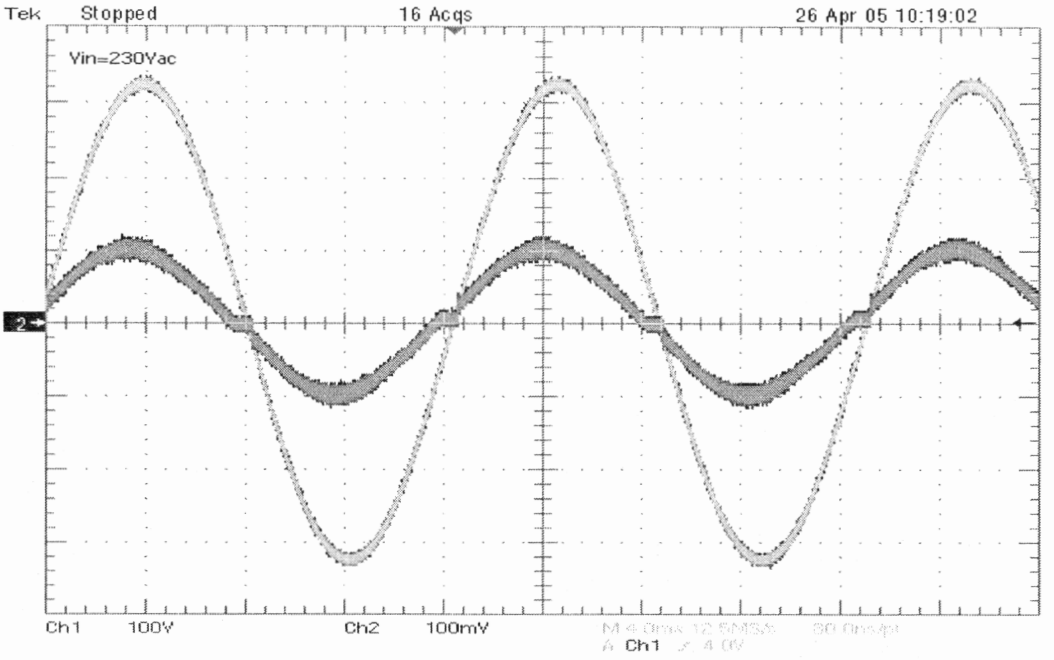

Figure 3.22: Experimental Results of Input Voltage and Input Currents at 230Vac (Ch2 – 100mV=1Amp)

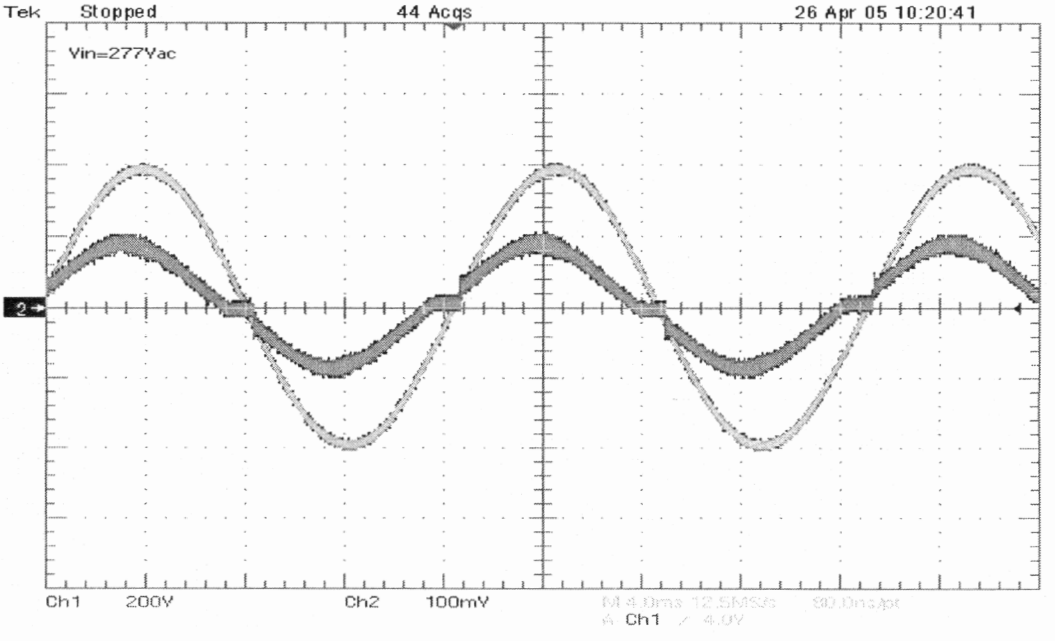

Figure 3.23: Experimental Results of Input Voltage and Input Currents at 277Vac (Ch2 – 100mV=1Amp)

The output voltage was tested for its output voltage dc value and peak to peak ripple and is shown along with the input voltage at four different input voltages in Figures 3.24 to 3.27 below.

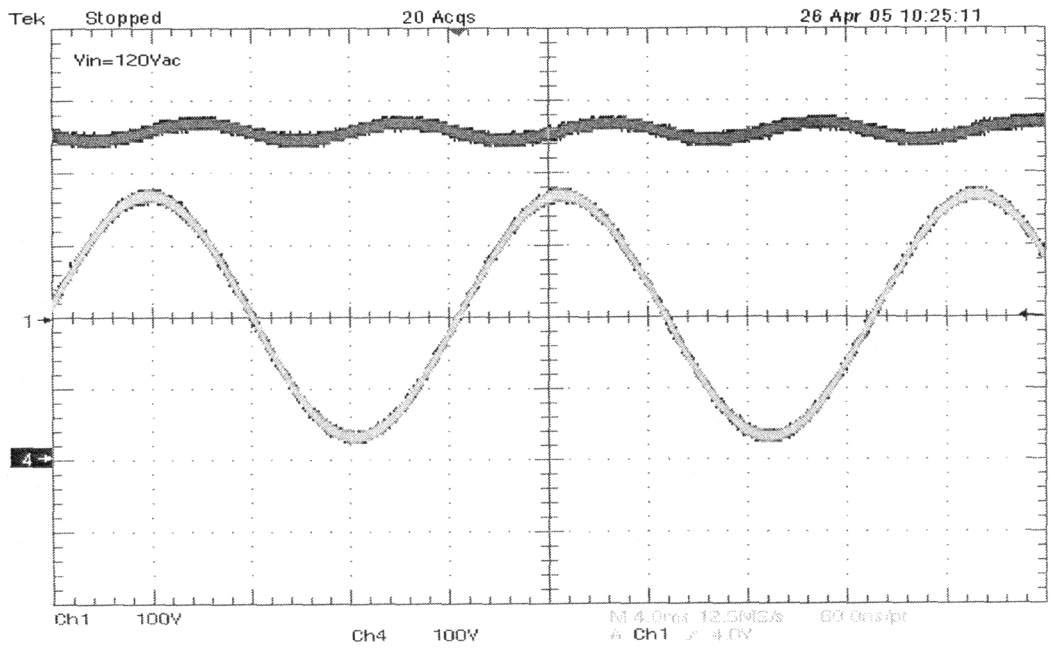

Figure 3.24: Experimental Results of Input Voltage and Output Voltage at 120Vac

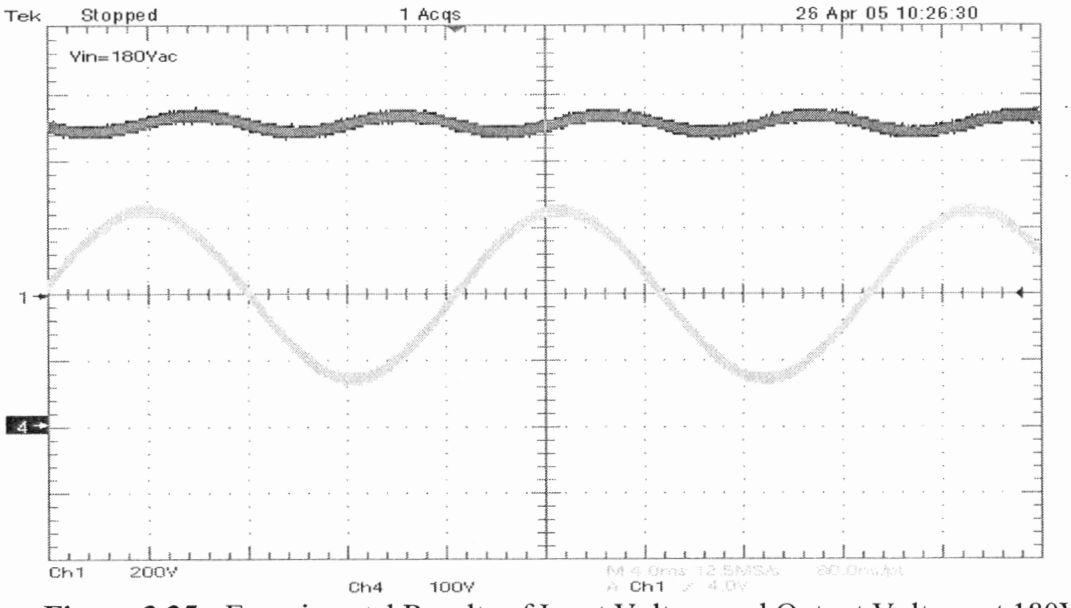

Figure 3.25: Experimental Results of Input Voltage and Output Voltage at 180Vac

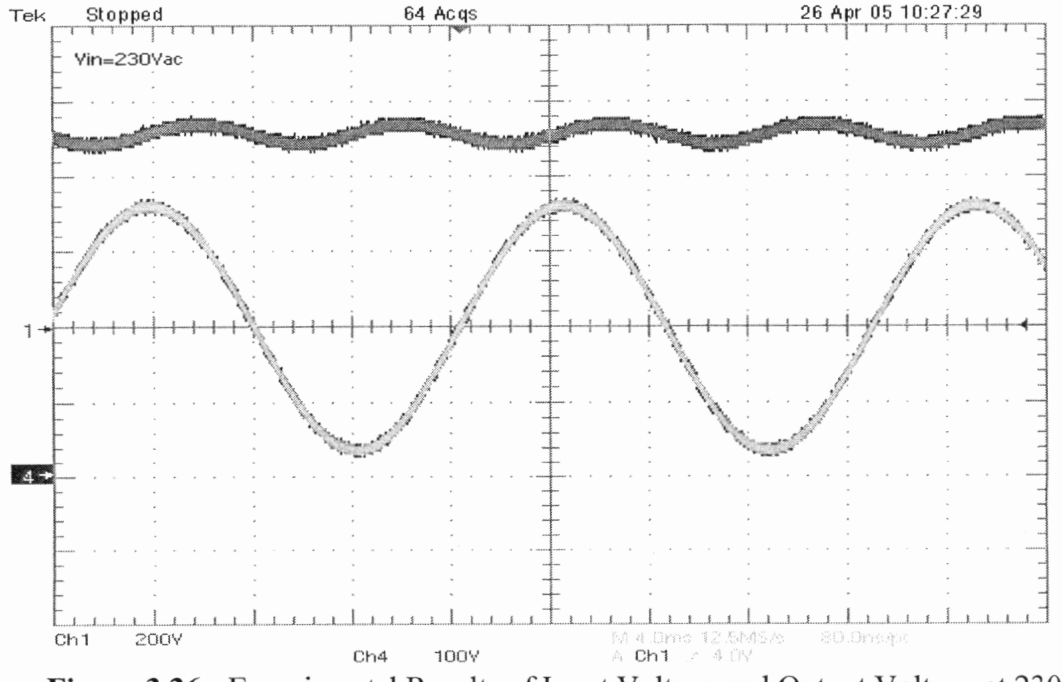

Figure 3.26: Experimental Results of Input Voltage and Output Voltage at 230Vac

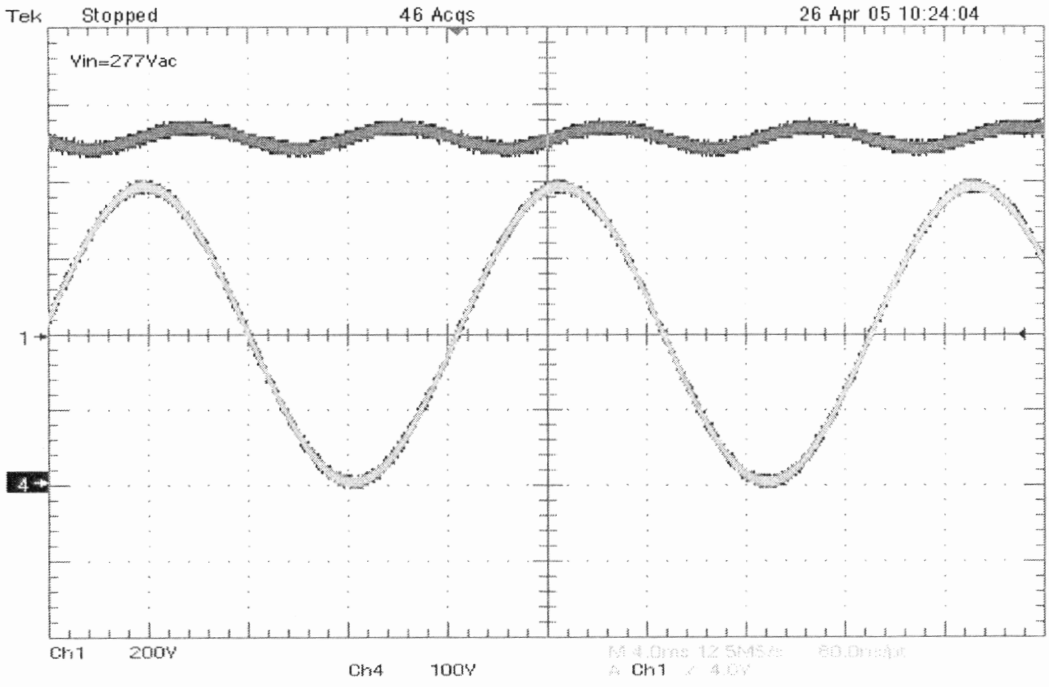

Figure 3.27: Experimental Results of Input Voltage and Output Voltage at 277Vac

The response of the system at different input voltages gives a 450 Volts output as expected with a small ripple at 120Hz (twice the input frequency).

Waveforms of the currents through the RCCC circuit and through the boost inductor are shown in Figures 3.28 to 3.31 below.

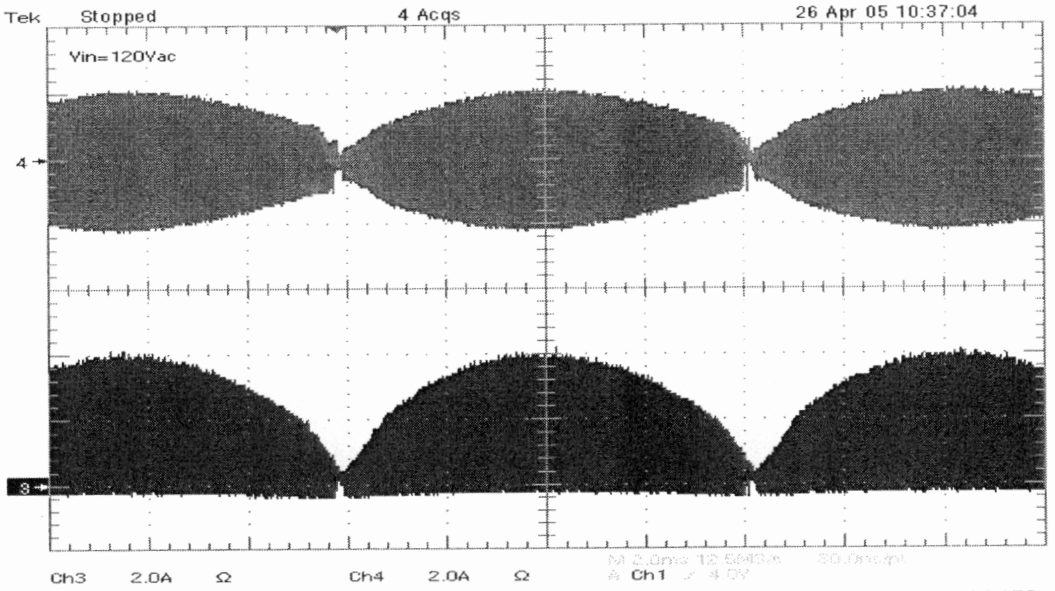

Figure 3.28: Experimental Results of Boost and RCCC Currents at 120Vac

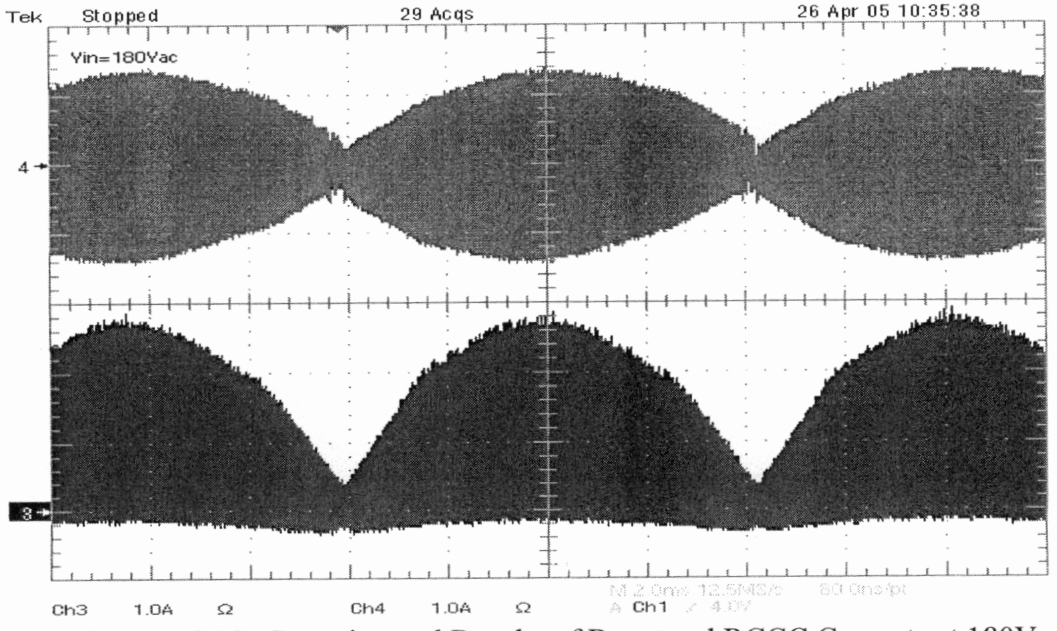

Figure 3.29: Experimental Results of Boost and RCCC Currents at 180Vac

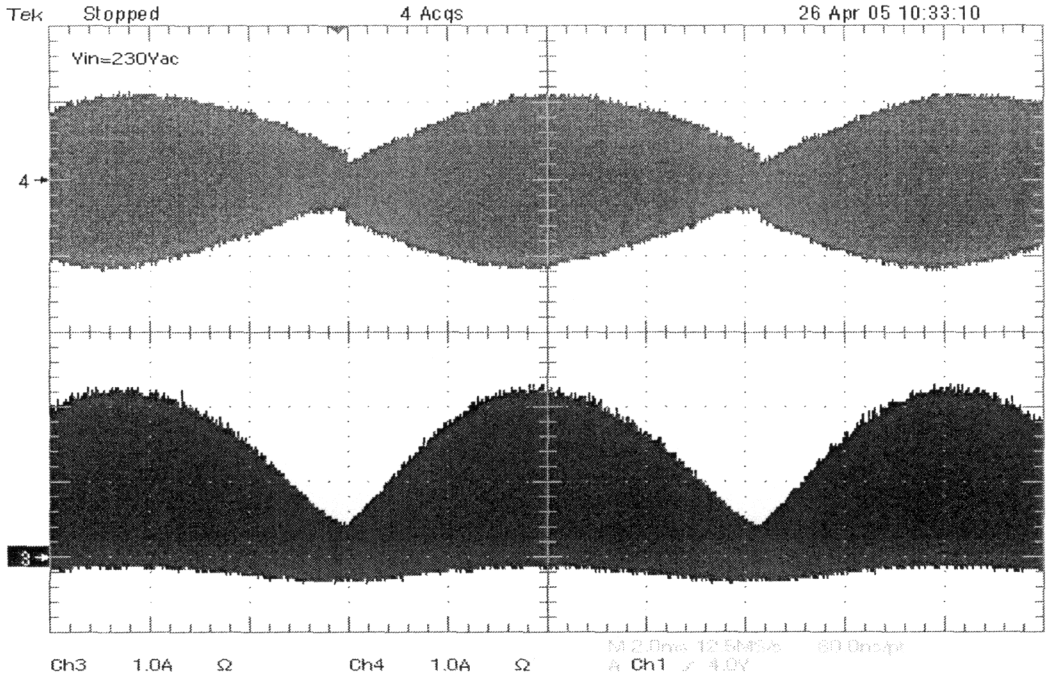

Figure 3.30: Experimental Results of Boost and RCCC Currents at 230Vac

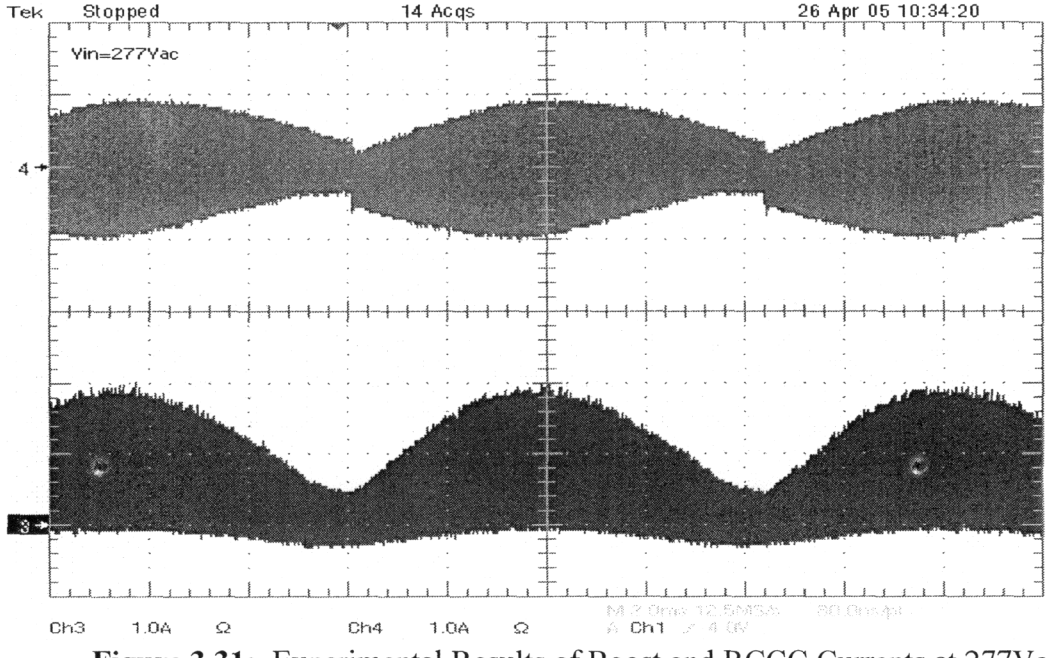

Figure 3.31: Experimental Results of Boost and RCCC Currents at 277Vac

The boost current waveform is reflected on the ripple cancellation circuit as a pure AC.

For a full comparison a closer look at the boost inductor current, along with the RCCC current, and the input current waveforms are shown in Figures 3.32 to 3.35 below.

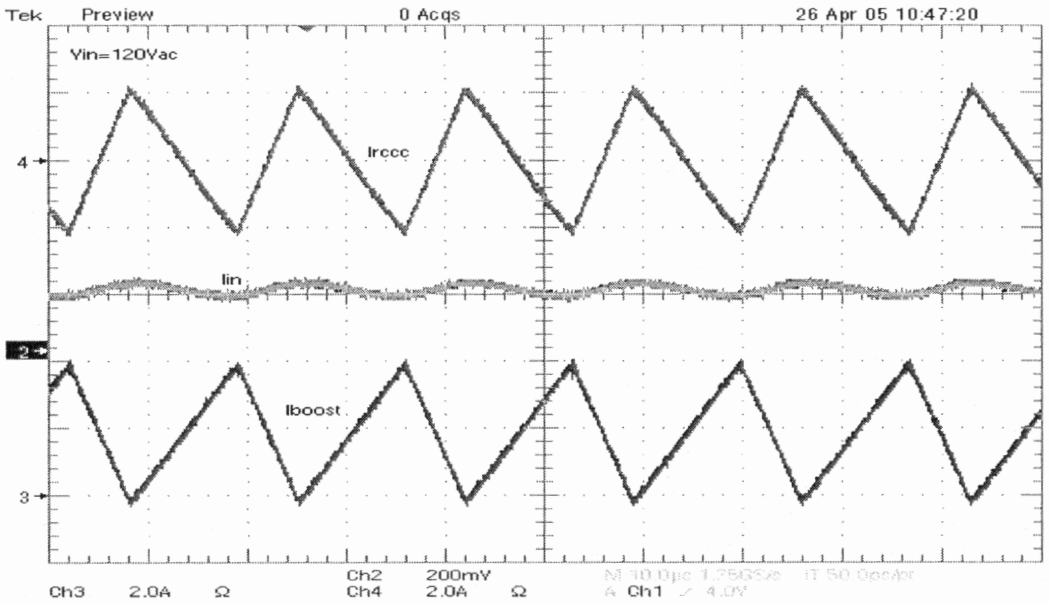

Figure 3.32: Experimental Results of Boost, RCCC, and Input Currents at 120Vac (Ch2 – 100mV=1Amp)

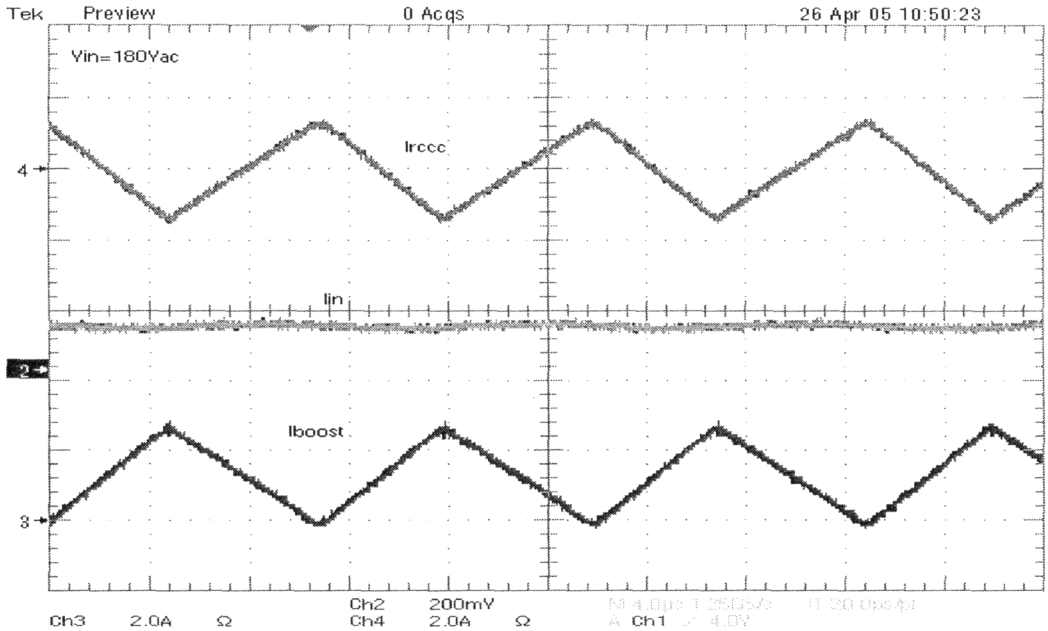

Figure 3.33: Experimental Results of Boost, RCCC, and Input Currents at 180Vac (Ch2 – 100mV=1Amp)

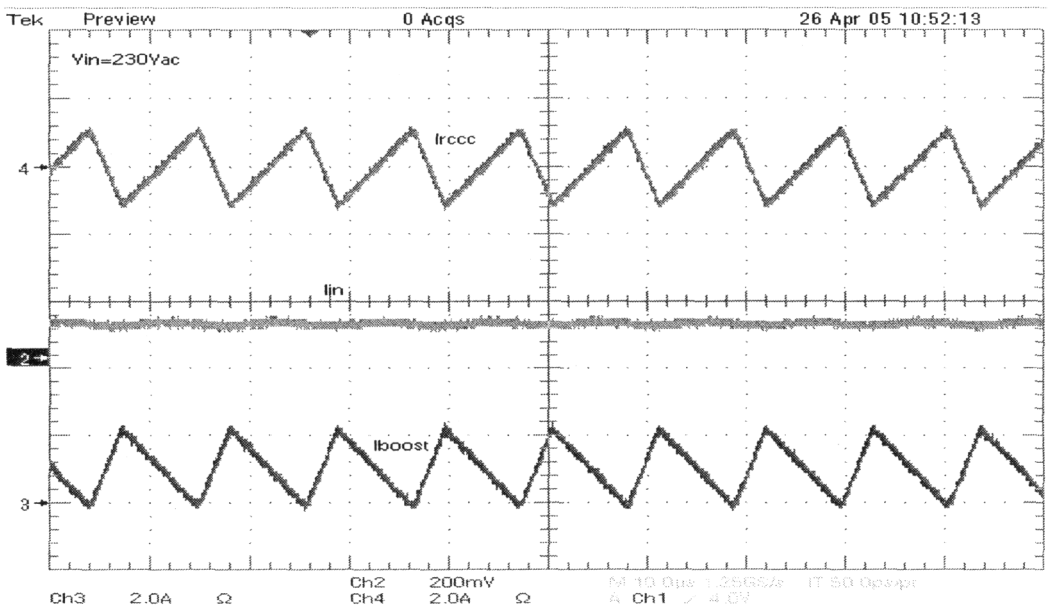

Figure 3.34: Experimental Results of Boost, RCCC, and Input Currents at 230Vac (Ch2 – 100mV=1Amp)

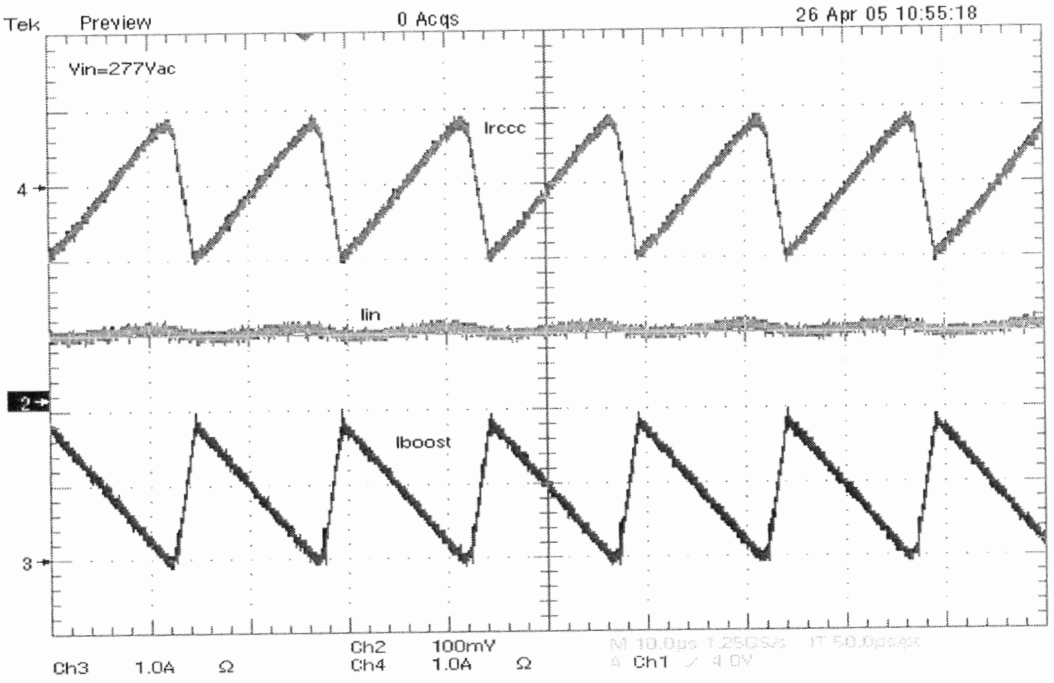

Figure 3.35: Experimental Results of Boost, RCCC, and Input Currents at 277Vac (Ch2 – 100mV=1Amp)

The results obtained from the bench model are in agreement with the results obtained from the simulation model.

CHAPTER IV

EMI FILTERING WITH RCCC METHOD VS. TRADITIONAL FILTERING METHOD AND COST ANALYSIS

In order to suppress the conducted EMI such that the noise level will not exceed the maximum limits prescribed by the regulatory agencies, additional filtering is necessary at the input of a converter. The filtering technique used to obtain EMI suppression typically requires a few capacitors and common mode inductors depending on the amount of noise level conducted back to the line.

A typical traditional filter commonly used in the lighting industry for ballast designed for a 150-Watt load is shown in Figure 4.1 below.

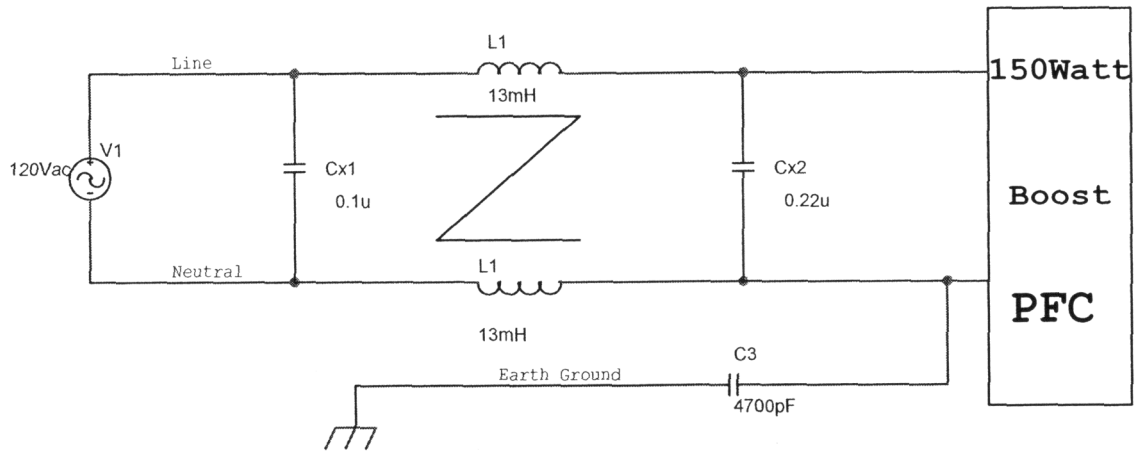

Figure 4.1: Traditional EMI Filter Schematic Representation

In this filtering method typically there is a common mode inductor (L_1) with two X type capacitors on both sides (Cx1 & Cx2). In addition there is a Y type capacitor that connects the earth ground (Cy1). This type of filter would suppress both common mode as well as differential mode noise such that the ballast will pass the EMI requirements. The cost of the filter components evaluated based on the current market prices is shown in Table IV below.

Table IV: Cost of the Traditional Filtering Method

No.	*Symbol*	*Description*	*Value*	*Vendor Part Number*	*Vendor*	*Cost ($)*
1	Cx1	EMI Suppression Cap. X2 type	0.1uF	B32922A2104M	Epcos	$0.13
2	Cx2	EMI Suppression Cap X2 type	0.22uF	B32922A2224M	Epcos	$0.138
3	L1	Common Mode Choke	13mH	LFZ28H08	Delta	$0.31
4	Cy1	EMI Suppression Cap. Y1 type	4700pF	B81123C1472M	Epcos	$0.12
		Total Cost				**$0.698**

The electronic components that make the EMI filter when the RCCC method is applied are shown in Figure 4.2 below.

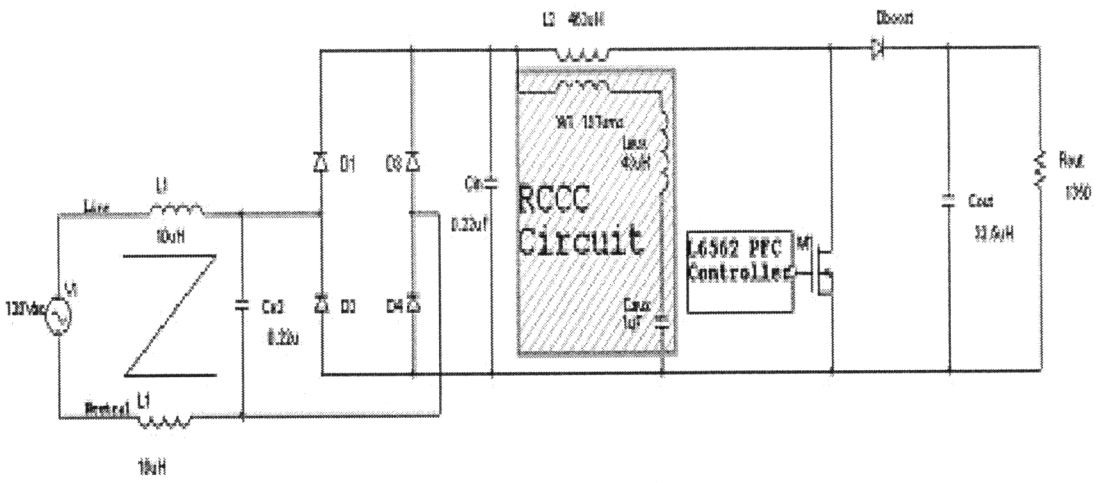

Figure 4.2: Schematic Diagram of the 150-Watt Boost Converter with RCCC Circuit and Input Filter for EMI Suppression.

In order to make the 150-Watt boost PFC converter pass the EMI test over the whole input voltage range when the RCCC method is used, a small common mode choke is added and an additional X type capacitor is placed between the line and neutral (Cx2). The cost of this filtering technique including the RCCC circuit is shown in Table V below.

Table V: Cost of the RCCC Filtering Method with EMI Choke

No.	*Symbol*	*Description*	*Value*	*Vendor Part Number*	*Vendor*	*Cost ($)*
1	W1	Auxiliary Winding on Boost Inductor	10 Turns	N/A	Delta	$0.01
2	Laux	Auxiliary Inductor EP13	43uH	T-1611/A/3	Epcos	$0.20
3	Caux	Auxiliary Capacitor for RCCC	1uF	B32592C3105K	Epcos	$0.133
5	L1	Common Mode Inductor	10mH	B82731-T2132-A20	Epcos	$0.21
6	Cx2	EMI Suppression Cap. X1 type	0.22uF	B81123C1472M	Epcos	$0.138
		Total Cost				**$0.691**

While the cost of both methods is approximately the same, the size of the input filter is greatly reduced when the RCCC method is used.

The RCCC method helps suppressing the differential mode noise while doing very little in suppressing the common mode noise. The RCCC method is recommended for use where the differential mode noise is predominant.

EMI results of the 150-Watt converter with the RCCC are shown below.

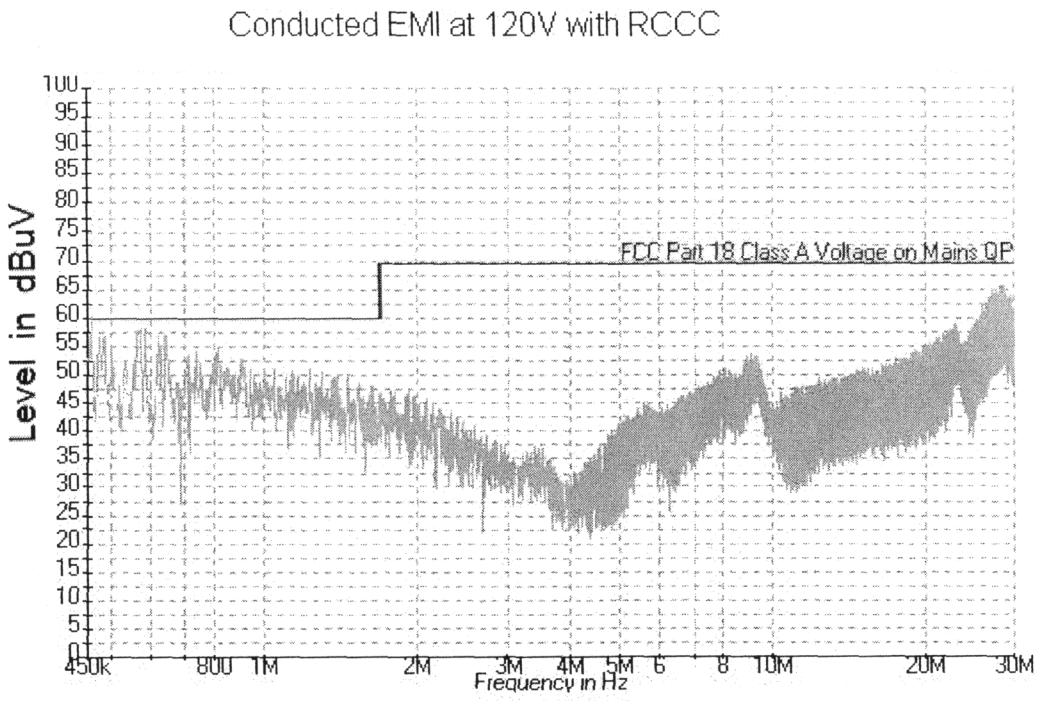

Figure 4.3: EMI Results of the System with RCCC at 120Vac (No EMI Choke)

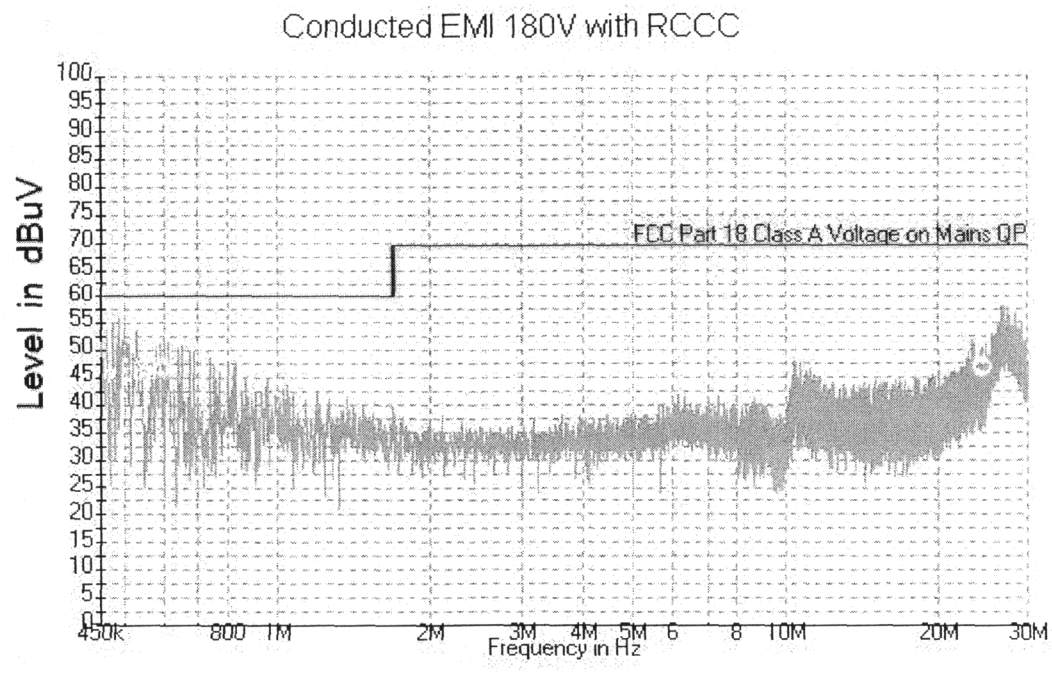

Figure 4.4: EMI Results of the System at 180Vac (EMI Choke added)

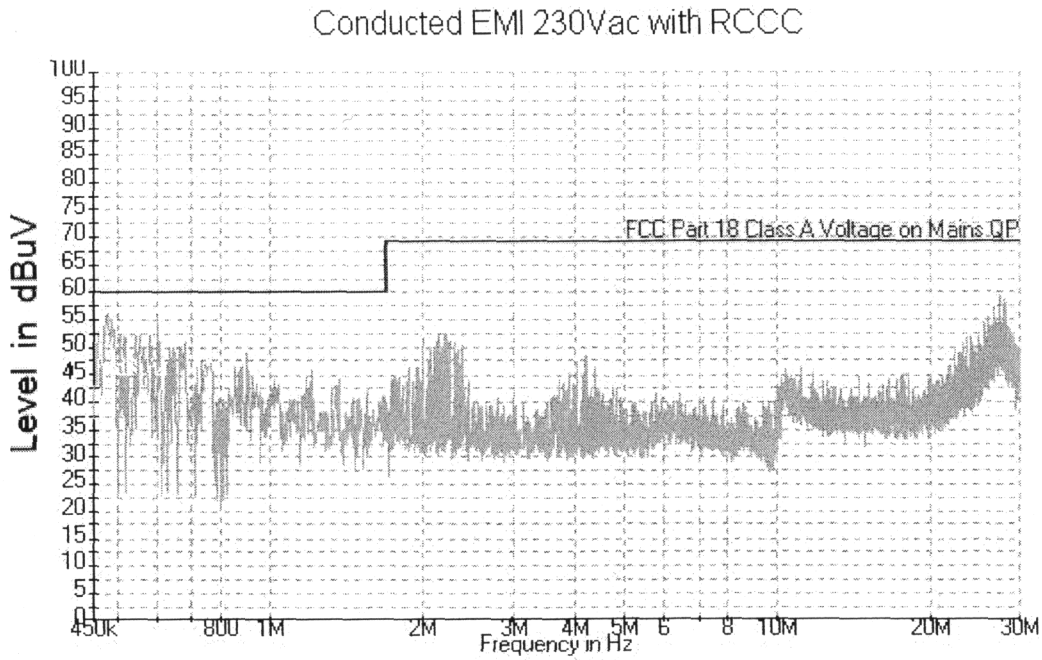

Figure 4.5: EMI Results of the System at 230Vac (EMI Choke Added)

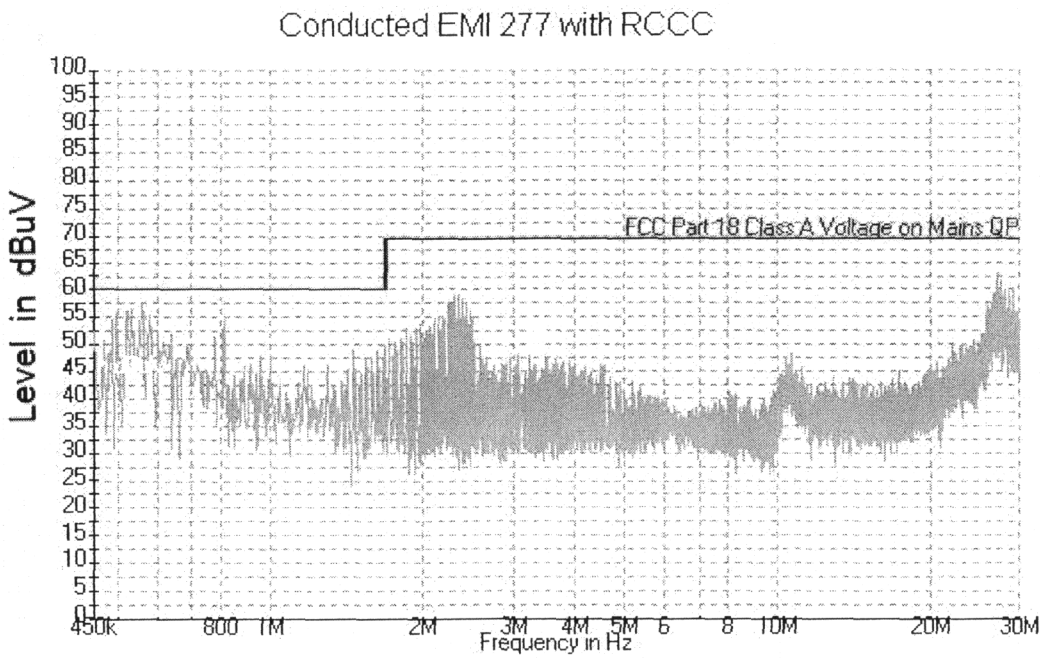

Figure 4.6: EMI Results of the System at 277Vac (EMI Choke Added)

For the input voltage of 120Vac there is no need for additional common mode inductor, and the system passes the EMI requirements. The total cost of the RCCC method at 120Vac input is $0.323 that is less then half of what the cost of the traditional method would be.

For comparison the results of the system without the RCCC method or any other additional filtering is shown at 120Vac and 277Vac

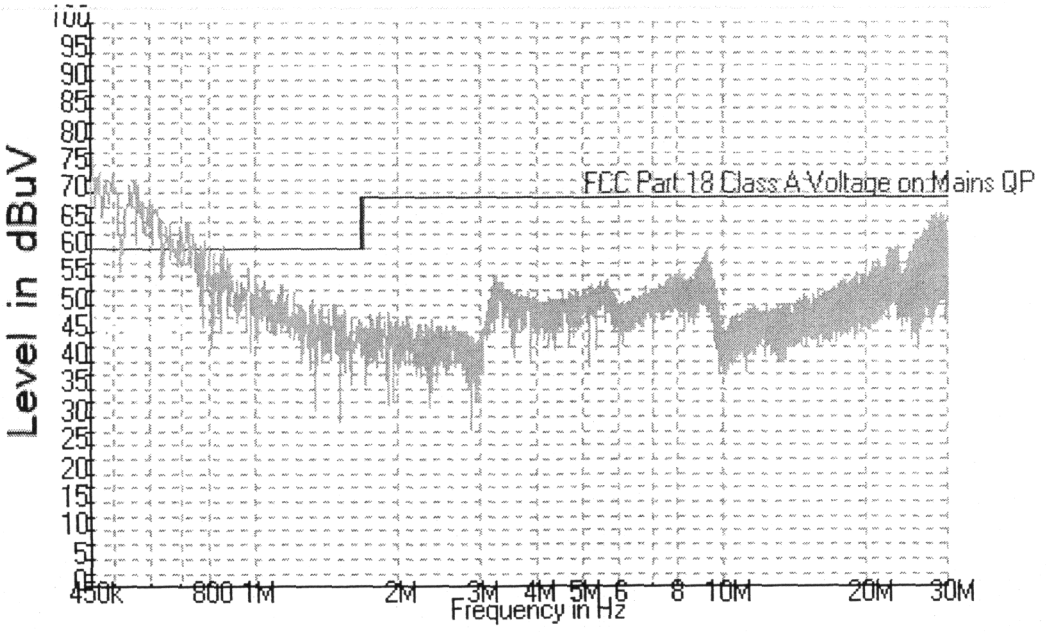

Figure 4.7: EMI Results of the System with No RCCC or Traditional Filter at 120Vac

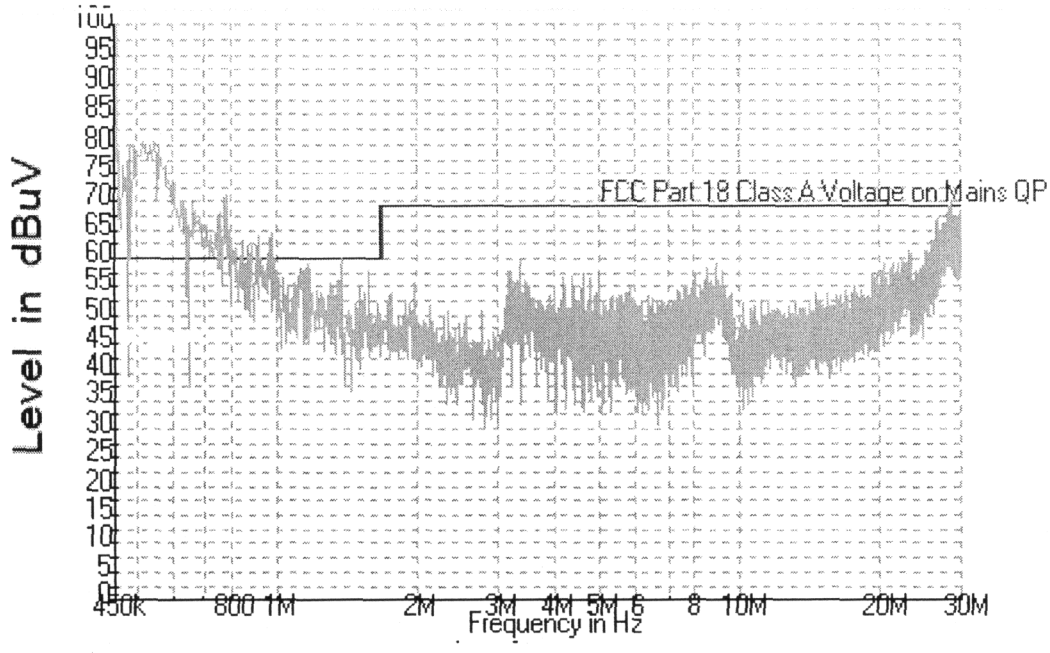

Figure 4.8: EMI Results of the System with No RCCC or Traditional Filter at 277Vac

There is more than 20dBuV suppression due to RCCC at 120Vac for low frequencies, and more than 25dBuV suppression when the common mode inductor is added at 277Vac input.

The EMI results of the system with the traditional filtering method for 120Vac and 277Vac input voltages are shown below.

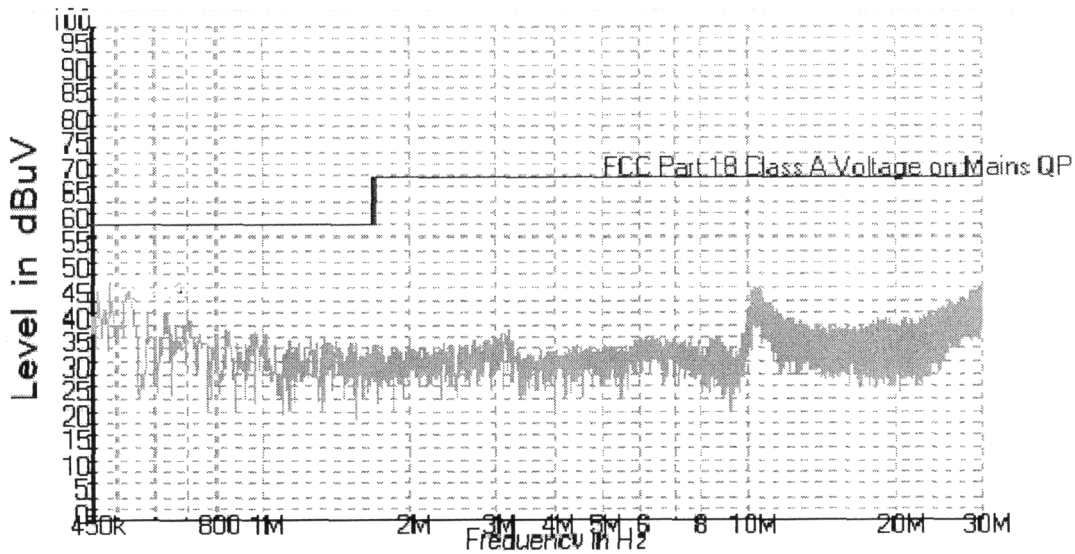

Figure 4.9: EMI Results of the System with Traditional Filter at 120Vac

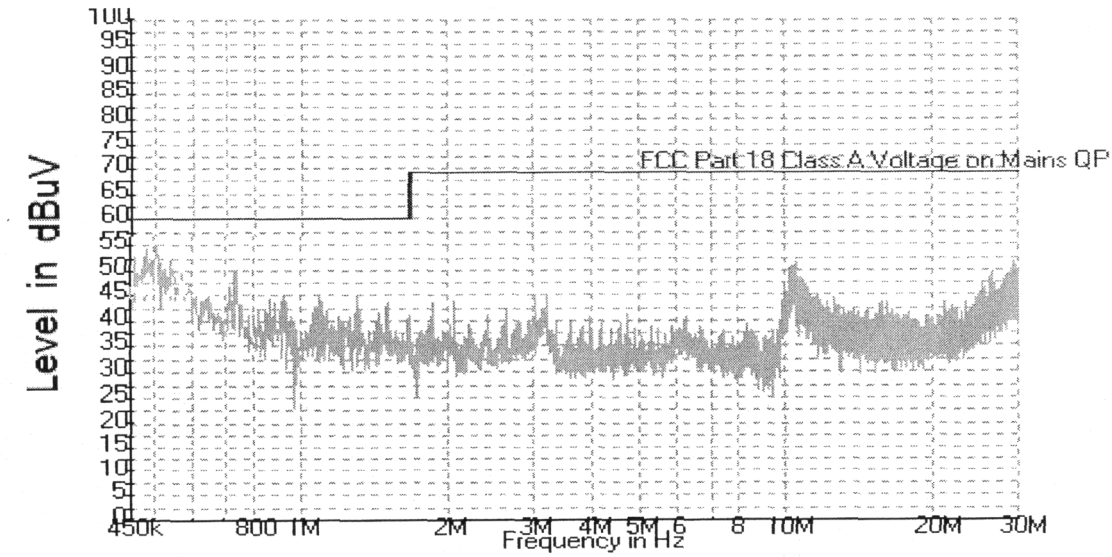

Figure 4.10: EMI Results of the System with Traditional Filter at 277Vac

While the traditional filtering method provides good margin over the entire frequency range, this design comes with a high inductance for the EMI choke, which adds to the total weight of the EMI filter.

The ripple current cancellation method helps suppress the noise level at a wide range of frequencies. EMI results of the 150-Watt boost converter were taken at frequencies ranging from 9kHz to 30MHz with the RCCC on and without the RCCC. Table VI below summarizes the results obtained and the gain due to the RCCC.

Table VI: EMI Results of the 150Watt Boost with and without the RCCC

EMI 150Watt Boost PFC @120Vac input source			
	Magnitude (dBuV)		*Gain*
Frequency (Hz)	*No RCCC*	*With RCCC*	*(dBuV)*
9k	85	90	-5
20k	105	100	5
30k	110	105	5
49k	120	115	5
50k	128	123	5
51k	93	80	13
100k	97	75	22
110k	83	65	18
200k	106	88	18
300k	85	70	15
450k	75	60	15
500k	75	60	15
800k	61	55	6
1000k	55	50	5
2000k	45	50	-5
3000k	52	50	2
5000k	52	52	0
6000k	55	55	0
10000k	60	57	3
11000k	48	48	0
21000k	60	60	0
30000k	65	67	-2

A plot of the results obtained in Table VI above is shown in Figure 4.11 below.

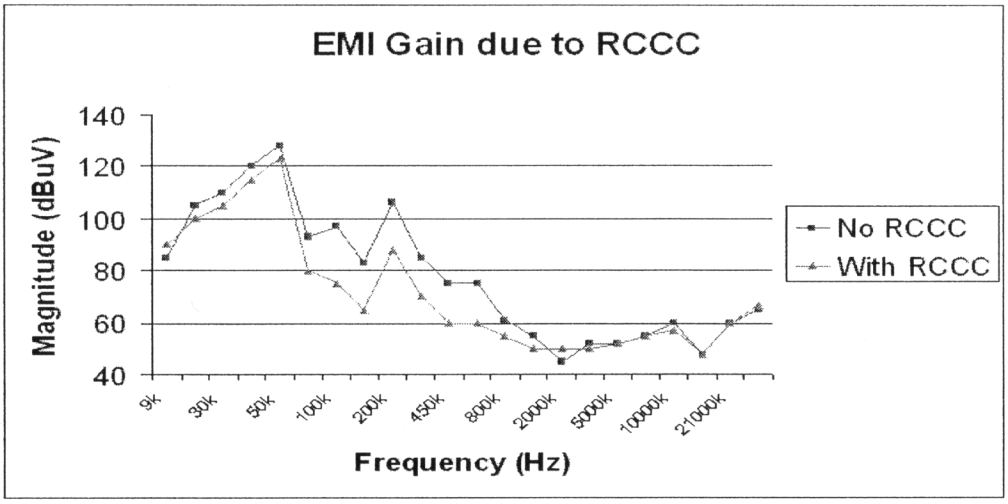

Figure 4.11: Conducted EMI plot of the 150Watt Boost Performance with and without the RCCC circuit.

The plot above shows the RCCC circuit contributing to the EMI suppression in the frequency ranging up to 1MHz. The RCCC circuit gives best results in the frequency range of 60kHz to 800kHz where it gains an average of 15dBuV improvement. Below this range there is only about 5dBuV gain reduction due to RCCC circuit. Above the 1MHz frequency range there is no gain reduction due to RCCC.

A 4-lamp linear fluorescent ballast was tested as well in the same way as the 150-Watt boost PFC and the results were even better and are summarized in the table and plot shown bellow.

Table VII: EMI Results of the 4 Lamp System with RCCC and Without the RCCC

EMI of a 4-H Ballast @120Vac input source			
	Magnitude (dBuV)		*Gain*
Frequency (Hz)	*No RCCC*	*With RCCC*	*(dBuV)*
9k	85	90	-5
20k	105	100	5
30k	110	105	5
49k	120	115	5
50k	128	123	5
51k	93	80	13
100k	97	75	22
110k	83	65	18
200k	106	88	18
300k	85	70	15
450k	75	60	15
500k	75	60	15
800k	61	55	6
1000k	55	50	5
2000k	45	50	-5
3000k	52	50	2
5000k	52	52	0
6000k	55	55	0
10000k	60	57	3
11000k	48	48	0
21000k	60	60	0
30000k	65	67	-2

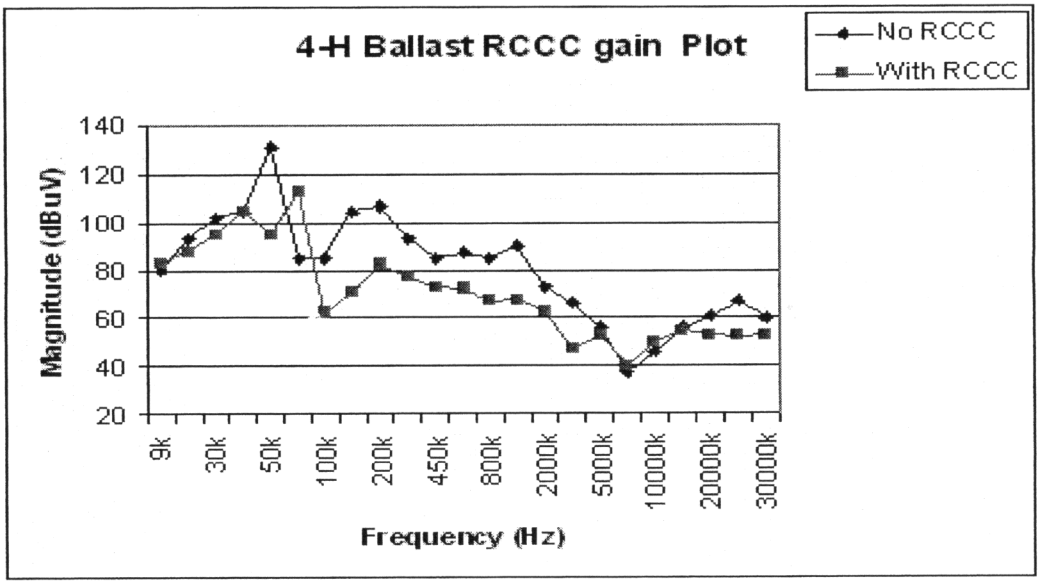

Figure 4.12: Conducted EMI Plot of the 4-Lamp Linear Fluorescent Ballast

For the 4-H ballast the RCCC contributes with an average of 19.5dBuV gain reduction between 100kHz to 3MHz frequency range. Below 100kHz the results are mixed but the highest peak is 18dBuV smaller with the RCCC on at these frequencies.

Overall the RCCC contributes to EMI gain reduction between the frequency range of 100kHz to 3MHz and this is where the filtering is the most difficult.

CHAPTER V

CONCLUSION

In this thesis a study of a particular ripple current cancellation technique was performed on a 150-Watt boost power factor correction circuit for electronic ballast. The 150-Watt boost PFC converter was developed based on reference [13]. The ripple current cancellation method was implemented on the boost converter, and the boost performance was analyzed with the ripple current cancellation circuit on it. A simulation model of the 150-Watt boost PFC was developed in Cadence-PSpice software. The response of the simulation model was compared with the results obtained from a bench model designed in the lab. The response of both simulation as well as bench models were in agreement. Then an EMI filter was added to the 150-Watt boost PFC, and its response and cost compared with a traditional filter of a typical 150-Watt boost of an electronic ballast.

A farther investigation of the ripple current cancellation circuit can be performed on systems where the predominant noise at the input is of differential type. One such example is the 6-step inverter motor control method. A look at a cúk converter

implemented with the RCCC method on both input and output filter is under investigation at GE-NELA Park location.

The RCCC has proved to be efficient in canceling out the ripple current at the input of a boost PFC circuit.

REFERENCES

[1] N. Mohan, T. Undeland, W. Robbins, "Power Electronics – Converters, Applications, and Design", John Wiley & Sons, New York 1995.

[2] M. J. Schutten, R. L. Steigerwald, J. A. Sabate, "Ripple Current Cancellation Circuit" IEEE PESC 2003, pp. 464-470.

[3] J. Wang, W. G. Dunford, K. Mauch, "Analysis of a Ripple-Free Input-Current Boost Converter with Discontinuous Conduction Characteristics" IEEE Transaction on Power Electronics, Vol. 12 No. 4, July 1997.

[4] R. Balog, P. T. Krein, and D. C. Hamill, "Coupled Inductors – A Basic Filter Building Block" IEEE Transaction on Power Electronics, 2004.

[5] D. C. Hamill, P. T. Krein, "A 'Zero' Ripple Technique Applicable to Any DC Converter", IEEE transaction April 1999, pp. 1165-1171.

[6] J. W. Kolar, H. Sree, "Novel Aspects of an Application of 'Zero'-Ripple Techniques to Basic Converter Topology," IEEE Power Electronics Specialists Conference 1997, pp796-803.

[7] K.K. Poon, J.C.P. Liu, C.K. Tse, and M.H. Pong, "Techniques for Input Ripple Current Cancellation: Classification and Implementation," IEEE 2000.

[8] G. B. Crouse, "Electrical Filter" US Patent No. 1,920,948, August 1933.

[9] R. L. Steigerwald, B. Hills, M. J. Schutten, "Ripple Cancellation Circuit For Ultra-Low-Noise Power Supplies," US Patent Application Publication No. US 2004/0022077 A1, February 2004.

[10] M. A. de Rooij, R. L. Steigerwald, B. Hills, M. J. Schutten, "Ripple Current Reduction for Transformers," US Patent Application Publication No. US 2005/0073863 A1, April 2005.

[11] G. B. Crouse, "Minimizing Filtering With Ripple Steering – A Practical Approach for Transition-Mode PFC Pre-Regulators" STMicroelectronics, July 2004.

[12] W. Wen, Y. Lee, "A Two-Channel Interleaved Boost Converter with Reduced Core Loss and Copper Loss," 35th Annual IEEE Power Electronics Specialists Conference, pp. 1003 - 1009, July 2004.

[13] C. Adragna, AN-966 Application Note "L6561, Enhanced Transition Mode Power Factor Corrector" STMicroelectronics, March 2003.

[14] C. Adragna, Application Note AN-1089 "Control Loop Modeling of L-6561-Based TM PFC," STMicroelectronics, March 2000.

[15] C. Ortmeyer, C. Adragna, Application Note AN-1214 "Design Tips for L-6561 Power Factor Corrector in Wide Range," STMicroelectronics, December 2000.

[16] A. V. Stankovic, D. Uppala, D. Kachmarik, M. C. Cosby Jr., and L. Nerone, "Design, Analysis and Optimization of a Universal Power Factor Correction Circuit for

Linear Fluorescent Lamps," Journal of the Illuminating Engineering Society, Winter 2004.

[17] Y. W. Lu, W. Zhang, Y. Liu, "A Large Signal Dynamic Model for Single-Phase AC-to-DC Converters with Power Factor Correction," IEEE Power Electronics Specialists Conference 2004, pp 1057-1063.

[18] J. Chen, R. Erickson, and D. Maksimovic, "Averaged Switch Modeling of Boundary Conduction Mode DC-to-DC Converters," The 27th Annual Conference of the IEEE Industrial Electronics Society 2001, pp. 844-849.

[19] S. C. Wong, C. K. Tse, "Method of Double Averaging for Modeling PFC Switching Converters," The 35th Annual IEEE Power Electronics Specialists Conference 2004, pp. 3202-3208.

[20] P. Athalye, R. Erickson, and D. Maksimovic, "Variable-Frequency Predictive Digital Mode Control," IEEE Power Electronics Letters, Vol. 2, NO. 4, December 2004, pp. 113-116

[21] E. Villaseca, "Notes on Small Signal Modeling and Control of Power Converters" Course taken at Cleveland State University, Spring 2003.

[22] S. Cuk, "Basics of Switched-Mode Power Conversion: Topologies, Magnetics, and Control" G.E. Cosumer and Industrial Lighting Library.

[23] Col. Wm. T. McLyman, "Transformer and Inductor Design Handbood" Marcel Dekker, Inc. New York and Basel, 1988.

[24] D. Perreault, "Power Electronics Notes," MIT website Course taught in 2003.

[25] Application Report SLVA061 "Understanding Boost Power Stages in Switchmode Power Supplies," Texas Instruments, March 1999.

[26] L. Salam, UTM Skudai, J. Bahru, "Notes on EMC Standards, Aspects and Solutions," Power Electronics and Drives, August 2000.

[27] K. Johnson, "EMC Emission Considerations In Power Supplies," Power-One Ireland, Ltd., The Annual Guide, 2004.

[28] R. West, "Common Mode Inductors for EMI Filters Require Careful Attention to Core Material Selection," PCIM Magazine, July 1995.

[29] Application Note AP-589, "Design for EMI," Intel, February 1999.

[30] M. Schutten, "EMI Filtering and Switch-Mode Power Converter Issues," GE Global Research Center, 2003.

[31] M. Sclocchi, "Input Filter Design for Switching Power Supplies," National Semiconductors.

APPENDICES

APPENDIX A

IDEAL BOOST MODELING

$$A_1 := \begin{pmatrix} 0 & 0 \\ 0 & \frac{-1}{R \cdot C} \end{pmatrix} \qquad A_2 := \begin{pmatrix} 0 & \frac{-1}{L} \\ \frac{1}{C} & \frac{-1}{R \cdot C} \end{pmatrix} \qquad B_1 := \begin{pmatrix} \frac{1}{L} \\ 0 \end{pmatrix} \qquad B_2 := \begin{pmatrix} \frac{1}{L} \\ 0 \end{pmatrix}$$

$$C_1 := (0 \quad 1) \qquad C_2 := (0 \quad 1)$$

$$A := \left[A_1 \cdot D + A_2 \cdot (1 - D) \right] \qquad B := \left[B_1 \cdot D + B_2 \cdot (1 - D) \right] \qquad C := \left[C_1 \cdot D + C_2 \cdot (1 - D) \right]$$

$$A := \left[\left[\begin{pmatrix} 0 & 0 \\ 0 & \frac{-1}{R \cdot C} \end{pmatrix} \cdot D + \begin{pmatrix} 0 & \frac{-1}{L} \\ \frac{1}{C} & \frac{-1}{R \cdot C} \end{pmatrix} \cdot (1 - D) \right] \right]$$

$$A := \left[\left[\begin{matrix} 0 & \frac{-1 + D}{L} \\ \frac{-(-1 + D)}{C} & \frac{-1}{R \cdot C} \end{matrix} \right] \right]$$

$$A := \left[\left[\begin{matrix} 0 & \frac{-(1 - D)}{L} \\ \frac{1 - D}{C} & \frac{-1}{R \cdot C} \end{matrix} \right] \right]$$

$$B := \left[\begin{pmatrix} \frac{1}{L} \\ 0 \end{pmatrix} \cdot D + \begin{pmatrix} \frac{1}{L} \\ 0 \end{pmatrix} \cdot (1 - D) \right] \qquad B := \begin{pmatrix} \frac{1}{L} \\ 0 \end{pmatrix}$$

$$C := [(0 \quad 1) \cdot D + (0 \quad 1) \cdot (1 - D)] \qquad C := (0 \quad 1)$$

$$A := \begin{bmatrix} 0 & \frac{-(1-D)}{L} \\ \frac{1-D}{C} & \frac{-1}{R \cdot C} \end{bmatrix} \qquad B := \begin{pmatrix} \frac{1}{L} \\ 0 \end{pmatrix} \qquad C := (0 \quad 1)$$

DC Analysis:

$$\frac{V_{out}}{Vin} := -C \cdot A^{\langle -1 \rangle} \cdot B$$

$$\frac{V_{out}}{V_{in}} := \left[-(0 \quad 1) \cdot \begin{bmatrix} 0 & \frac{-(1-D)}{L} \\ \frac{1-D}{C} & \frac{-1}{R \cdot C} \end{bmatrix}^{-1} \cdot \begin{pmatrix} \frac{1}{L} \\ 0 \end{pmatrix} \right]$$

$$\frac{V_{out}}{V_{in}} := \frac{-1}{-1 + D}$$

$\frac{V_{out}}{V_{in}} := \frac{1}{1-D}$ This is the DC Equation for Boost CCM.

The Small Signal Model of Boost Converter is:

$j := \sqrt{-1}$ $\quad f := 1, 10 .. 10^6$ $\quad \omega(f) := 2 \cdot \pi \cdot f$ $\quad s(f) := j \cdot \omega(f)$

$$I := \begin{pmatrix} 1 & 0 \\ 0 & 1 \end{pmatrix}$$

$$H_p(f) := \left[C \cdot (s \cdot I - A)^{-1} \cdot \left[(A_1 - A_2) \cdot \begin{pmatrix} i_L \\ v_c \end{pmatrix} + (B_1 - B_2) \cdot V_{in} \right] + (C_1 - C_2) \cdot \begin{pmatrix} i_L \\ v_c \end{pmatrix} \right]$$

Finding the Average Values of iL and Vc:

iL and vc are the average value of the state variables:

$v_c := V_{out}$

In terms of the input Vin and D (duty ratio), the vc is equal to:

$$v_c := V_{in} \cdot \frac{1}{1 - D}$$

Inductor Average Current can be expressed as:

$$i_L := \frac{I_{out}}{1 - D}$$

$$I_{out} := \frac{V_{out}}{R}$$

$$i_L := \frac{Vout}{R(1 - D)}$$

Now the calculation of the Small Signal Model is possible:

$$A_1 := \begin{pmatrix} 0 & 0 \\ 0 & \frac{-1}{R \cdot C} \end{pmatrix} \qquad A_2 := \begin{pmatrix} 0 & \frac{-1}{L} \\ \frac{1}{C} & \frac{-1}{R \cdot C} \end{pmatrix} \qquad B_1 := \begin{pmatrix} \frac{1}{L} \\ 0 \end{pmatrix} \qquad B_2 := \begin{pmatrix} \frac{1}{L} \\ 0 \end{pmatrix}$$

$$C_1 := (0 \ \ 1) \qquad C_2 := (0 \ \ 1)$$

$$A := \begin{bmatrix} 0 & \frac{-(1 - D)}{L} \\ \frac{1 - D}{C} & \frac{-1}{R \cdot C} \end{bmatrix} \qquad B := \begin{pmatrix} \frac{1}{L} \\ 0 \end{pmatrix} \qquad C := (0 \ \ 1)$$

$$v_c := V_{in} \cdot \frac{1}{1 - D} \qquad i_L := \frac{Vout}{R(1 - D)}$$

$$H_p(f) := \left[C \cdot (s \cdot I - A)^{-1} \cdot \left[(A_1 - A_2) \cdot \begin{pmatrix} i_L \\ v_c \end{pmatrix} + (B_1 - B_2) \cdot V_{in} \right] + (C_1 - C_2) \cdot \begin{pmatrix} i_L \\ v_c \end{pmatrix} \right]$$

Since B1=B2 and C1=C2 Hp becomes:

$$H_p(f) := C \cdot (s \cdot I - A)^{-1} \cdot (A_1 - A_2) \cdot \begin{pmatrix} i_L \\ v_c \end{pmatrix}$$

$$(s \cdot I - A)^{-1} := \Phi$$

$$\left[\left(A_1 - A_2 \right) \cdot \begin{pmatrix} i_L \\ v_c \end{pmatrix} \right] := A'$$

$$A' := \left[\begin{pmatrix} 0 & 0 \\ 0 & \frac{-1}{R \cdot C} \end{pmatrix} - \begin{pmatrix} 0 & \frac{-1}{L} \\ \frac{1}{C} & \frac{-1}{R \cdot C} \end{pmatrix} \right] \cdot \begin{pmatrix} I_L \\ V_{out} \end{pmatrix}$$

$$A' := \begin{pmatrix} \frac{1}{L} \cdot V_{out} \\ \frac{-1}{C} \cdot I_L \end{pmatrix}$$

$$\Phi := \left[s \cdot \begin{pmatrix} 1 & 0 \\ 0 & 1 \end{pmatrix} - \begin{bmatrix} 0 & \frac{-(1-D)}{L} \\ \frac{1-D}{C} & \frac{-1}{R \cdot C} \end{bmatrix} \right]^{-1}$$

$$\Phi := \begin{bmatrix} s & \frac{-(-1+D)}{L} \\ \frac{-1+D}{C} & \frac{s \cdot R \cdot C + 1}{R \cdot C} \end{bmatrix}^{-1}$$

$$\det(\Phi) := \left\| \begin{bmatrix} s & \frac{-(-1+D)}{L} \\ \frac{-1+D}{C} & \frac{s \cdot R \cdot C + 1}{R \cdot C} \end{bmatrix} \right\|$$

$$\det(\Phi) := \frac{s^2 \cdot L \cdot R \cdot C + s \cdot L + R - 2 \cdot R \cdot D + R \cdot D^2}{R \cdot C \cdot L}$$

$$\det(\Phi) := s^2 + \frac{1}{R \cdot L} \cdot s + \frac{1}{L \cdot C} \cdot (1 - D)^2$$

$$\Phi := \frac{1}{\det(\Phi)} \cdot \begin{pmatrix} \frac{s \cdot R \cdot C + 1}{R \cdot C} & \frac{-1 + D}{L} \\ \frac{1 - D}{C} & s \end{pmatrix}$$

$$\Phi := \frac{1}{s^2 + \frac{1}{R \cdot L} \cdot s + \frac{1}{L \cdot C} \cdot (1 - D)^2} \cdot \begin{pmatrix} \frac{s \cdot R \cdot C + 1}{R \cdot C} & \frac{-1 + D}{L} \\ \frac{1 - D}{C} & s \end{pmatrix}$$

$$H_p := C \cdot \Phi \cdot A'$$

$$H_p := \left[(0 \quad 1) \cdot \left[\frac{1}{s^2 + \frac{1}{R \cdot L} \cdot s + \frac{1}{L \cdot C} \cdot (1 - D)^2} \cdot \begin{pmatrix} \frac{s \cdot R \cdot C + 1}{R \cdot C} & \frac{-1 + D}{L} \\ \frac{1 - D}{C} & s \end{pmatrix} \right] \cdot \begin{pmatrix} \frac{1}{L} \cdot V_{out} \\ \frac{-1}{C} \cdot I_L \end{pmatrix} \right]$$

$$H_p := \left[\frac{1 - D}{C \cdot \left[s^2 + \frac{1}{R \cdot L} \cdot s + \frac{1}{L \cdot C} \cdot (1 - D)^2 \right] \cdot L} \cdot V_{out} - \frac{s}{\left[s^2 + \frac{1}{R \cdot L} \cdot s + \frac{1}{L \cdot C} \cdot (1 - D)^2 \right] \cdot C} \right] \cdot I_L$$

$$H_P := \frac{\frac{(1 - D)}{L \cdot C} V_{out} - \frac{1}{C} \cdot I_L \cdot s}{s^2 + \frac{1}{R \cdot L} \cdot s + \frac{1}{L \cdot C} \cdot (1 - D)^2}$$

APPENDIX B

TRANSITIONAL MODE PFC L6562 BOOST INDUCTOR DESIGN

DESIGN CHARACTERISTICS:

Mains Voltage Range:

$V_{irmsmin} := 108 \cdot V$ Minimum Input Voltage

$V_{irmsmax} := 305 \cdot V$ Maximum Input Voltage

Regulated DC Output Voltage:

$V_o := 450 \cdot V$

Rated Output Power:

$P_o := 150 \cdot W$

Minimum Switching Frequency:

$f_{sw} := 25 \cdot 10^3 \cdot Hz$

Maximum Output Voltage Ripple:

$\Delta V_o := 0.025 \cdot V_o$ $\Delta V_o = 11.25V$ Should be between 1 and 5% of the Output Voltage

Maximum Overvoltage Admitted:

$\Delta V_{OVP} := 60\ V$

Expected Efficiency:

$\eta := 0.90$

Input Power:

$$P_{in} := \frac{P_o}{\eta} \qquad P_{in} = 166.667W$$

Maximum Mains RMS Current:

$$I_{rms} := \frac{P_{in}}{V_{irmsmin}} \qquad I_{rms} = 1.543A$$

Rated Output Current:

$$I_o := \frac{P_o}{V_o} \qquad I_o = 0.333A$$

INPUT BRIDGE DESIGN:

Select standard slow recovery, low-cost diodes.
Factors to cosider: 1. Input Current, Irms 2. Maximum Peak mains Voltage 3. Thermal Data of the Diodes.

INPUT CAPACITOR:

High Frequency Ripple between 1 and 10% of the minimum rated Input Voltage:

$r := 0.05$ Choose a value between 0.01 and 0.1.

$$C_{in} := \frac{I_{rms}}{2 \cdot \pi \cdot f_{sw} \cdot r \cdot V_{irmsmin}} \qquad C_{in} = 1.819 \times 10^{-6}\,\text{F}$$

Higher Values of Cin will reduce the burden to the EMI filter but cause the power factor and the harmonic contents of the mains current to worsen.
Low Values of Cin Improve Power Factor and reduce Mains current distortion but requre heavier EMI filtering and increased power dissipation in the input bridge.
Right Choice up to the EE Designer.

OUTPUT CAPACITOR:

Depends on: 1. DC Output Voltage Vo 2. The Admitted Overvoltage DVovp
3. The Output Power Pout and 4. The Desired Voltage Ripple DVo.

$f := 100\,Hz$ f is twice the main frequency of the input votage.

$$C_{out} := \frac{P_o}{4 \cdot \pi \cdot f \cdot V_o \cdot \Delta V_o} \qquad C_{out} = 2.358 \times 10^{-5}\,\text{F}$$

Choose a value greater or equal to that of Cout.

Select Cout greater than the one obtained above:

$C_{out} := 23.5 \cdot \mu F$ Two 47uF Electrolytic Caps, 250V each in series.

Total RMS Ripple Current of the Capacitor is:

$$I_{Crms}(V_{irmsmax}) := \sqrt{\frac{32 \cdot \sqrt{2}}{9 \cdot \pi} \cdot I_{rms}^{\,2} \cdot \frac{V_{irmsmax}}{V_o} - I_o^{\,2}} \qquad I_{Crms}(V_{irmsmax}) = 1.572\text{A}$$

$$I_{Crms}(V_{irmsmin}) = 0.896\text{A}$$

$$I_{Crms} := if\left(I_{Crms}(V_{irmsmax}) > I_{Crms}(V_{irmsmin}), I_{Crms}(V_{irmsmax}), I_{Crms}(V_{irmsmin})\right)$$

$I_{Crms} = 1.572\text{A}$

BOOST INDUCTOR:

The Inductance L is usually determined so that the minimum switching frequency is greater than the maximum frequency of the internal starter, to ensure a correct Transitional Mode Operation.
Maximum Peak Inductor Current will be:

$$I_{Lpk} := 2 \cdot \sqrt{2} \cdot \frac{P_{in}}{V_{irmsmin}} \qquad I_{Lpk} = 4.365\text{A}$$

Assuming Unity Power Factor θ=0.

$\omega t := 0, 0.01 .. \pi$

$$L(V_{irmsmin}) := \frac{V_{irmsmin}^{2} \cdot (V_o - \sqrt{2} \cdot V_{irmsmin})}{2 \cdot f_{sw} \cdot P_{in} \cdot V_o}$$

$L(V_{irmsmin}) = 9.246 \times 10^{-4}\,\text{H}$ $\qquad$ $L(V_{irmsmax}) = 4.63 \times 10^{-4}\,\text{H}$

Choose the Smallest L of the two obtained:

$$L := if(L(V_{irmsmin}) > L(V_{irmsmax}), L(V_{irmsmax}), L(V_{irmsmin}))$$

$L = 463.013\ \mu H$ $\qquad$ Selected Value of L

$$f_{sw}(\omega t, V_{irmsmin}) := \frac{1}{2 \cdot L \cdot P_{in}} \cdot \frac{V_{irmsmin}^{2} \cdot (V_o - \sqrt{2} \cdot V_{irmsmin} \cdot \sin(\omega t))}{V_o}$$

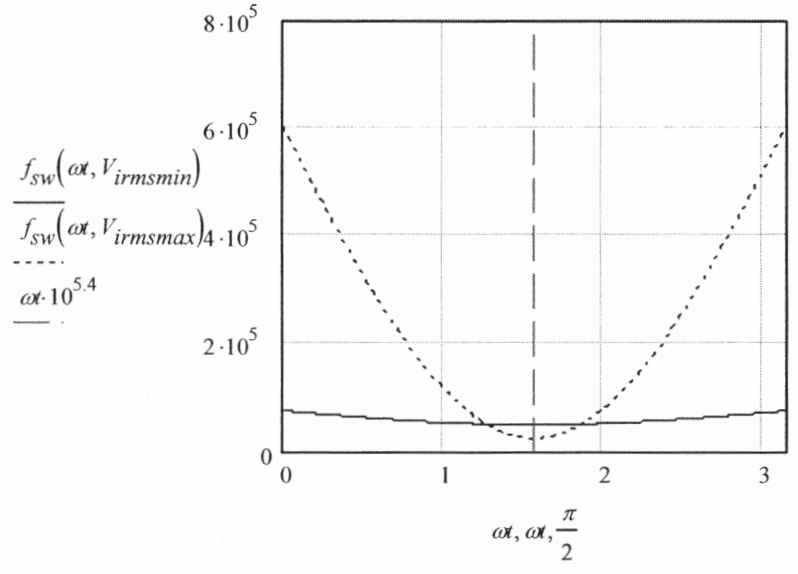

$f_{sw}\left(\frac{\pi}{2}, V_{irmsmax}\right) = 25\,KHz$ $\qquad$ Minimum Frequency

GUIDE : Use High Frequency Ferrite Gapped Core-Set With Bobbin for PFC applications.

ESTIMATE THE CORE SIZE:

$I_e := 57.5 \cdot mm$

$I_{gap} := 1.58\,mm$

$$K := 14 \cdot 10^{-6} \cdot \frac{I_e}{I_{gap}} \cdot \frac{m^3}{H \cdot A^2}$$

These Values are taken from the Datasheet or From Measuring the Ie-magnetic path length, and Igap. Igap has to be at least 1% of Ie.

To Calculate the Minimum Volume of the Core:

$Volume := 4 \cdot K \cdot L \cdot I_{rms}^{2}$ $\quad Volume = 2.247 cm^{3}$

$Volume_{ofAct} := 4500 mm^{3}$ $\quad Volume_{ofAct} = 4.5 cm^{3}$

DETERMINE THE WIRE SIZE AND NUMBER OF TURNS

$E := \frac{1}{2} \cdot L \cdot I_{Lpk}^{2}$ $\quad E = 4.411 \times 10^{-3} J$ Maximum Energy Stored in the Inductor

$A_e := 76.8 mm^{2}$ $\quad A_e = 0.768 cm^{2}$ Ae is the Efective Area of the Core Cross-Section

$\mu_0 := 4 \cdot \pi \cdot 10^{-7} \cdot \frac{H}{m}$

$N := \sqrt{\frac{L \cdot I_{gap}}{\mu_0 \cdot A_e}}$ $\quad N = 87.064$ Number of Turns

Wire gauge selection is based on limiting the copper losses at an acceptable value:

Litz wire or multiwire solutions are recommended due to high frequency Ripple (Rcu is increased by skin and proximity effects).

$t := 58 mm$ Bobbin Average Length of Turns

$R_{dc1} := 0.043 \cdot \frac{\Omega}{ft}$ Based on Wire Size

$R_{cu} := t \cdot N \cdot R_{dc1}$

$R_{cu} = 0.712 \Omega$

$P_{cu} := \frac{4}{3} \cdot I_{rms}^{2} \cdot R_{cu}$ $\quad P_{cu} = 2.262 W$ Power Loss in the Inductor

POWER MOSFET SELECTION:

$I_{Qrms}(V_{irmsmax}) := 2 \cdot \sqrt{2} \cdot I_{rms} \cdot \sqrt{\frac{1}{6} - \frac{4 \cdot \sqrt{2}}{9 \cdot \pi} \cdot \frac{V_{irmsmax}}{V_o}}$ $\quad I_{rms} = 1.543 A$ $\quad V_o = 450 V$

$I_{Qrms}(V_{irmsmax}) = 0.769 A$ $\quad I_{Qrms}(V_{irmsmin}) = 1.504 A$

$I_{Qrms} := if(I_{Qrms}(V_{irmsmax}) > I_{Qrms}(V_{irmsmin}), I_{Qrms}(V_{irmsmax}), I_{Qrms}(V_{irmsmin}))$

$I_{Qrms} = 1.504 A$

$R_{DSon} := 1.7 \cdot \Omega$ Select this value from the MOSFET Datasheet @ 100C

$P_{ON} := I_{Qrms}^{2} \cdot R_{DSon}$ $P_{ON} = 3.843\text{W}$ Conduction Losses

Switching Losses occur only at turn-off because of transition mode operation:

$t_{fall} := 70 \cdot 10^{-9} s$

$f_{sw} := 55 \cdot kHz$

$P_{CROSS} := V_o \cdot I_{rms} \cdot t_{fall} \cdot f_{sw}$ $P_{CROSS} = 2.674\text{W}$

BOOST DIODE:

A Fast Recovery Type should be Selected

$I_{Do} := I_o$ $I_{Do} = 0.333\text{A}$

$$I_{Drms}(V_{irmsmin}) := 2 \cdot \sqrt{2} \cdot I_{rms} \cdot \sqrt{\frac{4 \cdot \sqrt{2}}{9 \cdot \pi} \cdot \frac{V_{irmsmin}}{V_o}}$$

$$I_{Drms} := if\left(I_{Drms}(V_{irmsmin}) > I_{Drms}(V_{irmsmax}), I_{Drms}(V_{irmsmin}), I_{Drms}(V_{irmsmax})\right)$$

$I_{Drms} = 1.607\text{A}$

$V_{th} := 1.7V$ $R_d := .5 \cdot \Omega$

$P_{Don} := V_{th} \cdot I_{Do} + R_d \cdot I_{Drms}^{2}$

$P_{Don} = 1.858\text{W}$

L6561 BIASING CIRCUITRY:

Pin 1 (INV):

$$R_{11} := \frac{\Delta V_{OVP}}{40 \cdot \mu A}$$ R11 is the Upper Output Voltage Divider

$R_{11} = 1.5 \times 10^{6}\ \Omega$

$$R_{13} := \frac{R_{11}}{\left(\frac{V_o}{2.5 \cdot V} - 1\right)}$$ $R_{13} = 8.38 \times 10^{3}\ \Omega$

Pin 2 (COMP):

The Feedback Compensation Network reduces the bandwidth so to avoid the attempt of the system to control the output voltage ripple (100-120Hz).
This compensation can be achieved through a capacitor which provides a low frequency pole as well as high DC gain. Provide ~60dB attenuation at 100Hz.

$R_7 := 0.33 \cdot \Omega$ Resistance of Gate Circuit of the Mosfet, Pin 7.

$$C_{23} := \frac{10 \cdot 10^{-6}}{2 \cdot \pi \cdot R_7} \cdot \frac{F}{S} \qquad C_{23} = 4.823 \times 10^{-6}\,\mathrm{F}$$

Pin 3 (MULT):

To get a Sinusoidal Voltage Reference

$V_{MULTpkx} := 2.7 \cdot V$ Maximum Accepted Value for MULT pin.

$$V_{MULTpkmin} := V_{MULTpkx} \cdot \frac{V_{irmsmin}}{V_{irmsmax}} \qquad V_{MULTpkmin} = 0.956\,\mathrm{V}$$

$V_{XCSpk} := 1.65 \cdot V_{MULTpkmin}$ $V_{XCSpk} = 1.578\,\mathrm{V}$

If Vxcspk>1,6 the calculation should be repeated with Lower Vmultpkx.

Choose Lower Resistor Value:

$R_2 := 13 \cdot k\ \Omega$

$$R_1 := \frac{R_2 \cdot \left(\sqrt{2} \cdot V_{irmsmax} - V_{MULTpkx}\right)}{V_{MULTpkx}} \qquad R_1 = 2.064 \times 10^{6}\,\Omega$$

The values can be choosen to minimize the current through R3, in the hundreds uA or less to minimize power dissipation.

Pin 4 (CS):

$I_{Rspk} := 2 \cdot \sqrt{2} \cdot I_{rms}$

$$R_s := \frac{V_{XCSpk}}{I_{Rspk}} \qquad R_s = 0.361\,\Omega$$

Choose a value smaller or equal to that of Rs.

$$P_{Rs} := R_s \cdot I_{Qrms}^{2}$$

$P_{Rs} = 0.817\text{W}$ $\qquad I_{rspkmax} := \frac{1.8 \cdot V}{R_s}$ $\qquad I_{rspkmax} = 4.98\text{A}$

Make sure the Current above will not saturate the inductor at startup.

Pin 5 (ZCD):

m is the maximum main-to-auxiliary winding turn ratio:

$$m := \frac{V_o - \sqrt{2} \cdot V_{irmsmax}}{2.1 \cdot V}$$

$m = 8.888$

Can also use a resistor to limit the current to the pin to a maximum of 3mA.

Pin 6 (GND):

Pin 7 (GD):

Able to drive a MOSFET with 400mA source and sink capabilities.

Pin 8 (Vcc):

To start L6561, the voltage must exceed the start-up threshold (13V max). Current not exceeding 4.5mA.

APPENDIX C

L-6562 BOOST PFC CONTROLLER DESIGN

PFC Converter Data:

$V_O := 450 \cdot V$ $C_O := 33.5 \cdot \mu F$ $R_S := 0.33\,\Omega$ $OVP := 40 \cdot V$ $\eta := 0.9$

Multiplier Data:

$R_{up} := 2100\,k\Omega$ $R_{low} := 12.9\,k\Omega$

Analysis Setpoint:

$V_{irms} := 264 \cdot V$ $P_O := 150\,W$ $R_O := \frac{V_O^2}{P_O}$ $R_O = 1.35 \times 10^3\,\Omega$

Input Divider Gain: $KP := \frac{R_{low}}{R_{low} + R_{up}}$ $KP = 6.105 \times 10^{-3}$

Large signal Multiplier Gain: $KM(V_{comp}) := 0.651 \cdot \left[1 - 85.29(e)^{-1.776 \cdot V_{comp}}\right]$

Error Amplifier Quiescent Point: $V_{comp} := 4$

$$V_{comp} := \text{root}\left(2.5 + \frac{2 \cdot P_O \cdot R_S}{\eta \cdot KM(V_{comp}) \cdot KP \cdot V_{irms}^2} - V_{comp}, V_{comp}\right)$$

$V_{comp} = 3.105$

Small Signal Multiplier Gain: $km := \frac{d}{dV_{comp}}\left[KM(V_{comp}) \cdot (V_{comp} - 2.5)\right]$

$km = 0.668$

$j := \sqrt{-1}$ $f := 0.1, 1 .. 1000($ $\omega(f) := 2 \cdot \pi \cdot f$

****

Control to Output Transfer Function, Resistive Load:

$$G_R(f, V_{irms}) := \frac{km \cdot KP \cdot V_{irms}^{\,2}}{4 \cdot V_O} \cdot \frac{R_O}{R_S} \cdot \frac{1}{1 + j \cdot \omega(f) \cdot C_O \cdot \frac{R_O}{2}}$$

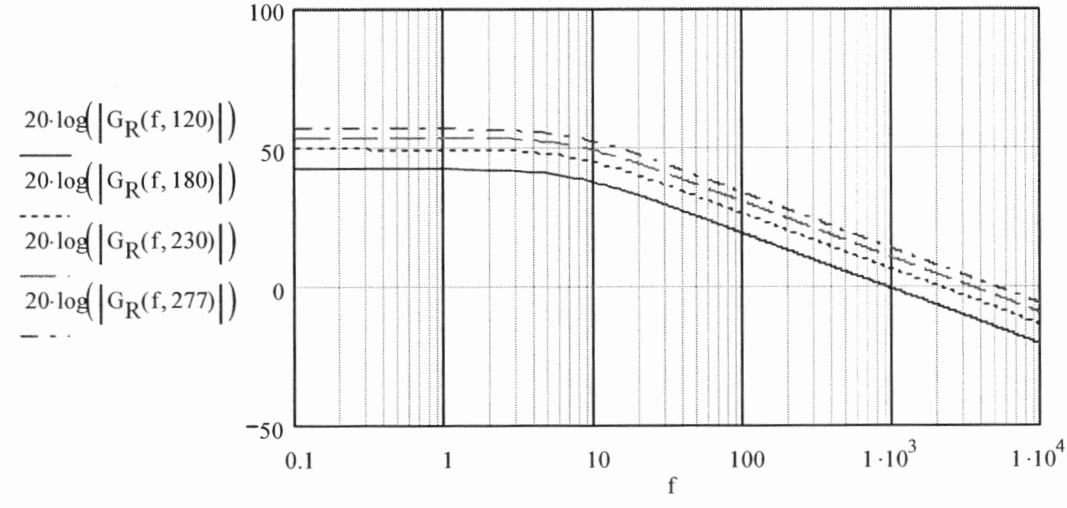

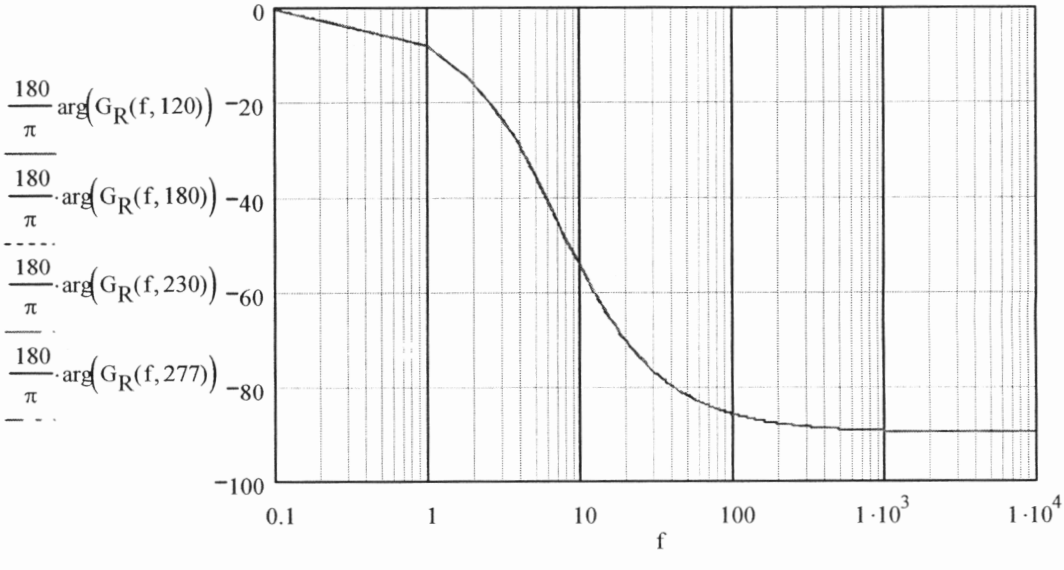

Pole Location: $p = 7.038\text{Hz}$

Compensated E/A Transfer Function (Resistive Load):

High Frequency Gain: $G_h := 0.00$

Zero : $z := 30 \cdot \text{Hz}$

Transfer Function: $G_1(f) := G_h \cdot 2 \cdot \pi \cdot z \cdot \dfrac{1 + j \cdot \dfrac{\omega(f)}{2 \cdot \pi \cdot z}}{j \cdot \omega(f)}$

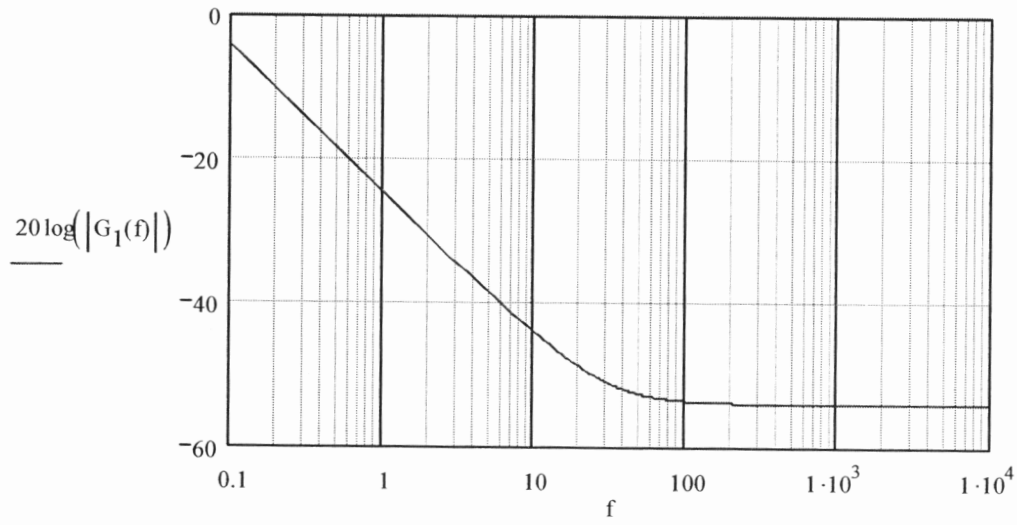

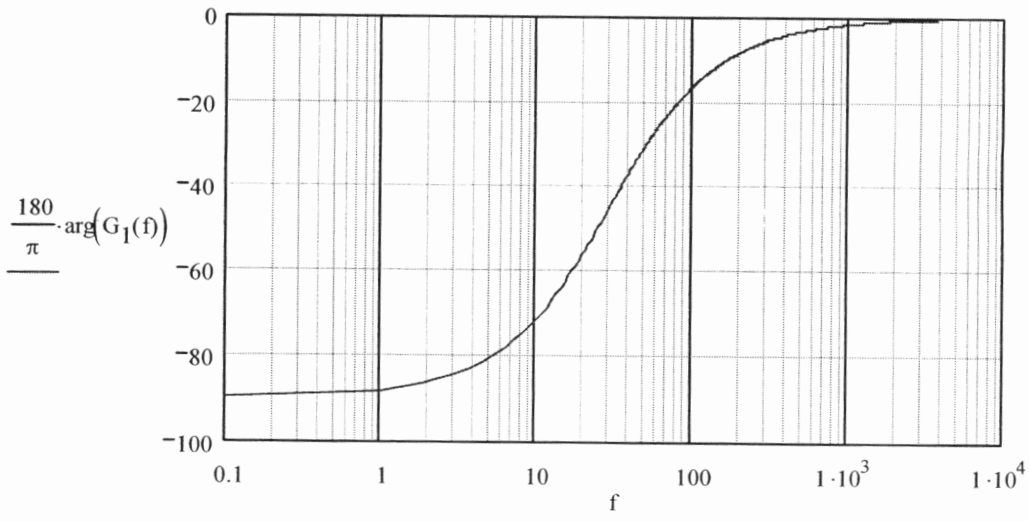

$$p := \frac{1}{\pi \cdot R_O \cdot C_O}$$

Open Loop Transfer Function:

$$F(f, V_{irms}) := G_R(f, V_{irms}) \cdot G_1(f)$$

$$\Phi F(f, V_{irms}) := \arg(F(f, V_{irms})) \cdot \frac{180}{\pi}$$

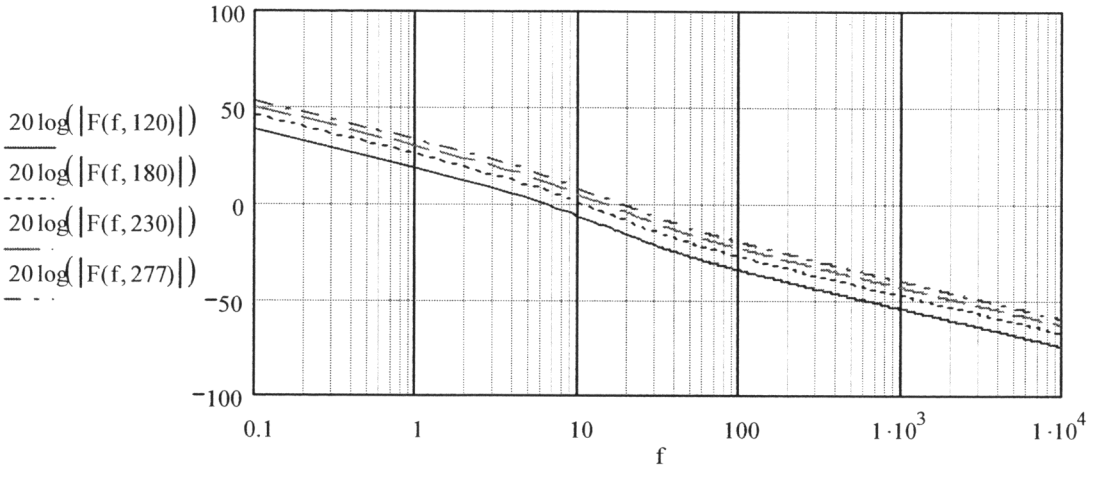

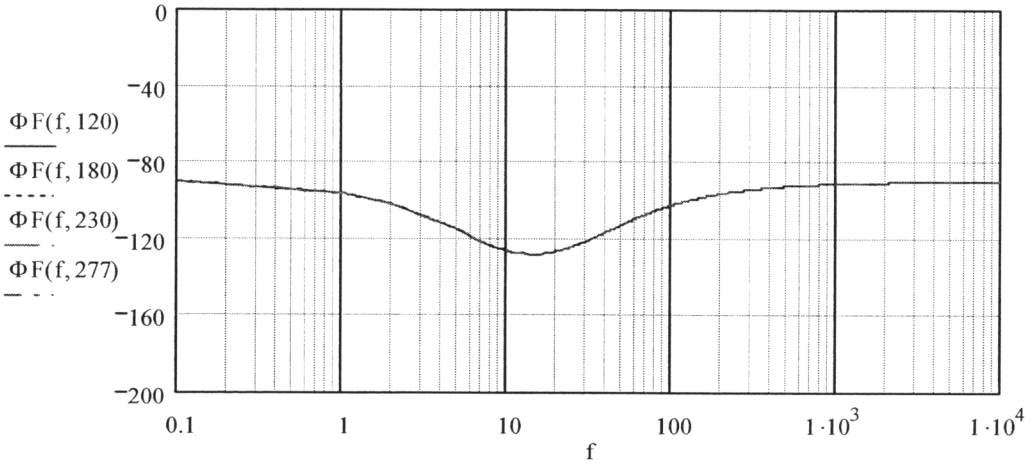

$f := 1 \cdot Hz$

Crossover Frequency: $f_c(V_{irms}) := |root(|F(f, V_{irms})| - 1, f)|$

$f_c(120) = 6.151Hz$ $f_c(180) = 10.574Hz$ $f_c(230) = 14.348Hz$ $f_c(277) = 18.068Hz$

Phase Margin: $\Phi(V_{irms}) := 180 + \Phi F(f_c(V_{irms}), V_{irms})$

$\Phi(120) = 60.435$ $\Phi(180) = 53.065$ $\Phi(230) = 51.69$ $\Phi(277) = 52.342$

Feedback Network Implementation for Resistive Load:

Equivalent Load Resistance: $R_7 := \frac{OVP}{40 \cdot V} \cdot 10^3 \cdot K\Omega$ $R_7 = 1\,M\Omega$

Output Divider Lower Resistor: $R_8 := \frac{2.5 \cdot V}{V_O - 2.5 \cdot V} \cdot R_7$ $R_8 = 5.587k\Omega$

Series Feedback Capacitor: $C_3 := \frac{1}{2 \cdot \pi \cdot z \cdot G_h \cdot R_7}$ $C_3 = 2.653\mu F$

Series Feedback Resistor: $R_{11} := \frac{1}{2 \cdot \pi \cdot z \cdot C_3}$ $R_{11} = 2k\Omega$